REPUBLIC OF TURKIYE
DOKUZ EYLUL UNIVERSITY
IZMIR INTERNATIONAL BIOMEDICINE AND GENOME INSTITUTE

INVESTIGATION OF THE ROLE OF EXTRACELLULAR MATRIX AND TUMOR MICROENVIRONMENT KERATAN SULFATE PROTEOGLYCAN COMPOSITION IN CANCER METASTASIS

ESRA ERSÖZ GÜLSEVEN

DEPARTMENT OF GENOMICS AND MOLECULAR BIOTECHNOLOGY

MASTER OF SCIENCE THESIS

IZMIR-2023

THESIS CODE: DEU.HSI.MSc number/2019850034

REPUBLIC OF TURKIYE
DOKUZ EYLUL UNIVERSITY
IZMIR INTERNATIONAL BIOMEDICINE AND GENOME INSTITUTE

INVESTIGATION OF THE ROLE OF EXTRACELLULAR MATRIX AND TUMOR MICROENVIRONMENT KERATAN SULFATE PROTEOGLYCAN COMPOSITION IN CANCER METASTASIS

DEPARTMENT OF GENOMICS AND MOLECULAR BIOTECHNOLOGY

MASTER OF SCIENCE THESIS

ESRA ERSÖZ GÜLSEVEN
Supervisor: Dr. Hani ALOTAIBI
Co-Supervisor: Dr. Gülçin ÇAKAN-AKDOĞAN
This project funded by TUBITAK Project No: 219S943 and
Esra ERSOZ was supported by TUBITAK Project No: 219S943 and
TUBITAK-BIDEB 2210-A scholarship fund.

Thesis Code: DEU.HSI.MSc number/2019850034

T.C.
DOKUZ EYLÜL ÜNİVERSİTESİ

İZMİR ULUSLARARASI BİYOTIP VE GENOM ENSTİTÜSÜ

MASTER'S THESIS DEFENSE EXAM REPORT

Esra Ersoy Güleyen, who is a student at the Department of Genomics And Molecular Biotechnology - Molecular Biology Master's program of the Dokuz Eylul University's Izmir International Biomedicine and Genome Institute, with the student ID 2019850034, ~~succeeded/failed~~ ~~his~~/her Master's thesis titled "Investigation of the role of EGM and IMS Keratan Sulfate Proteoglycan Composition in cancer metastasis" as a result of ~~his~~/her thesis defense on February 1st 2023 at 10.00 am.

JURY HEAD

Dr. Hani ALOTAIBI

JURRY MEMBER

Dr. Serif SENTURK

JURRY MEMBER

Prof. Dr. Ralph MEUWISSEN

CONTENTS

1. INTRODUCTION AND AIM 7

1.1. STATEMENT OF THE PROBLEM 7

1.2. AIM 8

1.3. HYPOTHESIS 8

2. GENERAL INFORMATION 9

2.1. CANCER AND INITIATION OF METASTASIS 9

2.2. EXTRACELLULAR MATRIX 11

2.3. STRUCTURAL PROPERTIES OF PROTEOGLYCANS (PGs) 14

2.4. KERATAN SULFATE PROTEOGLYCANS 18

2.5. SULFATION OF GLYCOSAMINOGLYCANS 19

2.6. CHST6: CARBOHYDRATE SULFOTRANSFERASE -6 24

2.7. ZEBRAFISH AS A MODEL ORGANISM 24

3. MATERIALS AND METHODS 31

3.1. TYPES OF RESEARCH 31

3.2. TIME AND PLACE OF RESEARCH: 31

3.3. MATERIALS 31

3.3.1. Laboratory Reagents 31

3.3.2. Primers 33

3.3.3. Enzymes, Antibodies and Kits 33

3.3.4. Laboratory Equipment 34

3.3.5. Cell Culture Products 35

3.3.6. General Solutions 35

3.4. TOOLS FOR DATA COLLECTION 37

3.4.1. Design and Production of gRNAs and Cas9 mRNAs 37

3.4.2. Microinjection 38

3.4.3. Preparation Of DNA Lysates 38

3.4.4. Mutation analyses from Genomic DNA 38

3.4.6. Sequence Analysis 39

3.4.7. Western Blot 39

3.4.8. ELISA 39

3.4.9. Immunofluorescence Staining of Wildtype and Mutant Zebrafish 40

3.4.10. Cell Preparation for Xenograft 41

3.4.11. Xenograft 41

3.4.12. Imaging of Xenograft 41

3.4.13. Visualization and Analysis of Cells 42

3.5. RESEARCH PLAN 42

3.6. DATA EVALUATION 43

3.7. LIMITATION OF STUDY 43

3.8. ETHICS COMITTEE APPROVAL 43

4. RESULTS 44
4.1. SYNTHESIS OF GRNAS, CAS9 MRNAS AND MICROINJECTION 44
4.2. GENERATING OF THE CHST6 CRISPR MUTANTS 45
4.3. SEQUENCING ANALYSIS OF MUTANTS 48
4.4. SELECTION OF MUTANTS 51
4.5. PROTEIN EXPRESSION ANALYSIS OF MUTANTS BY WESTERN BLOT 54
4.6. FUNCTIONAL ANALYSIS OF MUTANTS BY ELISA 55
4.7. TISSUE DISTRIBUTION OF SULFATED KSPGS IN MUTANT AND WT LARVAE 56
4.8. GENERATION OF XENOGRAFT MODEL 57
5. DISCUSSION 66
5.1. DELETING THE CODING SEQUENCE OF THE CHST6 GENE IS FATAL 67
5.2. MUTATION OF THE PAPS REGION WAS CONFIRMED BY SEQUENCE ANALYSIS 68
5 3. MUTATION OF THE PAPS DOMAIN LEADS TO LOSS OF FUNCTION IN THE CHST6 GENE 69
5.4. METASTATIC CAPACITY OF BREAST AND MELANOMA CANCER CELLS ARE INCREASED IN CHST6 MUTANT XENOGRAFT MODELS 70
6. CONCLUSION 73
7. REFERENCES 74
8. APPENDIX 83
8.1 ETHICS COMITTEE APPROVAL 83
8.2 Curriculum Vitae 84

INDEX OF TABLES

Table 1 Disease related with abnormal GAG sulfation *22*
Table 2 List of laboratory reagents and chemicals used for experiments *31*
Table 3. List of the primers used in experiments. *33*
Table 4 List of kits, enzymes and antibodies used for experiments. *33*
Table 5 List of laboratory equipment *34*
Table 6 Table of products used cell culture applications. *35*
Table 7 Recipe of 10X PBS Stock Solution *35*
Table 8 Recipe of 1X PBST Solution *35*
Table 9 Recipe of Tricaine Stock Solution *36*
Table 10 Recipe of 60X E3 Medium Stock Solution *36*
Table 11 Recipe of %2 Agarose Gel *36*
Table 12 Recipe of %4 PFA Solution *36*
Table 13: Coding sequence deletion mutation A) Shows the number of F1 embryos, *B)* shows the number of F2 embryos. *48*
Table 14 Transmission and homozygous rates of chst6pd4 allele *51*
Table 15 Transmission and homozygous rates of chst6f42 allele *53*

INDEX OF FIGURES

Figure 1 Schematic representation of extracellular matrix with their components..... 12
Figure 2 Illustration of components of extracellular matrix..... 13
Figure 3 Basic structural illustration of Proteoglycans. 16
Figure 4 Illustration of glycosaminoglycans chains..... 17
Figure 5 Structure of Keratan Sulfate 18
Figure 6 Illustration of glycosaminoglycans chains..... 19
Figure 7 Diagram of advantages for using a zebrafish as a model..... 25
Figure 8 CRISPR Cas9 mediated genom editing..... 27
Figure 9 Schematic representation of the xenograft technique 28
Figure 10 Distribution of cKS expression in 8 dpf zebrafish larva 29
Figure 11 Metastatic cells were shown as map via ImageJ software 42
Figure 12 Targeted mutation sites in the zebrafish chst6 gene..... 44
Figure 13 Production of Cas9 and gRNAs 44
Figure 14 Mutations screening of chst6^{del5} allele 46
Figure 15 Coding region deletion mutant chst6^{del5} F_2 homozygous screening. 47
Figure 16 chst6^{del5} allele heterozygous single embryo sequence analysis.....49
Figure 17 Sequence analysis of coding region deletion mutants with gRNA3+5..... 50
Figure 18 Targeted mutation sites in the zebrafish chst6 gene..... 51
Figure 19 Sequence analysis of the chst6^{pd4} deletion homozygous mutant..... 52
Figure 20 Sequence analysis of the chst6^{f42} frameshift mutation homozygous mutant..... 53
Figure 21 Western blot results. 54
Figure 22 cKS amount decreased in mutants 55
Figure 23 Inhibition of keratan sulfate proteoglycan sulfation in CHST6 mutant zebrafish larvae 56
Figure 24 Workflow of a xenograft experiment and analysis 58
Figure 25 Results of Metastatic Capacity change of MCF7 cells in mutant larvae 59
Figure 26 Results of Metastatic Capacity change of MCF7 cells in mutant larvae 60
Figure 27 Results of Metastatic Capacity change of Malme-3M cells in mutant larvae..... 61
Figure 28 Results of Metastatic Capacity change of Malme-3M cells in mutant larvae..... 63
Figure 29 Summary of Metastatic potential comparison of xenografts which are used chst6 mutants as hosts. 64
Figure 30 Representative images of DiI stained NMuMG cells injected wildtype and chst6$^{pd4/+}$ incross mutants zebrafish larvae. Black dots represent NMuMG cells. 65

ABBREVIATIONS

BM	Basal Membrane
bp	Base pair
CAF	Cancer Associated Fibroblast
Cas9	CRISPR-associated protein 9
CDS	Coding Sequence
CHST	Carbohydrate sulfotransferase
cKS	Corneal Keratan Sulfate
CRISPR	Clustered Regularly Interspaced Short Palindromic Repeats
CS	Chondroitin Sulfate
DNA	Deoxyribonucleic acid
DPF	Day Post Fertilization
DPI	Day Post Injection
DS	Dermatan Sulfate
ECM	Extracellular Matrix
EMT	epithelial-mesenchymal transition
FF	Founder Fish
F0	First Parents or the Origins
F1	First Filial Generation
F2	Second Filial Generation
GAG	Glycosaminoglycan
Gal	Galactose
gRNA	Guide RNA

HA	Hyaluronic Acid
hpi	Hour Post Injection
HS	Heparan Sulfate
IM	Intestinal Membrane
KS	Keratan Sulfate
KSPG	Keratan Sulfate Proteoglycan
mRNA	Messenger RNA
NHEJ	Non-Homologous End Joining
nls	Nuclear Localization Signal
PAM	Protospacer Adjacent Motif
PAPS	3'-phosphoadenosine-5'-phosphosulphate
PG	Proteoglycan
SLRP	Small Leucine-Rich Proteoglycans
WT	Wildtype

to my Family, who always believed in me…

ACKNOWLEDGEMENTS

First of all, I would like to express my gratitude to my valuable supervisor, my wedding witness, Dr. Gülçin ÇAKAN-AKDOĞAN, who surrounded me with her deep knowledge, guided me, educated me and took me by the hand when I was a new graduate and a young and uninformed student without a clear vision, and made me who I am. Throughout this process, she tried to transfer all her knowledge and experience to us. Thanks to the creative working environment she offered us, I learned to take responsibilities with confidence and to deal with the consequences, good or bad. She has always been with me whenever I needed help. The fact that she was always fair but also compassionate, made me feel close to her. I hope I can be as much of a luminous, encouraging and guiding person as she is. She shaped my life with her vision, I would like to be a mother, scientist and teacher like her.

I am grateful to my official advisor Dr. Hani ALOTAIBI, who accepted me as his student, for supporting and my studies and making an impact in the scientific progress of this thesis study.

I would like to thank my jury members Assoc. Prof. Dr. Şerif ŞENTÜRK and Prof. Dr. Ralph MEUWISSEN for their valuable time that they spent to evaluate my thesis work.

I would like to express my gratitude and regards to Scientific and Technological Council of Turkey - TUBITAK BIDEB 2210-A Program for supporting me during my graduate education and financial support with TUBITAK grant number #219S943,

I have also special thanks;

To my dear friend Merve BAŞOL, with whom we were like two halves of the same apple in this project. She shared her knowledge with me, stood by me when I had existential crisis moments. She always walked with me, was there for me on all my special days, and was even a big sister to me,

To Ebru ÖNAL, my partner in trouble, who has added joy to my life since she came, who has been sad and happy with me, who has made every day great with her energy, found a way to cheer us up in my most troubled times,

To my dear Özlem EREZ, whom I will be friends with for life. Even though she started came as my intern, now I see myself when I look at her. I want her to be with me in every moment of my life. Without her help this thesis would not have been completed in time,

To all my teammates, especially Emine GELİNCİ who taught me her secret skills and who was always there when I needed help. To Çiğdem KARAKOYUN, who guided me in my academic career with all her friendliness and always listened to me. To Helin ÖZAKTAŞ who made me laugh with her sweetness, to Serhat SONGÖREN and Metehan GÜZELKAYA who, in all his kindness, helped me with my experiments. I also thank Khalid ABDALLA who guided me whenever I ask to him. And lastly to Meryem Özaydın who took safe care of my fish,

I would like to thank my best friends Ezgi ERGÜL, Şeyda Nur POLAT, Şeyma Nur SOYYİĞİT, Cerennur YALÇIN, Meltem KAYSI, who have witnessed this journey with me for years, who have always loved me even when I could not spare time for them, who have always been there for me in every mistake, who think of me more than me, who have supported me at every step,

I would like to thank Bensu GÜNAY and Nur Deniz BİNGÜL, with whom I have been on the same path since my undergraduate education, who have been more than friends to me, treating me like their little sister, and always thinking of each other even though we are far away.

My biggest thank is to my most precious ones, my dear mother and father, who raised me and made me grow up to this day, who stood behind me in every decision, who did everything I wanted, who beared all my tiredness, stress and troubles, who deserve this diploma more than me. To my beloved father-in-law and mother-in-law who see me as their own daughter, who value me very much, who took me into their lives with kindness.

To my elder sister Kamile KUTLU and her family. She is the most caring and thoughtful mother I have ever known, who came into my life with all her kindness and gentleness, who accepted me as her own sister and loved me very much.

To my sister Ayşegül ERSÖZ. I am so lucky to have you as my best friend and my sister. I will do everything I can to set an example for you. I am always with you. Thank you so much for never making me sad and always making me happy despite all my annoyances, my little baby.

Last but not least, I would like to extend my endless love to my beloved husband Ahmet GÜLSEVEN, my life partner, my most precious one, for being with me in every moment, for supporting me and being proud of me. I am grateful to him for being with me every day, for changing my perspective on life, for relieving all my troubles with his beautiful smile.

Investigation of the Role of Extracellular Matrix and Tumor Microenvironment Keratan Sulfate Proteoglycan Composition in Cancer Metastasis

Esra ERSOZ-GULSEVEN, Dokuz Eylul University Izmir International Biomedicine and Genome Institute, Health Campus, Balcova 35340- Izmir / TURKEY

ABSTRACT

The extracellular matrix (ECM) is a complex structure that consists of several macromolecules including proteoglycans, collagens and adhesion molecules. ECM plays important roles in determination of physical properties such as stiffness and elasticity, regulation of cell-cell and cell-ECM interactions, chemokine diffusion and modulation of signal transduction. Recent findings suggests that ECM takes part in cancer metastasis; not only by affecting the permissiveness of the microenvironment for migration but also by regulation of signal transduction. Proteoglycans (PGs) are important ECM components, that have been implicated in cancer progression. PGs are a large family that contain several proteins covalently bonded with different types of glycosaminoglycan chains. They are divided into four groups according to their Glycosaminoglycan (GAG) types: hyaluronans, dermatan/chondroitin sulfates, heparan sulfates and keratan sulfates. There is extensive research that implicates heparan sulfate and chondroitin sulfate in tumor development, and cancer progression but the roles of Keratan Sulfate Proteoglycans are less understood. Some KSPGs of the cancer cell such as lumican has been implicated in metastasis. However, no studies were reported that investigated the effect of KSPGs in the tissue microenvironment.

In order to inactivate different KSPGs, sulfation can be inhibited since sulfation of glycosaminoglycans is the most important modification required for KSPG function. In this study, a zebrafish KSPG sulfating enzyme has been mutated, and loss of function mutants were obtained.

Next, the metastatic potential of breast cancer and melanoma cancer cells were examined by xenograft method in the host environment where Keratan Sulfate sulfation levels were altered. The results indicate to the importance of KSPGs in tumor microenvironment and metastasis initiation.

Key Words: Extracellular matrix, Keratan Sulfate Proteoglycans, carbohydrate sulfotransferase, Zebrafish xenograft model

Tümör Mikroçevresi ve Hücre Dışı Matriks Keratan Sülfat Proteoglikan Kompozisyonun Kanser Metastazındaki Rolünün Araştırılması

Esra ERSOZ-GULSEVEN, Dokuz Eylül Üniversitesi, İzmir Uluslararası Biyotıp ve Genom Enstitüsü, Sağlık Kampüsü, Balçova 35340- Izmir / TURKEY

ÖZET

Hücre dışı matriks (HDM), proteoglikanlar, kollajenler ve adezyon molekülleri dahil olmak üzere çeşitli makromoleküllerden oluşan kompleks bir yapıdır. HDM, sertlik ve elastikiyet gibi fiziksel özelliklerin belirlenmesinde, hücre-hücre ve hücre-HDM etkileşimlerinin düzenlenmesinde, kemokin difüzyonunda ve hücre sinyal iletiminin düzenlenmesinde önemli roller oynar. Son bulgular, HDM'nin, tümör mikroçevresinde kanser hücrelerinin sadece migrasyonunu değil aynı zamanda sinyal iletiminin düzenlenmesini de etkileyerek metastazda rol aldığını göstermektedir. Proteoglikanlar (PG'ler), kanserin ilerlemesinde rol oynayan önemli HDM bileşenleridir. PG'ler, farklı tipte glikozaminoglikan zincirleri ile kovalent olarak bağlanmış protein içeren çok geniş bir ailedir. Glikozaminoglikan (GAG) tiplerine göre hiyalüronanlar, dermatan/kondroitin sülfatlar, heparan sülfatlar ve keratan sülfatlar olmak üzere dört gruba ayrılırlar. Heparan sülfat ve kondroitin sülfat hakkında tümör gelişiminde ve kanser ilerlemesinde rol oynadığını gösteren kapsamlı araştırmalar vardır; ancak Keratan Sülfat Proteoglikanların rolü daha az anlaşılmıştır. Lumikan gibi bazı KSPG'ler hücre çalışmalarında metastazla ilişkilendirilmiştir. Bununla birlikte, KSPG'lerin doku mikroçevresindeki etkisini araştıran hiçbir çalışma bildirilmemiştir. Farklı KSPG'leri inaktive etmek için, sülfasyon inhibe edilebilir çünkü glikozaminoglikanların sülfasyonu, KSPG işlevi için gereken en önemli modifikasyondur. Bu çalışmada, bir zebrabalığı KSPG sülfatlama enzimi mutasyona uğratılmış ve işlev kaybı mutantları elde edilmiştir. Daha sonra, meme kanseri ve melanom kanseri hücrelerinin metastatik potansiyeli, KS sülfasyon seviyelerinin değiştirildiği konakçı ortamda ksenograft yöntemiyle incelenmiştir. Bu çalışma sonuçları KSPG'lerin tümör mikroçevresi ve metastaz oluşumundaki önemine işaret etmektedir.

Anahtar Kelimeler: Hücre dışı matriks, Keratan Sülfat Proteoglikanlar, karbonhidrat sülfotransferazlar, Zebrabalığı ksenograft modeli

1. INTRODUCTION AND AIM

1.1. STATEMENT OF THE PROBLEM

Cancer metastasis is the process where tumor cells leave the primary tumor site, invade other tissues passing through the vessels and the extracellular matrix (ECM) and migrate to distant sites. While character of cells such as mesenchymal properties are essential factors, the tumor microenvironment, and the tissues through which the cells pass through are inarguably important in metastasis. The ECM not only provides physical support to tissues but also it regulates important processes such as cell differentiation, proliferation, and migration (Clause & Barker, 2013). Extracellular matrix is produced by fibroblasts, and the interaction between the ECM components and fibroblasts is a dynamic process that can influence disease progression and homeostasis. Chemokines in ECM can activate fibroblasts, and in case of cancer the activated fibroblasts can transform into cancer associated fibroblasts that can induce malignant transformation of cells. Proteoglycans are important components of ECM, which are found in close interaction with collagens, and can bind to other proteins including integrins and chemokines (Clause et. al 2013). Proteoglycans are a large family of macromolecules that all have a core protein and linked glycosaminoglycan (GAG) side chains that come in many flavors including heparan sulfate, chondroitin/dermatan sulfate or keratan sulfate, each of is characterized by different disaccharide repeats (Cho et al., 2022). The roles of these complex macromolecules are not completely clarified. And keratan sulfate proteoglycans are one of the less understood proteoglycan family in cancer progression (Ren et al., 2021). Keratan sulphate (KS) is an interesting GAG, found mainly in KSPGs but also in mucins and side chains of other complex PGs such as aggrecan. KS is characterized by Galactose: N-Acetylated Glucosamine (Gal: GlucNAc) disaccharide repeats, where sulfation of these residues is an important regulation of structure and function (Caterson & Melrose, 2018). KS is found in proteoglycans of various tissues including the brain, cartilage, cornea, uterus as well as in cell surface glycans of stem cells, tumor cells and stroma (Funderburgh, 2000). Role of KS in tumor progression is an emerging field. Lumican, a KSPG, on the cell surface of cancer cells is known to be involved in metastasis and

mesenchymal-epithelial-transition (Giatagana et al., 2021; Hayes et al., 2013a; Karamanou et al., 2017). Interestingly, sulfation status of KS is correlated with tumor cell invasiveness and several carbohydrate sulfotransferase (CHST) genes are associated with cancer prognosis (Lee et al., 2017; Ren et al., 2021).However, earlier studies focused on the cellular KSPGs, while the KSPGs in the tumor microenvironment and ECM, and importance of their sulfation status is not studied to our knowledge. Animal models are valuable tools to address the role of ECM and its components on metastatic invasion of cancer cells. Zebrafish xenograft model has been widely used to assess metastatic behaviors of cancer cells, however the role of host tissues and ECM in zebrafish xenograft model has not been studied in detail (Gamble et al., 2021)
.

1.2. AIM

Here, we aim to explore the effects of KS composition of the ECM and tissue microenvironment in cancer progression and metastasis by employing a zebrafish xenograft model and CRISPR mediated mutagenesis. Zebrafish larval xenograft is a robust in vivo model that allows analysis and imaging of metastatic behavior and invasion of tissues within days. In order to generate a microenvironment where KS sulfation is reduced or diminished, we aimed to generate CHST6 loss of function mutants via CRISPR/cas9 mediated mutagenesis technology and explore the influence of keratan sulfate proteoglycan content of host tissues on the metastatic behavior and epithelial/mesenchymal character of cancerous cells. Since keratan sulfate expression of breast and melanoma cells has been associated with cancer progression, we aimed to evaluate their metastatic behavior in wildtype and CHST6 mutant zebrafish hosts which will provide microenvironments with different KS compositions.

1.3. HYPOTHESIS

Keratan sulfate proteoglycans (KSPG) in the tumor microenvironment and extracellular matrix can regulate metastatic potential of breast and melanoma cells. Mutant zebrafish that lack CHST6 activity can be used to modulate sulfation status of KSPGs in zebrafish tissues, and metastatic behaviors of cancer cells can be studied in a xenograft model by changing the KS composition in the zebrafish host.

2. GENERAL INFORMATION

2.1. CANCER AND INITIATION OF METASTASIS

Cancer is one of the leading causes of death, killing nearly 10 million people - one in six - by 2020 alone. (Ferlay et al., 2021). The loss of cellular regulatory mechanisms caused by genetic changes that lead to uncontrolled cell division, leading in either benign or malignant neoplasms, is the significant marker that characterizes all cancers. Several common characteristic features, referred to as hallmarks of cancer, were first described by Hanahan and Weinberg (Hanahan & Weinberg, 2011) The hallmarks of cancer have been proposed as a master plan to guide research efforts aimed at understanding the core characteristics of cancer and deriving treatments for this extraordinarily complex disease (Meirson et al., 2020).

Initially, six characteristics were put forth: preservation of proliferative signaling, avoidance of growth inhibitors, facilitation of replicative immortality, facilitation of cell death, induction of angiogenesis, and activation of invasion and metastasis. These are now joined by four new enabling characteristics and hallmarks, including genomic instability and mutation, tumor promoting inflammation, metabolic reprogramming, and tolerance to immune destruction (Jayatilleke & Hulett, 2020). In his research, Lazebnik pointed out that five of the six original characteristics, except for invasion and metastasis, are common to benign and malignant tumors (Lazebnik, 2010). Invasion and metastasis, on the other hand, are not typical of benign diseases, with very few exceptions. The term "cancer" is used to describe a broad spectrum of genetically unique disorders characterized by cell cycle dysregulation, which results in unchecked cell proliferation and the development of primary tumors. These abnormal cells develop traits that improve their capacity to penetrate the bloodstream, disperse, and reach further regions where they can grow into secondary tumors. The primary cause of cancer-related incidence and death is this occurrence, also known as metastasis. (Cabezas-Sáinz et al., 2020).

Briefly, to gain the ability to exit the primary tumor and become intravascular, cells undergo complex transcriptional reprogramming and alter their morphology through a process known as the epithelial-mesenchymal transition (EMT). The intravasation of tumor cells into blood or lymphatic arteries and their associated translocation through the vasculature are thought to need EMT as a critical precursor step. Cells that reach a secondary target tissue extravasate and undergo the reverse transition (Mesenchymal-Epithelial Transition, MET), resulting in micro metastasis and eventually secondary tumors. (Cabezas-Sáinz et al., 2020). Both intrinsic and external factors influence this complicated process. The extracellular matrix, a noncellular component of tissues, is a significant extrinsic impact.

In the tumor microenvironment tumor cells can transform normal fibroblasts into cancer-associated fibroblasts (CAFs) to proliferate more vigorously (Dituri et al., 2022). This relationship between tumor cells and fibroblasts creates a positive feedback loop that ensures rapid progression of cancer. Type I and III fibrillar collagen as well as non-collagen glycoproteins such fibronectin, laminin, hyaluronate, elastin, and proteoglycans are synthesized by CAFs and released into the ECM (Bataller & Brenner, 2005). In both healthy and pathological conditions, such as hepatocellular carcinoma, where stromal cells, primarily cancer-associated fibroblasts release of extracellular matrix (ECM) proteins, including proteoglycans. For example, Versican and biglycan expression is overexpressed by TGF- β in cells of mesenchymal origin (Cross et al., 2005; Heegaard et al., 2004). In response to TGF-β, CAFs of ovarian cancer can release versican (Yeung et al., 2013). Furthermore, it was discovered that after being exposed to TGF- β, HCC CAFs expressed more versican mRNA (Bataller & Brenner, 2005).

In this thesis, the effects of keratan sulfate proteoglycans in the extracellular matrix to the metastasis of cancer cells will be addressed. Therefore, the composition of extracellular matrix and types of proteoglycans involved are introduced in the following sections.

2.2. EXTRACELLULAR MATRIX

The extracellular matrix (ECM) is a complex structure containing several macromolecules such as structural proteins, glycoproteins, and proteoglycans, providing the physical scaffolds necessary to maintain tissue integrity as well as the biochemical signals necessary to regulate the functions of cells.

The extracellular matrix is one of the core components of tissues and organs in all living organisms and is essential for the existence of multicellular organisms. It regulates and stabilizes all cellular processes in the organism from the earliest stages of organismal development to the death (Winkler et al., 2020). Constitutively altered genetic ECM (Vigetti et al., 2014) as well as both activation and inhibition modifications of degrading enzymes may be key factors promoting or restricting cancer growth and migration. In the cancerous tumor microenvironment, the extracellular matrix is altered at biochemical, structural, and topographical levels. Studies that suggest the significance of extracellular matrix in solid tumors have proliferated significantly over the past decade. The extracellular matrix is now emerging as a target for inhibition cancer progression mediated by interactions between tumor cells and their microenvironment (Belli et al., 2018; He et al., 2021; Huang et al., 2021)

Basement membrane (BM) and Interstitial Matrix (IM) are the two primary forms of extracellular matrix. Type IV collagen, which is present in enormous amounts, and PGs such laminin and perlecan build up the Basement Membrane (Xiong & Xu, 2016). The basement membrane is in close contact with cells, holding epithelial and endothelial cells together to support them and protect them from disintegration (Madsen and Bugge, 2015). The interstitial matrix is composed of collagen I and III also the proteoglycans such as fibronectin, which surround the cells and support the stromal compartment (Theocharis et al., 2016). Fibroblasts, vasculature, and lymphatics are embedded in the interstitial matrix (Mecham, 2012).

The basement membrane acts as a barrier to prevent cancer cells from invading and extravasating, especially in epithelial cancer types. During cancer progression, the basement membrane is invaded by forcing through its pores. In addition, during angiogenesis, basement membrane matrix is synthesized to strengthen the durability

of vessels. As matrix density and stiffness increase, vascularization decreases, cell-cell interaction decreases, and consequently barrier integrity is compromised, resulting in leaky vascular (Huang et al., 2021).

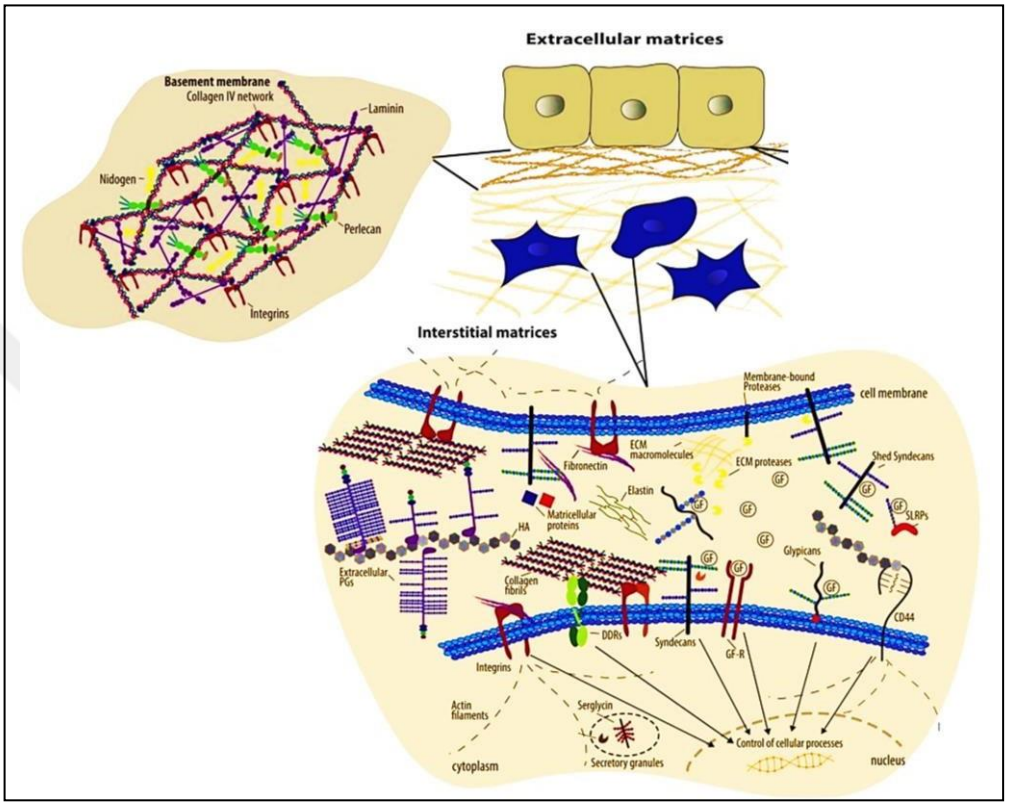

Figure 1 Schematic representation of extracellular matrix with their components. The extracellular matrix composed of Basement membrane and interstitial membrane. Adapted from (Theocharis et al., 2016)

The ECM contains three main types of macromolecules:

1. Structural proteins: collagens and elastins

2. Adhesion proteins: fibronectin, laminin, tenascin

3. Proteoglycans (PG): Biglycan, aggrecan, versican, perlecan, KSPG, HSPG, CSPG, Hyaluronan (Frantz et al., 2010).

Structure and roles of the ECM is maintained by interactions of its components. Collagen constitutes 90% of the extracellular matrix, with 28 distinct types identified to date (Burgeson & Nimni, 1992). Collagens are in direct interaction with proteoglycans in the extracellular matrix. Collagens together with proteoglycans regulate cellular signals by interacting with cell surface receptors in various signaling pathways. In cases where the extracellular matrix is remodeled, such as in tumor formation, the synthesis and structure of collagens change. Excess collagen accumulation in tumor microenvironment, not only disturbs tissue integrity but also stiffens the ECM which in turn enhances malignant tumor development (Oxford et al., 2019a).

Another key part of ECM are fibronectins. Fibronectins bind to collagens, proteoglycans, fibrils, and cell surface adhesion molecules. Even though are not as abundant in the extracellular matrix as collagens, they are incredibly important in intracellular signal transduction. Thanks to the presence of abundant arginine-glycine-aspargine (RGD) sequences, they recognize and bind to integrins in the cell membrane (Oxford et al., 2019b).

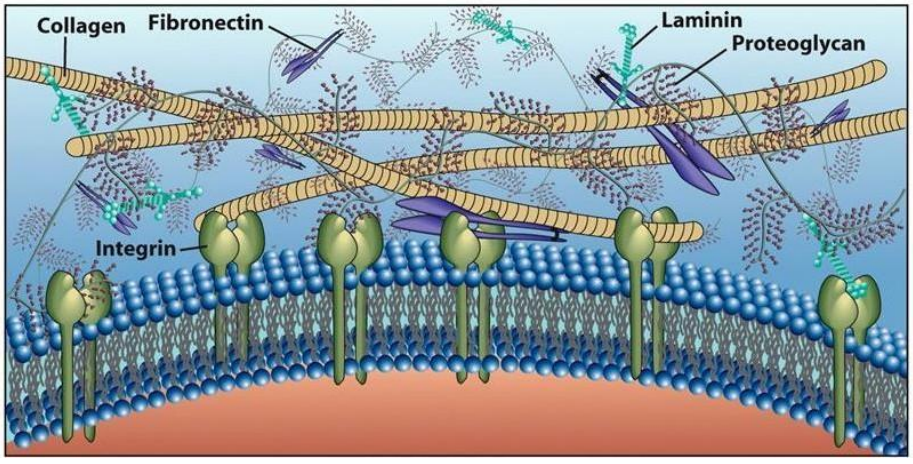

Figure 2 Illustration of components of extracellular matrix: collagens, integrins, fibronectins and proteoglycans. Adapted from Jhon Wiley and Sons, 2007.

Proteoglycans (PG) are second most abundant macromolecules of ECM, after collagens. As in collagens PGs is also a large family that contains various core proteins associated with different glycosaminoglycan (GAG) side chains including, keratan sulfates. Proteoglycans regulate the structure of ECM in tissues such as cornea and skeletal tissues both by hydrating tissues due to their negative charge, and by binding to collagens and other proteins that are important for ECM regulation (Soares Da Costa et

al., 2017a). Proteoglycans interact with various growth factors, cytokines and chemokines, cell surface receptors and many ECM molecules via both the glycosaminoglycans (GAGs) and the core proteins.

The structure and types of PGs as well as their importance in cancer metastasis is discussed further in the following sections.

2.3. STRUCTURAL PROPERTIES OF PROTEOGLYCANS (PGs)

PGs are complex molecules in which glycosaminoglycan (GAG) chains are covalently linked to a protein core, and they are a rather large family, divided into several subclasses as shown in detail in Figure 3. Approximately 45 PGs have been found to date, with each of the PG elements showing considerable variability.
PGs are classified according to several criteria:

I) Cellular and Subcellular Location:

- There are extracellular PGs that are embedded in ECM. In total, ECM-associated PGs consist of 25 members: 4 hyalectans, which participate in the major structural components of cartilage, blood vessels and the central nervous system; 18 small leucine-rich proteoglycans (SLRPs) which are help stabilize and regulate collagen fibers. SLRPs also have other roles in the regulation of innate immunity and growth factor signaling (Ajit Varki et al., 2022) and 3 calcium-binding HSPG testicans (Iozzo & Schaefer, 2015).
- Pericellular PGs that are heparan sulfate (HS)-charged perlecan and agrin, together with collagen, are participating in the formation of basement membranes.
- Cell surface PGs syndecans and glycans are loaded with HS. While syndecans play important roles in growth factor and growth factor receptor signaling (Afratis et al., 2017) glycans participate in regulating key cellular signaling pathways such as Hedgehog signaling (Filmus & Capurro, 2014) and Wnt signaling (Pez et al., 2013).
- The only intracellular PG, serglycin (Kolset & Tveit, 2008) is mostly known for its role in inflammatory responses.

II) -General gene/protein homology,

III) Their core proteins (Nikitovic et al., 2018).

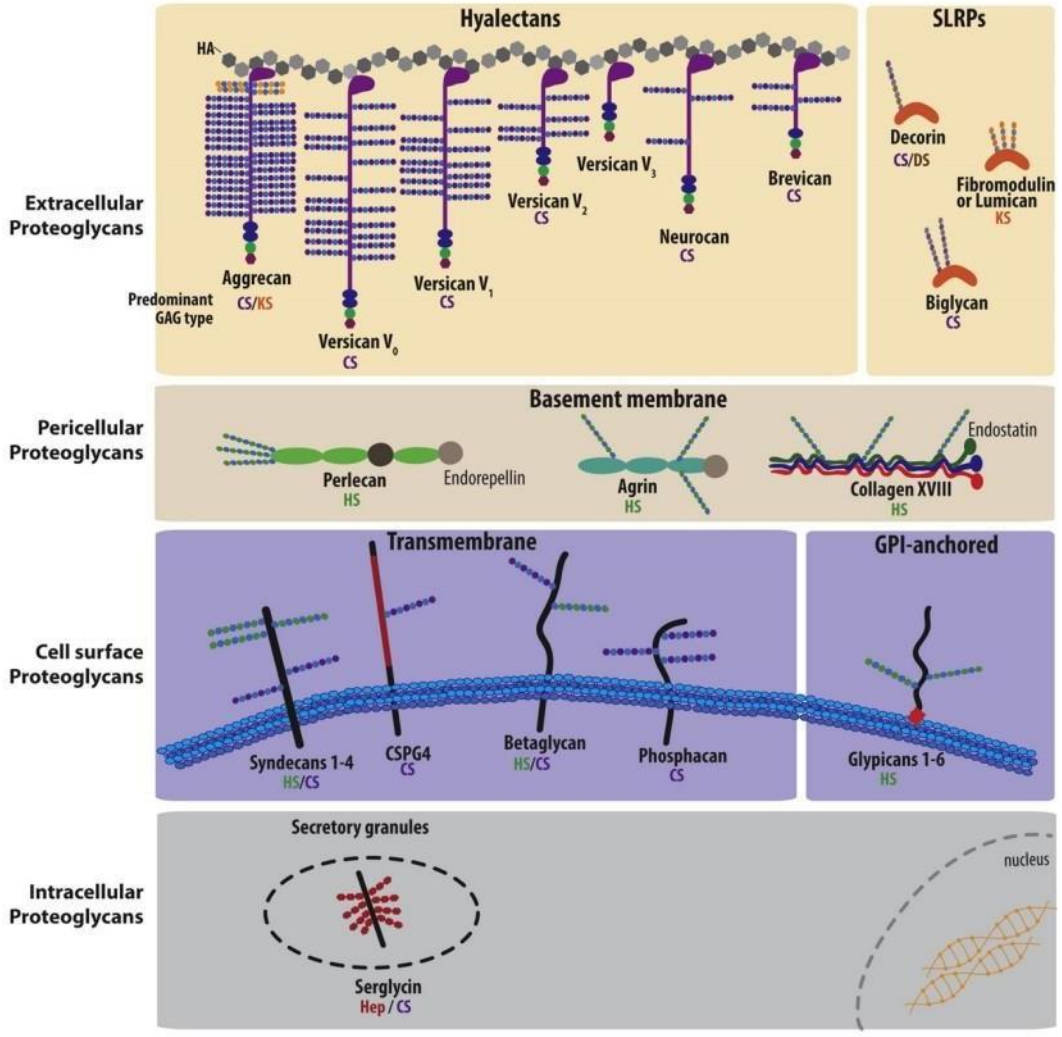

Figure 3 An exhaustive classification of proteoglycans. Adapted from: (Theocharis et al., 2016)

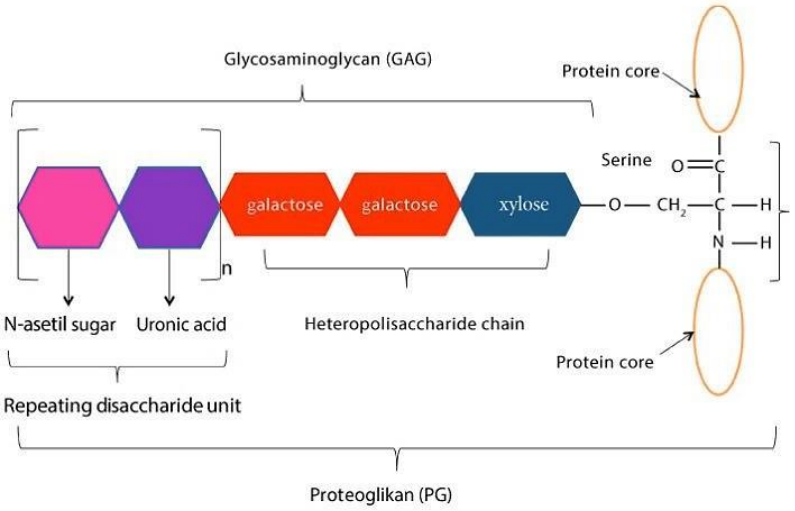

Figure 3 Basic structural illustration of Proteoglycans. Adapted from (Derya et al., 2014)

Structurally, GAGs are linear carbohydrate molecules that contains disaccharide repeats of sugars, amino sugars (a sugar molecule in which the OH group is replaced with an NH_2 group) and sugar acids. The disaccharide repeats of a GAG chain contains one amino sugar + a sugar acid or amino sugar + galactose.

These amino sugars are:

- N-acetylated Glucosamine [GlcNAc]
- N-sulfated Glucosamine [GlcNS] or
- N -acetylgalactosamine [GalNAc].

Sugar acids are:

- iduronic acid [IdoA]
- glucuronic acid [GlcA]

In addition, the stem of the disaccharide repeat contains sugars (Xylose, Galactose or D-Mannose) and/or glucosamines. The GAG chains are linked to the core protein by covalent binding of this stem to a Serine, Asparagine or Thereonine of the core protein (Figure 3).

GAGs are divided into four families based on their chemical composition (Esko et al.,2009):

- Heparin/heparan Sulfate (HS),
- Chondroitin/Dermatan Sulfate (CS/ DS),
- Keratan Sulfate (KS) and
- Hyaluronic Acid (HA).

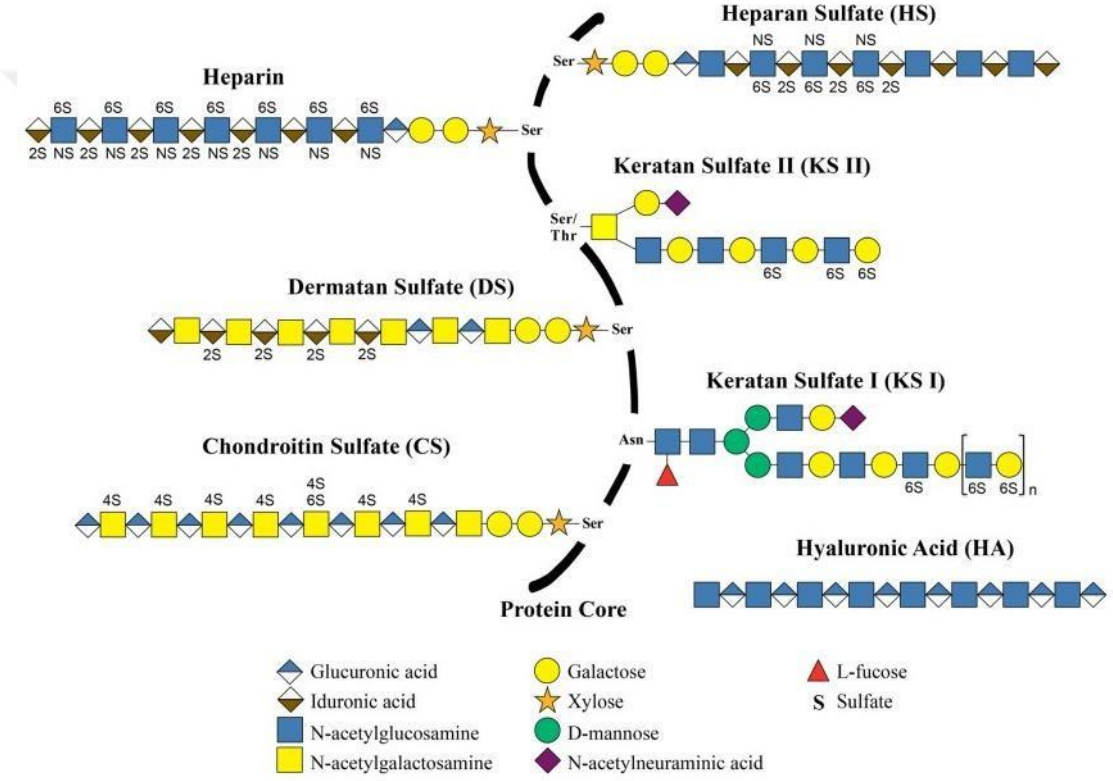

Figure 4 Illustration of glycosaminoglycans chains. Adapted from: (Merida-De-Barros et al., 2018)

Among them, KSPGs are a notable PG group, and there are few studies suggesting a role for some of their members in cancer development. Moreover, there are genetic diseases that point to the importance of their role in the ECM. This thesis aims to investigate the effects of changing Keratan Sulfate composition in the ECM.

2.4. KERATAN SULFATE PROTEOGLYCANS

Keratan sulfate is characterized with galactose (Gal)-N-Acetylated glucosamine (GlcNac) disaccharide repeats in the GAG chain. KSs are found as an N-linked or O-linked chain in a subset of proteins. Sulfation is an important modification and keratan sulfate chains contains of a mixture of unsulfated (Galβ4GlcNAcβ3), monosulfated (Galβ4GlcNAc6Sβ3) and disulfated (Gal6Sβ4GlcNAc6Sβ3) disaccharide units.

There are three types of keratan sulfate according to the differences in the stem of the GAG chain and their linkage to the core protein (Soares Da Costa et al., 2017b).

- **KS I**: Has a stem region that contains 2 GlcNac, 1 fucrose and 3 mannose residues, which is linked to the core the protein via an asparagine residue. The KSI is first described in cornea.
- **KS II**: Has a GalNac in the stem region that links the disacchraide chain to a serine or threonine of the core protein. The KS II is found mainly in skeletal tissues.
- **KS-III**: Has a mannose residue in the stem region that links the disaccharide chain to a serine of the core protein. The KS III is found in brain.

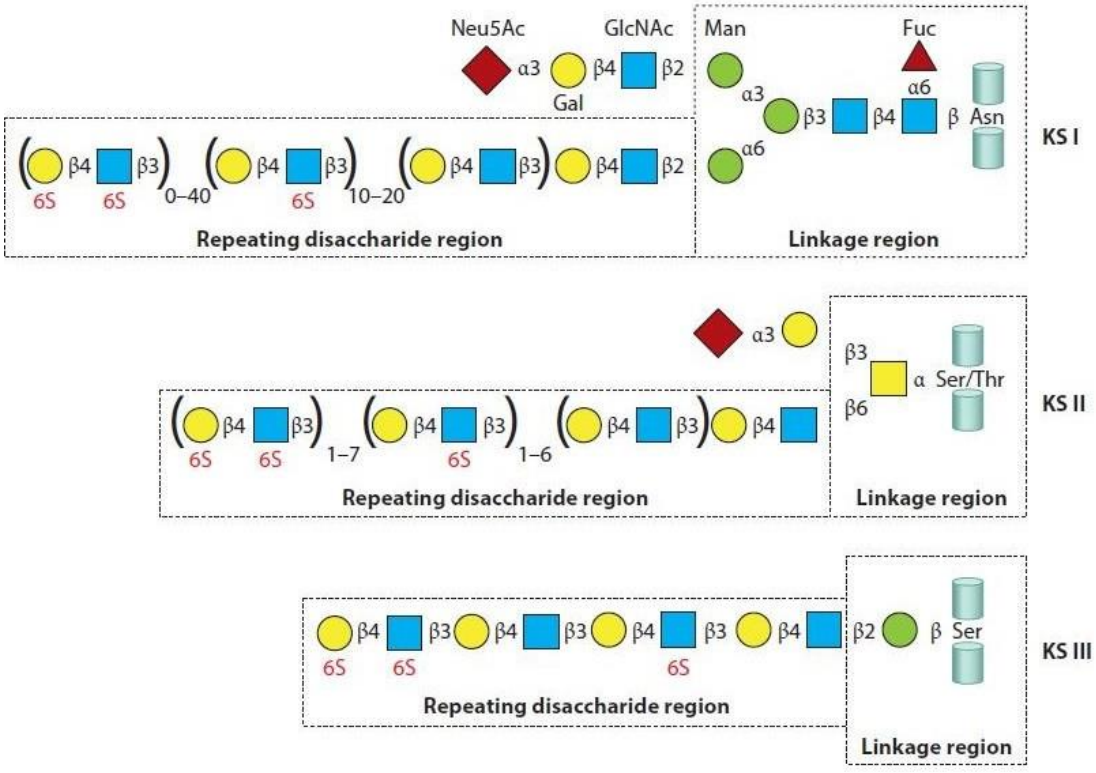

Figure 5 Structure of Keratan Sulfate with disaccharide repeat and types of Keratan Sulfate and their core proteins. Adapted from: (Soares Da Costa et al., 2017).

Keratan Sulfate I was first described in keratocan which is a proteoglycan encoded by KERA gene. The most common form of KS I, has been detected in the cornea in association with lumican and mimecan. It has also been observed on fibromodulin and osteoadherin proteins in cartilage. Known defects in KS I proteoglycan formation are associated with ocular dysfunction. The defective sulfation of keratan sulfates causes macular corneal dystrophy and defects in keratan sulfate chain formation result in keratoconus (Caterson & Melrose, 2018).

Lumican and Keratocan are the main core proteins of KSPGs, and they are members of the small leucine-rich repeat proteins. The importance of these KSPGs in ECM organization is exemplified by their regulation of collagen fibril organization in cornea (Ajit Varki et al., 2022 & Sifaki et al., 2006) . Aggrecan is a hyalectan and its major GAGs are CS, however it also carries Keratan Sulfate chains. In an adult cartilage there are 100 CS chains and about 25-50 KS chains. These glycosaminoglycan chains account for about 90% of the molecule. Aggrecan acts as a gap filler and water retainer, especially in cartilage tissues (Kiani et al. 2002).

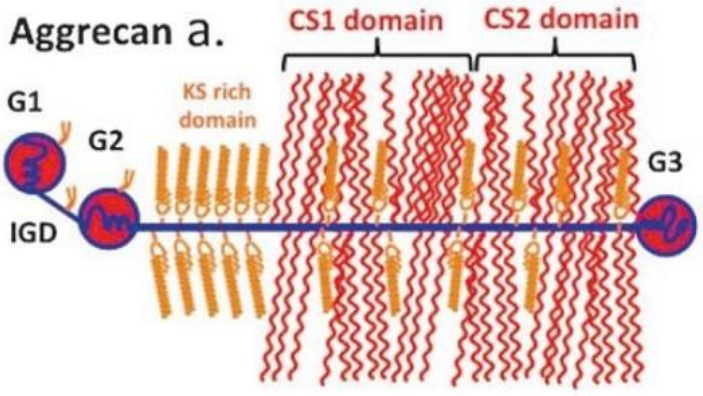

Figure 6 Illustration of glycosaminoglycans chains: KS and CS chains of Aggrecan. Adapted from: (Caterson and Melrose 2018).

2.5. SULFATION OF GLYCOSAMINOGLYCANS

The biological roles of proteoglycans are highly regulated by their associated GAGs. The monosaccharides of the GAGs, the length of the disaccharide chains, the nature of bonds between these are all key factors. A major regulation of PG function is the sulfation of GAG chains, which is a determinant of the negative charge and water holding capacity of GAGs. Changes that occur during glycan synthesis may play a role

in the development of diseases. Understanding these changes can improve disease diagnosis and/or treatments. Altered glycosylation is also a common feature of cancer cells and specific glycans are recognized as markers of tumor development. While most glycosaminoglycans contain sulfates in various positions, hyaluronan lacks sulfate groups. Heparan sulfate and heparins are sulfated from their N-acetylglucosamine residues. Sulfation of chondroitin sulfates is carried out at the C-2 position of uronic acid residues and at the C-4 and/or C-6 positions of GalNAc residues. The sulfation of dermatan sulfates is conducted at the C-2 position of iduronic acid residues and at the C-4 and/or C-6 positions of GalNAc residues. Keratan sulfates, on the other hand, do not contain uronic acid but are composed of sulfated galactose and N-acetylglucosamine residues.

Carbohydrate sulfotransferases are essential in the synthesis of glycosaminoglycans. Sulfotransferases are a major group of enzymes produced both in the cytoplasm and in the Golgi. All sulfotransferases utilize 3′-phospho-adenosine-5′-phosphosulfate (PAPS) as a sulfate donor. While sequence similarity between sulfotransferases is remarkably weak, the sequence motifs necessary for binding the 5′ and 3′ phosphate groups of PAPS are preserved in all of them. Sulfation reactions are conducted by carbohydrate sulfotransferase enzymes. There are 15 different CHST genes in the human genome. Dysregulation or dysfunction of some of these genes can lead to genetic diseases.

CHST3-Related Skeletal Dysplasia: Skeletal dysplasia, also known as Larsen syndrome, is associated with the CHST-3 gene. In studies conducted in patients, it has been found that the ratio of 6-O-sulfated disaccharide units is significantly decreased and there is an increase in nonsulfated proteins.

Noninflammatory Peeling Skin Syndrome: Although the exact cause is unknown, recent studies suggest a link with mutations in CHST8, which alters the hydrophilicity of amino acids. In addition, it has been observed that the amount of total sulfated GAG is reduced in mutants in which GalNAc4ST1 proteins are dysfunctionalized (Soares Da Costa et al., 2017).

Ehlers–Danlos Syndrome, Musculocontractural Type 1: It is also known as Dundar syndrome. Patients with EDS have highly elastic (supple) and fragile, soft skin. Patients have mutations in several genes that regulate collagen structure. Recently, EDS has been linked to mutations in the CHST14 gene.

Macular Corneal Dystrophy: Mutations in the CHST6 gene that cause disruption in the KS sulfation pattern led to Macular Corneal Dystrophy, in which the fibril organization of the cornea is disrupted and causes the corneal opacity. CHST6 encoded N-acetylglucosaminyl-6-sulfotransferase sulfates GlcNAc residues at the 6th carbon, during the synthesis of the KS chain. The sulfation of the the next Gal residue is dependent on sulfation of the GlcNAc. Sulfation in keratan sulfates is catalyzed by the enzyme encoded by the carbohydrate sulfotransferase 6 (CHST6) gene, originally called corneal (Faria-Ramos et al., 2021; Funderburgh, 2002).

Many enzymes responsible for GAG sulfation are changed in malignant cells. Alterations in the CS 4-O-sulfotransferases expression have been described in both ovarian and breast cancers, while cancerous lung tissues exhibit increased 6-O-sulfated CS when compared to non-cancerous tissues. Likewise, enhanced levels of 6-O-sulfotransferases have been observed in ovarian and colorectal cancers, and increased levels of 3-O-sulfotransferases in breast and pancreatic cancers. (Ajit Varki et al., 2022). However, the effect of ECM GAGs and proteoglycans is largely unknown.

Disease	GAG	Consequence of
Interstitial cystitis	**CS**	Defective addition of sulfate residues
Macular Corneal dystrophy	**KS**	Defective GAG synthesis
Alzheimer disease	**HS*** **CS** **DS***	Abnormal control of HS *O*-sulfotransferases
Gastric cancer	**6S-CS**	Increased activity of chondroitin sulfate 6-*O*-sulfotransferase
Laryngeal squamous cancer	**4S-DS** **CS**	Low expression of CHST3 and D4ST1
Breast cancer	**HS** **CS**	Underexpression of 3-*O*-sulfotransferase; High heparanase expression levels and activity
Brain cancer (Glioblastoma)	**HS**	Upregulation of HS3ST3a1 and downregulation of 6-*O*-sulfotransferases 1-3
Prostate cancer	**CS** **HS**	Overexpression of 2-*O*-sulfotransferases
Ovarian cancer	**CS** **HS**	Increased expression of GalNAc4S-6ST Up-regulation of 6-O-sulfotransferase 2 Irregular expression of CHST3 and D4ST1
Colorectal cancer	**CS** **HS** **CS/DS**	
Pancreatic cancer	**CS**	
Lewis lung cancer	**CS** **HS**	

Table 1 Disease related with abnormal GAG sulfation.

Adapted from: (Soares Da Costa et al., 2017b)

Alterations of glycans, such as loss of expression or over-expression of certain glycans, increased levels proteoglycans with truncated glycans or those lacking the glycans, are seen in malignant cells. Recently it was proposed that, alterations in the sulfation of glycosaminoglycans may guide diagnostic and therapeutic approaches for cancer. (Afratis et al., 2017).The content and distribution of many proteoglycans change during tumorigenesis and HS chains have been implicated in tumor pathogenesis. HS chains are covalently linked to syndecans, glycans and perlecans. Syndecan-1 is an HS which has been shown to accumulate in the tumor microenvironment and induce activation of both chemokine and growth factor signaling (Afratis et al., 2017). Of particular importance is the finding that Syndecan-1 ectodomains promote metastasis to bone tissue in breast and prostate carcinoma (Faria-Ramos et al., 2021).

There are studies indicating importance of the sulfation of chondroitin sulfates and keratan sulfates in cancer (Crusio et al., 2018). The proteoglycans that have been implicated in tumor progression are listed below:

- **Decorin** is a CS/DSPG. Decorin is present in significant amounts in the healthy mammary gland, whereas its expression is reduced in breast cancer (Theocharis et al., 2010). Decorin was shown to be a metastasis suppressor in a breast tumor (Neill et al., 2012).

- **Biglycan** is a CS/DSPG. It is highly abundant in the dermis and other connective tissues. Biglycan and decorin can bind to TGF-β and inhibit its activity in vitro (Kolb et al., 2001). Some studies have shown significantly higher biglycan expression in endometrial, pancreatic and colon tumor tissues (Iozzo & Sanderson, 2011).

- **Fibromodulin** is a KSPG which regulates collagen fibrillogenesis by interacting with type I and II collagens (Iozzo & Schaefer, 2015). In solid tumors, fibromodulin accumulation has been observed supporting the formation of a dense stroma ((Dituri et al., 2022)).

- **Lumican** is a leucine rich KSPG that is mainly found in mesenchymal tissues and tumor stroma (Iozzo & Schaefer, 2015). Lumican is highly expressed in breast cancer and melanoma (Sifaki et al., 2006). In breast cancer, lumican accumulation in their stromal tissues is correlated with high cancer grade, decreased estrogen levels and younger age (Leygue et al., 2000). Furthermore, in a mouse model of metastatic breast cancer, exogenous expression of lumican reduced both primary tumor growth and lung metastasis (Sharma et al., 2013). According to these findings lumican may act as a tumor suppressor in breast cancer; however, further cellular and molecular studies are needed to establish its role.

2.6. CHST6: CARBOHYDRATE SULFOTRANSFERASE -6

The human CHST6 (OMIM 605294) gene is located on chromosome 16, includes 3 exons. The product of gene is a 395 amino acid protein with a molecular weight of 44 kDa (Zhang et al.,2019). CHST6 encodes the corneal N-acetylglucosamine-6-O-sulfotransferase (C-GlcNAc6ST) enzyme, which is a transmembrane sulfotransferase localized in the Golgi of keratocytes. C-GlcNAc6ST performs the first sulfation step in keratan sulfate biosynthesis by binding sulfate groups to carbon 6 of N-Acetylglucosamine (GlcNAc) in the disaccharide chain of proteoglycans (Funderburgh, 2000). As mentioned, Chapter 2.4. The enzyme GlcNAc6ST (N-acetylglucosamine-6-O-sulfotransferase) sulfate keratan sulfates into Galactose and Glucosamine, respectively. GlcNAc6ST only works during chain formation as it can transfer sulfate to the terminal N-acetylglucosamine. Reduced GlcNAc sulfation leads to reduced or lost Gal sulfation (Funderburgh, 2000). Thus, GlcNAc6ST enzyme function greatly influences the total sulfate content of KSPGs. Mutations seen in MCD patients have been shown to negatively affect CHST6 protein function and lead to non-sulfation or under-sulfation of keratan sulfate proteoglycans (Niel et al., 2003).

2.7. ZEBRAFISH AS A MODEL ORGANISM

Zebrafish is a small vertebrate model, preferred for its ease of genetic modifications, transparency during preliminary stages that facilitates for imaging, ease of manipulations and high fecundity. Oocytes are fertilized ex utero, which makes the zygote accessible for microinjections and allows for easier production of transgenics or mutants. Moreover, embryos reach adulthood in a short period of 3 months and can be produced at lower cost in the laboratory environment compared to models. Although zebrafish came to the forefront in the 1980s with its suitability for developmental biology research, today it is used in different fields such as toxicology, drug efficacy testing, metabolism, neuroscience and cancer biology (Haldi et al., 2006; Patton et al., 2005; White et al., 2013) . Despite some physiological differences, many biological processes and tissue functions are conserved in zebrafish.

The initial genetic mutation scans were performed in 1992-93, and first draft of the genome sequence of zebrafish was published at the beginning of the 21st century (Driever et al., 1996). Homology analyses showed that 70% of human genes and 82% of disease genes are represented in zebrafish genome (Howe et al., 2013). By expressing human genes in zebrafish or mutating zebrafish homologs of disease genes, it is possible to replicate disease phenotypes in fish and assess the effect of mutations (Michailidou et al., 2009; Poon et al., 2017; Santoriello and Zon, 2012). Another important advantage of zebrafish is its suitability for high-throughput screening, by adding drugs/inhibitors/chemicals to ambient water in 24-96-well plates during embryonic and larval stages. All these features make zebrafish a unique organism for disease modeling and therapeutic development. Pioneering researchers demonstrated the speed and effectiveness of the model, by discovering drug molecules in drug screening in the zebrafish model and started clinical phase studies in a record time of 36 months (van Rooijen et al., 2017; Zon, 2014).

These advantages of zebrafish also offer opportunities for modeling rare diseases, elucidating molecular mechanisms and drug trials.

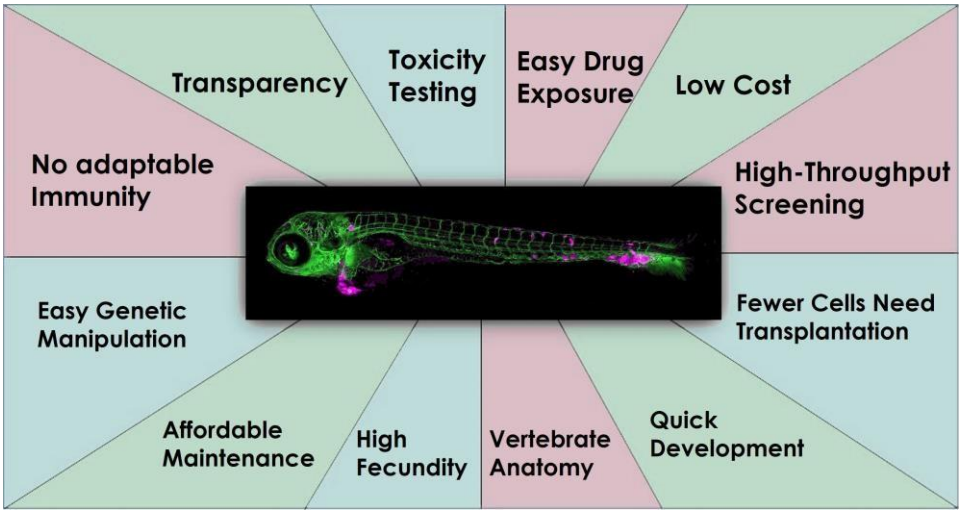

Figure 7 Diagram of advantages for using a zebrafish as a model.

Targeted Genome Editing in Zebrafish:

A new phase in zebrafish research has started with TILLING, TALEN, ZincFinger and finally CRISPR/Cas9 methods developed to create targeted gene mutations. These methods are based on the principle that base insertions and deletions occur during the repair of double-strand DNA breaks caused by nuclease directed to specific DNA sequences by the Non-Homologous End Joining (NHEJ) pathway. The first of these methods, Zinc Finger Nuclease, has been replaced by TALEN and CRISPR/Cas9 methods due to its difficulty of application and low efficiency. TALEN (Transcription activator like effector nuclease) consists of 33-35 amino acid repeats that recognize the target DNA sequence and FokI nuclease. To create DNA sequence-specific TALEN, TALE sequences need to be assembled modularly using the TALEN library (Zhang et al., 2016). The RNA which is produced by TALEN was injected into zebrafish embryo for the first time (Sander et al., 2011). Although this method has high DNA specificity and efficiency, it is not practical due to cloning difficulties and excessive cost. The CRISPR/Cas9 method is a simple system that required only 1 protein and guide RNA. The Cas9 enzyme, which forms a complex with the CRISPR-RNA heterodimer that binds to the complementary sequence in DNA, searches for the Protospacer Adjacent Motif (PAM) motif. When RNA binding is achieved next to the PAM motif, Cas9 is activated and cuts DNA ~3 nucleotides above the PAM sequence (Moreno-Mateos et al., 2015). With this system, targeted mutation is created with the designed single-stranded guide RNA (gRNA) and recombinant Cas9. gRNA consists of a skeletal sequence and 18-20 nt target-specific sequence and directs the Cas9 enzyme to the target sequence (Vejnar et al., 2016) To mutate in zebrafish by CRISPR/Cas9 method, gRNA(s) and Cas9 capped mRNA are microinjected into single-cell zebrafish embryos to mutate the target sequence(s). In the literature, it has been shown that different alleles of the same gene can be created, or multiple genes can be mutated simultaneously by injecting different gRNAs simultaneously (Jao et al., 2013; Ota et al., 2014). In 2013, a CRISPR/Cas system engineered for zebrafish was demonstrated to target the reporter gene in the transgenic line efficiently (Hwang et al., 2013). CRISPR/Cas9 method was preferred for mutation generation due to its high efficiency, low cost, and ease of application.

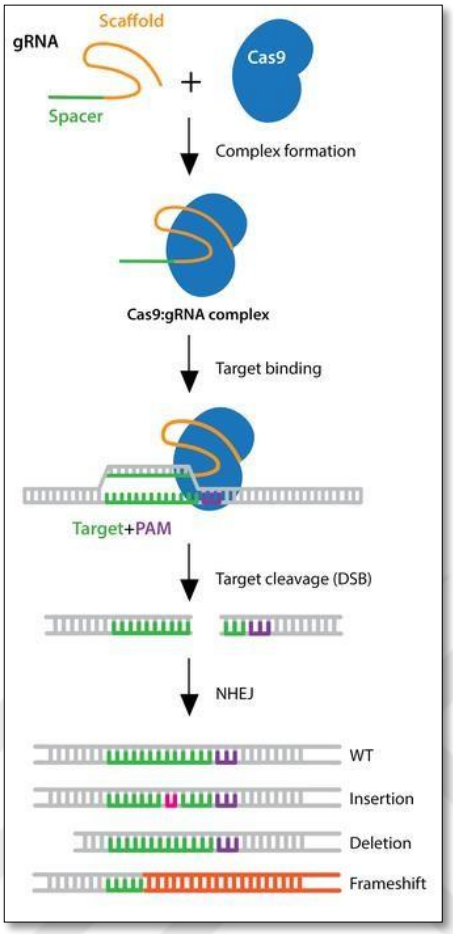

Figure 8 CRISPR Cas9 mediated genom editing Adapted from: addgene.org/guides/crispr/

Cancer Modeling in Zebrafish:

In in vitro platforms using cancer cell lines, the cells lose their biomarkers after a while in the culture environment, the effects of the cancer microenvironment and healthy stroma are ignored and therefore do not accurately reflect the in vivo response. In addition, the fact that mouse xenograft tumors created with these lines require weeks/months, technical difficulty and high cost are seen as disadvantages (Scott et al. 2013).

Due to such disadvantages, zebrafish cancer modeling has been preferred as a in vivo model in recent years (Chen et al., 2021). Cancer modeling in zebrafish has gained attention in last 2 decades (Chen et al., 2021). Cancer studies in zebrafish model began with the observation of spontaneous tumors that displayed histological and genetic

similarity human tumors (White et al., 2013). In addition, zebrafish transgenic cancer models can be developed by either tissue specific overexpression of human oncogenes or mutagenesis of zebrafish tumor suppressor or oncogenes (Li et al., 2013; Patton et al., 2005; Santoriello et al., 2010). Finally, avatar cancer models are generated via transplantation of human cancer cells into zebrafish by xenograft method which is mostly preferred for metastasis studies.

Xenograft models developed in the zebrafish model organism are in vivo models that have attracted attention in recent years with low cost and short response time. In this method, cancer cells injected into 48-hour larvae show cancer characteristics such as proliferation, metastasis, and vascularization. Since the adaptive immune system develops between days 14-28, it does not develop immune response to human cells injected before this period (Haldi et al. 2006). Cell transplantation was first performed by Langenau et al. in 2003 by zebrafish T cells were injected into adult zebrafish. Furthermore, the first xenograft using human melanoma cells was performed by Lee et al. in 2005. Since then, hundreds of xenograft studies with cell lines for many cancers such as melanoma, breast cancer, hepatocellular carcinoma have repeatedly proven the efficiency of the model (Gunes et al. 2018; Lu et al. 2017; Topel et al. 2020). (Costa et al. 2020; Konantz et al. 2012).

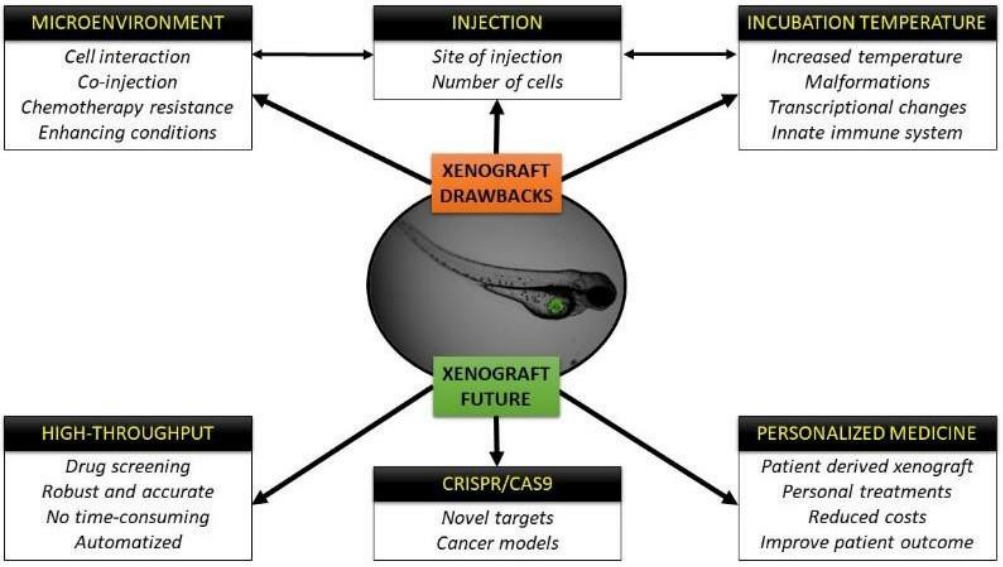

Figure 9 Schematic representation of the xenograft technique and future perspectives and fields of application Adapted from (Chen et al., 2021)

In this thesis, zebrafish chst6 mutants obtained by CRISPR method are used as hosts for xenograft with breast and melanoma cancer cell lines to study the metastatic properties of zebrafish larvae with mutated gene encoding carbohydrate sulfotransferase enzyme. Therefore, Keratan Sulfates in zebrafish are discussed below.

Keratan sulfate proteoglycans in zebrafish:

Several proteoglycans are reported, and some of the KSPGs including keratocan (zKera) and lumican (zLum) are shown to be expressed in zebrafish although no mutants have been generated to date (Hayes et al., 2013a; Yeh et al., 2008). Souza et al., showed that KS and CS glycosaminoglycans are the major sulfated GAGs found in adult zebrafish and KSs account for nearly 80 % of total GAGs in the whole body (Souza et al., 2007). Furthermore Hayes et al., showed that sulfated KSPG epitopes are found in brain, cartilage and notochord of zebrafish larvae (Figure 10) (Hayes et al., 2013a). Lumican is widely expressed in the body of zebrafish, especially in the cornea, bone and cartilage. Similarly, zebrafish keratocan (zKera) is expressed widely in the embryo, and in the cornea and brain.

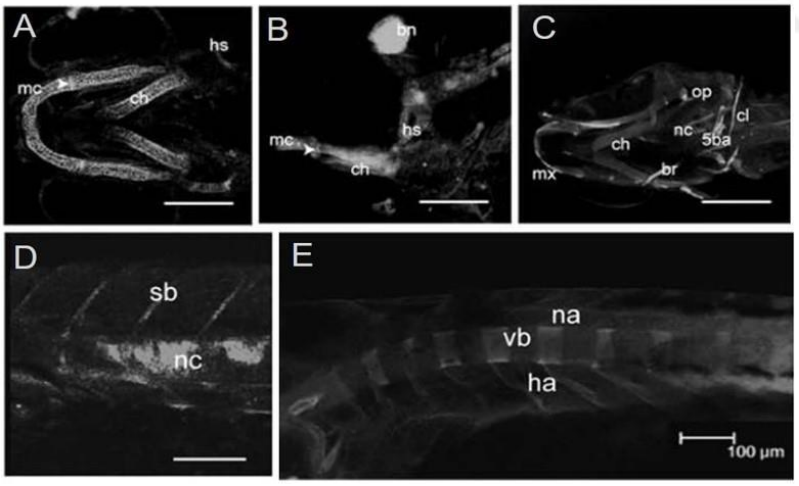

Figure 10 Distribution of cKS expression in 8 dpf zebrafish larva. A) jaw, B) lateral jaw, C) head, D) close-up view of end of the notochord E) notochord Adapted from: (Hayes et al., 2013a)

As mentioned above, sulfation of the proteoglycans is an important regulation. Carbohydrate transferase (CHST) encoded enzymes are responsible from GAG sulfation, and of the 15 human CHSTs 12 have orthologs in the zebrafish genome. Of these enzymes, chst1, chst2, chst4, chst5 and chst6 are responsible for sulfate transfer to KSPG (Soares Da Costa et al., 2017a).

The KS chains are sulfated in galactose and N-acetylated glucosamine at C-6 positions and these steps are catalyzed by Gal6ST and GlcNAc6ST enzymes, respectively. GlcNAc6ST enzymes are responsible for the first sulfation step of keratan sulfates, as this step is a prerequisite for Gal sulfation these enzymes are critical for KSPG structure and function (Uchimura and Muramatsu, 2002). ZFIN and UNIPROT databases show 3 zebrafish GlcNAc6ST enzymes (CHST2,6,7), of which CHST7 shows activity on chondroitin sulfates, while no information is available on CHST2 (Habicher et al., 2015). This suggests that CHST6 may be the major GlcNAc6ST enzyme in the zebrafish genome. The fact that CHST6 is expressed in the eye and other tissues from early embryonic stages suggests that it is important for keratan sulfate modification outside the cornea (Thesis, Merve Basol). There are studies showing that keratan sulfate proteoglycans have structural and regulatory roles in many processes such as development, cancer, and regeneration (Caterson & Melrose, 2018; Insua-Rodríguez & Oskarsson, 2016).

3. MATERIALS AND METHODS

3.1. TYPES OF RESEARCH

The type of research of this thesis study is experimental.

3.2. TIME AND PLACE OF RESEARCH:

All experiments were performed at Çakan Zebrafish Modelling Laboratory at Izmir Biomedicine and Genome Center between July 2020 and December 2022.

3.3. MATERIALS:

3.3.1. Laboratory Reagents

Common laboratory reagents and kits used for experimental procedures are given in Table 2 along with catalog number and company name information.

Table 2 List of laboratory reagents and chemicals used for experiments.

Product Name	Company	Catalog Number
10 000X Gelred	Biotium	41003
50X TAE	GeneMark	GB01-1
Agar bacteriological (agar no.1)	OXOID	LP0042
Agarose Basic	PanReac AppliChem	A8963,0250
Ampicilin sodium	Gold Bio	A30125
Biomax Agarose	Prona	HS-8000
CaCl2.2H2O	Carlo Erba	327607
Citric Acid Monohydrate	Emsure® Sigma aldrich	1.00244.1000
DEPC	PanReac AppliChem	A0881,0020
Ethanol	Emsure® Merck	1.00983.2500
Formamide	Merck	S4117
Glycerol 99%	Isolab	927.043.1000
Heparin	PanReac AppliChem	A3004,0001
Hidrogen Peroxide 35% (H_2O_2)	Isolab	932.122.2500
Magnesium chloride hexahydrate (MgCl2)	Emsure® Sigma Aldrich	1.05833.1000

Methanol	Merck	1060072500
MgSO4.7H2O	Sigma-Aldrich	M2773
NBT (Nitro Blue Tetrazolium)	CHEM IMPEX INT'L INC.	225
NBT/BCIP	Boehringer Mannheim GmbH	1697471
Normal Goat Serum	Vector Laboratories	S-1000
N-Phenylthiourea	Sigma-Aldrich	P7629-25G
Paraformaldehyde	Emprove® Merck	1.04005.1000
Phenol Red	Sigma-Aldrich	P0290-100ML
Potassium chloride (KCl)	Emsure® Merck	1.04936.1000
Potassium dihydrogen phosphate (KH_2PO_4)	Emsure® Merck	1.04873.1000
Potassium Hydrate (KOH)	Emsure® Merck	1.05033.1000
Sodium chloride (NaCl)	Emsure® Merck	1.06404.1000
Sodium Hydroxide (NaOH)	Merck	
Sodium phosphate dibasic dihydrate	Sigma-Aldrich	04272-1KG
Tricaine methanesulfonate	Sigma-Aldrich	E1052
Tris Base	Gold Bio	T-400-1
tri-Sodium Citrate dihydrate	Emsure® Sigma aldrich	1.064448.1000
Tryptone	OXOID	LP0042
Tween-20	Merck	8.22184.0500
Ulta Pure Water	KD Medical	REG-3410
Yeast extract	OXOID	LP0011
HCl	Isolab	932.106.2500
EDTA	Gold Bio	E-210-1
Isopropanol	Emprove® Merck	1.00995.2500
Bovine Serum Albumine	Gold Bio	A-420-100
Milli-Q water	KD Medical	RGE-3410
Methylene Blue	Merck	1592700010

3.3.2. Primers

Table 3. List of the primers used in experiments.

Primers	Sequence
CHST6 Genotyping Forward Primer	CCACTGCTAATGTCGTGATGTT
CHST6 Genotyping Reverse Primer - 1	CGCAGTGCTTTTTGCAGTCT
CHST6 Genotyping Reverse Primer - 2	AATGCACAAATGCCCCAGAA
CHST6 Start Codon Forward	ATGCTGCGCTGGAGAGTGT
CHST6 Sequencing Reverse	AATGCACAAATGCCCCAGAA
gRNA1 Specific Primer	taatacgactcactataGGTGACTCAGCCTGAGGGAAgttttagagctagaa
gRNA2 Specific Primer	taatacgactcactataGGTGAATACCTGGCCCAGGAgttttagagctagaa
gRNA3 Specific Primer	taatacgactcactataGGAGCCGTCGTGCTTTTGGGgttttagagctagaa
gRNA5 Specific Primer	taatacgactcactataGGGCTGGAGAGTGTCGAAGGgttttagagctagaa
gRNA Template Universal Primer	AAAAGCACCGACTCGGTGCCACTTTTTCAAGTTGATAACGGACTAGCCTT ATTTTAACTTGCTATTTCTAGCTCTAAAAC

3.3.3. Enzymes, Antibodies and Kits

Table 4 List of kits, enzymes and antibodies used for experiments.

Kits, Enzymes and Antibody	Company	Catalog Number
Keratan sulfate, ELISA Kit	MyBioSource	MBS288502
Pierce™ BCA Protein Assay Kit	Thermo Fisher Scientific	23225
NucleoSpinGel and PCR Clean-up Kit.	Macherey-Nagel	740609.50
Plus PCR Product Clean-up	GeneMark	DP04P-300
SP6 mMessage mMachine Transcription	Invitrogen	AM1340
TranscriptAid T7 High Yield Transcription	Thermo Fisher Scientific	KO441
VitaTaq PCR Kit	Procomcure Biotech	PCCSKU1003
DIG-RNA Labelling Mix. 10X Concentarion	Roche	11277073910
dNTPs	Thermo Fisher Scientific	LSG-R0192
EcoR I	Thermo Fisher Scientific	FD0278
NotI	Thermo Fisher Scientific	FD0598
Proteinase K	GoldBio	480-100
T7 Endonuclease I	New England Biolabs Inc.	MO302-L
Taq Polymerase	New England Biolabs Inc.	M0480L
Collagenase		
Chst6 Antibody (rabbit – polyclonal)	Novus Biologicals	NBPI 57928
Anti Col1A Antibody	Santa Cruz	Sc59772
Anti – Keratan Sulfate antibody	Merck	mab2022
beta-Actin Antibody (AC-15) (mouse – monoclonal)	Novus Biologicals	NB600-501SS
Anti-rabbit IgG (H+L) (DyLight 680 Conjugate)	Cell Signaling Technology	5366S
Anti-mouse IgG (H+L) (DyLight 800 4X PEG Conjugate)	Cell Signaling Technology	5257S

3.3.4. Laboratory Equipment

Table 5 List of the laboratory equipments.

Equipment	Company	Cat. No:/Model
-20°C Freezer	Bosch	GSN51AW30
28°C Incubator	Witeg	WiseCube
4°C Refrigerator	Bosch	KSV36AI31
Electrophoresis System	Major Science	M15-7-10-15
Fluorescence Microscope	Olympus Corporation	SZX2-ILLB
Fluorescence Source	Olympus Corporation	U-RFL-T
Electrophoresis Gel System	BioRad	Gel Doc™ XR + System
Shaking incubators	Thermo Fischer	88880020
Microcentrifuge	Thermo Scientific	MicroCL 17R
Microinjection Pump	World Precision Instruments Inc.	PV830
Micromanipulator	NARISHIGE	MN-151
NanoDrop	Thermo Scientific	2000
OD-Spectrophotometer	Implen	P330
PCR	Applied Biosystem	SimpliAmp Thermal Cycler
Sensitive Balance	Sartorius	32908543
Stereo Camera	Olympus Soft Imaging Solutions	SC50
SZX10 Stereo microscope with SC50 Camera	Olympus Corporation	SZX2-ILLB
SZX16 Stereo microscope equipped with XC50 camera	Olympus Corporation	
LSM 880 Confocal Laser Scanning Microscopy	Zeiss	
INCO 153 Incubator	Memmert	
SAFE 2020 Biological Safety Cabinet	Thermo Scientific	
Water bath	Nuve	NB9

3.3.5. Cell Culture Products

Table 6 List of the materials used in cell culture applications.

Product Name	Company	Catalog Number
RPMI Medium 1640 (1X)	Thermo Fisher Scientific	21875-034
Fetal Bovine Serum	Thermo Fisher Scientific	10500-064
0.05% Trypsin-EDTA (1X)	Thermo Fisher Scientific	25300-054
Penicillin/Streptomycin	Thermo Fisher Scientific	15140-122
Vybrant Dil cell-labeling solution	Invitrogen	V22885

3.3.6. General Solutions

Table 7 Recipe of 10X PBS Stock Solution

10X PBS (pH: 7.4) (1L)	
Component	**Amount (g)**
NaCl	80
KCl	2
$Na_2HPO4.2H_20$	17.8
KH_2PO_4	2.4
dH_2O	Complete to 1L and autoclave

Table 8 Recipe of 1X PBST Solution

0,1% Tween-20 in PBS (100 ml)	
Component	**Volume**
80% Tween-20	0,125
1X PBS	99,875

Table 9 Recipe of Tricaine Stock Solution

50 mg/ml Stock Tricaine (50 ml)	
Component	**Amount**
Tricaine	2.5 g
dH_20	50 ml

Table 10 Recipe of 60X E3 Medium Stock Solution

E3 Medium (60X) (1L)	
Component	**Amount**
NaCl	17.2 g
KCl	0.76
CaCl2.2H2O	2.9 g
MgSO4.7H2O	4.9 g
dH_20	Complete to 1L and autoclave

Table 11 Recipe of %2 Agarose Gel

2% Agarose	
Component	**Volume**
Agarose	1 g
1X TAE	Complete to 50 ml

Table 12 Recipe of %4 PFA Solution

4% PFA (pH: 7.5) (100 ml)	
Component	**Amount**
PFA	4 g
1X PBS	Complete to 100 ml

3.4. TOOLS FOR DATA COLLECTION

3.4.1. Design and Production of gRNAs and Cas9 mRNAs

For design and the protocol published by Vejnar et al was followed. In summary gRNA sequences were designed with the CRISPRScan web tool, and a template DNA was generated by PCR using a gene-specific gRNA oligo and a universal oligo for each guide RNA based on. (Moreno-Mateos et al., 2015; Vejnar et al., 2016). The template DNA was used for synthesis of gRNA by in vitro transcription. Design of gRNAs were explained in Results chapter of in this thesis and the thesis of Merve BAŞOL, named "Generation of Chst6 Zebrafish Mutants Via Crispr/Cas9 System, And Phenotypic Analysis of Mutants".

For generating the template DNA, 10 pmol of specific oligonucleotide and 10 pmol of universal oligonucleotide were used for PCR with Taq polymerase in 50 µl volume. After PCR, samples were run on 2.5% agarose gel and visualized. The targeted 117 bp long template DNA was produced for each gRNA separately. The resulting template DNA was purified with a PCR Product Clean-Up Kit. Using 130 ng of template DNA, gRNA was synthesized with T7 in vitro transcription (IVT) kit at 37°C for 2 hours. To isolate the gRNA 0.8VEtOH and 75mM Sodium acetate (pH5.2) was added and incubated at -80°C for 1 hour gRNA was precipitated at 16,000xg for 10 min and washed with 70 % ethanol. RNA samples dissolved in 50 µl ultrapure water were visualized on agarose gel and their concentration was measured with a spectrophotometer (Nanodrop2000, Thermo Scientific). It was aliquoted at a concentration of 100 ng/µl and stored at -80°C.

Cas9 mRNA was also produced by in vitro transcription method. For this purpose, two different plasmids 1) PCS2_nlsCas9nls (Addgene, #47929) containing the zebrafish codon-optimized Cas9 with 2 nuclear-localization signals, and 2) pCS2:nlsCas9nls_nanos3'UTR (Addgene, #62542) plasmid that encodes Cas9 fused to the nanos gene 3'UTR sequence, that directs localization of mRNA to the nuclei of germ cells (Jao et al., 2013; Moreno-Mateos et al., 2015). Plasmids were produced in DH5-α E. coli strain and confirmed by control digestion with EcoRI after isolation. The

plasmids were linearized with NotI enzyme, isolated from the gel, and capped mRNA synthesis was performed with SP6 mMessage mMachine RNA synthesis kit. Produced RNA was checked on the gel for integrity and, after measuring its concentration, it was aliquoted at 500 ng/µl concentration and stored at – 80ºC.

3.4.2. Microinjection

To generate the mutant fish, single cell embryos from wildtype type AB+/+ fish were injected with a mixture of gRNA and Cas9 mRNA by microinjection system. First, 100 ng of each gRNA, 250-500 ng Cas9 mRNA and 0.05 % phenol red solution were mixed in water and 5 µl injection solution was prepared. Single-cell embryos were injected in a volume of approximately 1-5 nl. After the post-injection mutation yield analysis was performed, the injection was repeated if necessary.

3.4.3. Preparation Of DNA Lysates

To figure out the injection efficiency, DNA was prepared from pools of 5-8 24-hour embryos. Total of 3 pools (15-24 embryos) were analyzed. For this purpose, the embryos were placed in PCR tubes and the ambient water on them was completely removed. By adding 10 µl of 50 mM NaOH per embryo, lysis was performed at 95 °C for 30 minutes, and at the end of incubation, 10 µl of 100 mM Tris-HCl (pH: 8.0) per embryo was added to the tubes.

For extraction of DNA from adult fish fin, the ¼ of fin was cut with sterile razor blade when fish under anesthesia. Tissue was placed in a PCR tube and 50 µl of 50mM NaOH was added and incubated at 95°C for 30 minutes, and at the end of the incubation 50 µl of 100 mM Tris-HCl was added to the tube.

3.4.4. Mutation analyses from Genomic DNA

Genomic DNA was amplified by PCR to find the rate of mutation in embryos injected with a mixture of gRNA - Cas9 mRNA. For this purpose, PCR reaction was established using 1 µl DNA lysate, 10 pmol Forward primer, 10 pmol Rev primer, 0.1 mM dNTP mixture, 1 U Taq polymerase, and a standard PCR for 30 cycles was performed with 60°C annealing temperature.

As a result of the use of gRNA3 and gRNA5 together, it was aimed to create a deletion of approximately 1150 bp with simultaneous breakage at the beginning and end of the

coding region. In order to distinguish mutant DNA resulting from deletion from WT DNA, a 1302 bp long genomic region containing the entire coding region was amplified by PCR. WT DNA is 1302 bp, whereas mutant DNA is expected to be 150-160 bp in length and visualized with agarose gel at a density of 1.5 %.

3.4.6. Sequence Analysis

Sanger Sequencing method was used for determining the mutant sequences. A 1302 bp genomic DNA covering the entire exon2 of the CHST6 gene was amplified. The sequencing reaction was performed by Eurofins Genomic using the CHST6 ID Forward primer. Sequence analyzes were performed with the Clustal Omega web-based software and SnapGene program.

3.4.7. Western Blot

The BCA Protein Assay Kit (Thermo Scientific, USA, 23225) was used to measure the concentrations of isolated proteins. Proteins were boiled with 4X Laemmli Loading Buffer at 95°C for 5 minutes. 20-30 µg protein sample was run on 12 % SDS-PAGE gel. Transfer of proteins to the PVDF membrane was achieved by wet transfer at 350 mA for 90 minutes. After transfer, blocking was performed in a blocking solution (5 % BSA-Phosphate-buffered saline, PBS) for 1 hour at room temperature. After blocking the membranes incubated with the primary antibodies (1:1000 dilution) overnight at 4°C. After overnight incubation, the membranes were washed 3 times with PBS-T for 5 minutes and incubated with anti-mouse (5257S, Cell Signaling Technologies) or anti-rabbit (5366S, Cell Signaling Technologies) secondary antibodies in 5 % skim milk-PBST for 1 hour at room temperature. Then washed membranes were imaged with Licor Odessy.

3.4.8. ELISA

Larvae (at least 50) were collected in 600 µl test tubes 5 days after fertilization (5dpf). The ambient water of the larvae was withdrawn from the test tubes and snap freezing was performed in liquid nitrogen for 30 minutes to stop the metabolic activity. PBS containing 1 µl of protease inhibitor added per larva. Larvae were crushed manually with a micro pestle (Eppendorf). Crushing was continued until the viscosity was removed. The samples were centrifuged at 12000 rpm at 4°C for 5 minutes and the supernatant was transferred to new test tubes. Total protein was calculated by the

BCA assay using 1:10 dilution. If the process was not to be continued, the samples were kept at -20°C overnight.

Standard plotting for ELISA was performed using the kit manufacturer's protocol. The lyophilized 20 ng/ml standard in the kit was dissolved with the sample dilution solution included in the kit. It was incubated at room temperature for at least 15 minutes before serial dilutions were made. Standard solutions were prepared at the concentrations indicated in Figure 22B. Sample dilution solution was used for 0 ng/ml standard. In accordance with the kit protocol, the standard graph was drawn using the non-linear 4-parameter sigmoidal curve method and the concentration calculation equation was calculated.

ELISA protocol for Wildtype and Mutant Fish: 50 µl of standard, blank and samples were added to antibody coated wells. 50 µl of fixative reagent A solution was added to the wells and incubated at 37°C for 1 hour. At the end of the incubation, the wells were washed 3 times with 400 µl wash buffer. 100 µl of detection reagent B solution was added to the wells and incubated at 37°C for 45 minutes. At the end of the incubation, washing was done 5 times with wash buffer. 90 µl of substrate solution was added to the wells and incubated at 37°C for 10-20 minutes, protected from light. Then 50 µl of stop solution was added and absorbance was read at 450 nm. Concentrations were calculated by applying the formula in the Microsoft Excel program.

3.4.9. Immunofluorescence Staining of Wildtype and Mutant Zebrafish

After the larvae were fixed with 4 % PFA for 4 hours at room temperature, they were incubated in 100 % Methanol at -20°C for 24 hours. Larvae transferred to PBS were washed 2 times for 30 minutes with 1X PDT (1X PBS 0.3% Triton-X, 1% DMSO) washing solution. Then incubated for 1 hour at 37°C with 10 µg/µl Proteinase K and 0.5 U/ml chondrotinase to ensure penetration. Samples were blocked with 1X PBST containing 10 % FBS and 2 % BSA for 1 hour at room temperature. The primary antibody, Anti-Keratan Sulfate (1:200, Millipore MAB2022) was added to the blocking solution and incubated at 4°C overnight. Samples stained with the secondary Goat Anti-Mouse, Alexa Flour 594 (1:400, Invitrogen, A11005) and they were visualized with the confocal microscope (ZEISS LSM880).

3.4.10. Cell Preparation for Xenograft

Both Malme-3M and Mcf-7 cells culture medium include RPMI-1640 (Gibco) and 10 % Fetal Bovine Serum (FBS) (Thermo Fisher Scientific) supplemented with 1 % penicillin (50 IU/mL) and streptomycin (50 l g/mL). Cells were incubated at 37 °C in the incubator with 5 % CO_2. Cells were collected when 75% confluence, via 0.05 % trypsin treatment for 3 min in 37°C.

For xenograft, 500.000 cells were stained with a fluorescent membrane dye which is DiI (Invitrogen, V22885). After counting, cells were incubated with DiI in 1X PBS at 37°C for 20 minutes. The celllu suspension was mixed by gentle swirling every 5 minutes. Then cells washed once with FBS and 2 times with PBS at 1500 rpm for 2 minutes, resuspended in PBS containing 10 % FBS to a final density 30000 cells/µl. Stained cells were kept on ice and injected within 2 hours.

3.4.11. Xenograft

2 dpf zebrafish embryos were dechorionated, placed on an injection plate under anesthesia. Cell suspension was injected using an electronic microinjector (PV820 pneumatic picopump, World Precision Instruments) and a micromanipulator (Narishige MN-151). 250 - 300 cells were tried to be given to the yolk of each embryo. Embryos were kept at 34°C for the next 4 days. 2-3 hours after the injection, embryos were checked with an Olympus SZX16 (Olympus, Japan) fluorescent stereomicroscope to select local injected larvae. Embryos with the targeted cell count (250 - 300) were selected. At 1 dpi, representative bright field and fluorescent images of all selected embryos were taken under the fluorescent stereomicroscope using cellSens Entry software (Olympus, Japan). After 4-day post injections larvae were fixed with 4 % PFA for 2 hours at room temperature or overnight at 4°C.

3.4.12. Imaging of Xenograft

Zebrafish fixed with 4 % formaldehyde 4 days after microinjection were visualized with a fluorescent microscope, and tumor sizes and metastatic distribution were analyzed in groups wildtypes and mutants. For each experimental group, it was evaluated in 3 groups containing 20-25 larvae, the whole-body image of larvae and close images of different regions were recorded with the help of a fluorescent microscope.

3.4.13. Visualization and Analysis of Cells

Xenografted cells visualized by an ImageJ plugin as explain in detail in our publication (Cakan-Akdogan et al., 2022). Briefly images of xenografted larvae turned into grayscale and threshold was adjusted to clarify cells to be analyzed. Analyze Particles plugin was used, to count cells. Map of metastasized cells were generate using "Show outlines" command. Finally, to calculate and analyze statistically total cell number "summarize" command was run (Cakan-Akdogan et al., 2022).

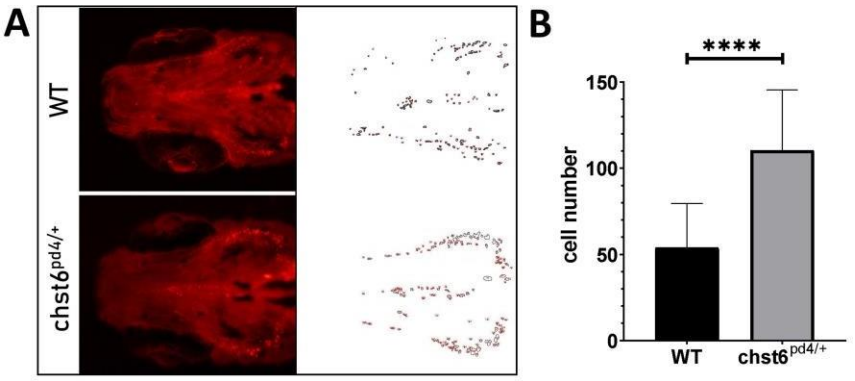

Figure 11 A) Metastatic cells were shown as map via ImageJ software B) A graph of counted cells.

3.5. RESEARCH PLAN

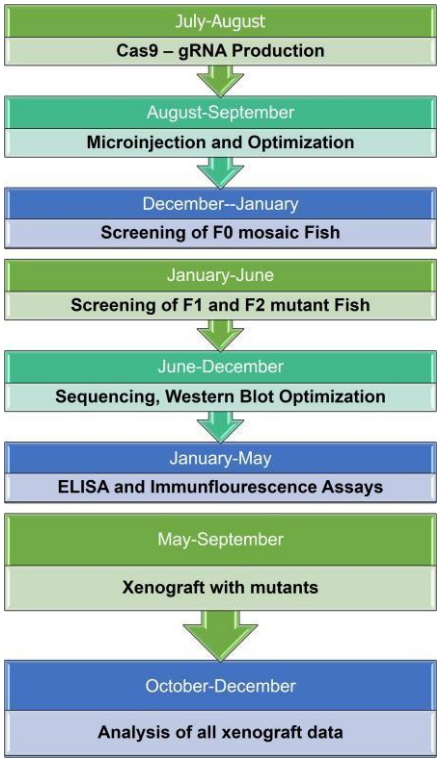

3.6. DATA EVALUATION

Data were analyzed statistically and graphed by using GraphPad (Prism 9.0).

All xenografts were carried out at least in triplicate. Two-way analysis of variance (ANOVA) was employed for the comparison of multiple groups, while multiple t-test was utilized for the analysis of two groups. Significance is accepted as * ; $P < 0.05$, ** ; $p < 0.001$ and *** ; $p < 0.0001$.

3.7. LIMITATION OF STUDY

At the beginning of the thesis study, the strategy of deleting the entire coding sequence was applied, but it could not be continued due to reasons such as low survival rate, low homozygous fish number, insufficient number of larvae for experiments. One of the biggest problems experienced was the lack of a primary antibody recognizing the zebrafish chst6 gene. Western blot was tried with chst6 antibody from 2 different brands, but it did not work in zebrafish samples. In addition, the ELISA Keratan Sulfate kit was used as a quantitative analysis, but the number of experiments that could be performed with the kit limited the experiments and the experiments remained in one repetition. This kit, which is quite expensive, could not be bought again and the experiment could not be repeated.

3.8. ETHICS COMITTEE APPROVAL

The ethics committee approval was obtained for the HADYEK protocol number 2021-003 with the approval of the Izmir Biomedicine and Genome Center.

4. RESULTS

4.1. SYNTHESIS OF gRNAS, CAS9 mRNAs AND MICROINJECTION

In order to generate loss of function CHST6 mutants, deletion of the entire coding sequence (CDS) was aimed. The CRISPRSCAN web tool found highest scoring gRNA (gRNA5) that targets 5th aa of the CHST6. Another gRNA that anneals to the 3' end of the CDS was annotated gRNA5 (Figure 12-B).

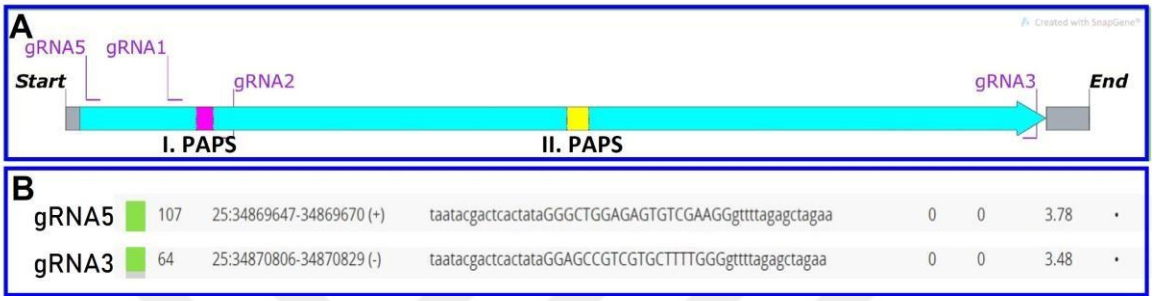

Figure 12 Targeted mutation sites in the zebrafish chst6 gene: A) chst6 mRNA is shown in the graph. Noncoding regions are shown in gray, the protein-coding sequence in turquoise, PAPS region 1 in magenta, and PAPS region 2 in yellow. B) Sequence of selected gRNAs based on Crispr scan web-based program.

The Cas9 capped mRNA was produced by in vitro transcription from pCS2:nlsCas9nls_nanos and pCS2:nlsCas9nls plazmids. The plasmids were confirmed with EcoRI, and linearized with NotI enzyme (Figure 13-A, B). The produced mRNA was checked in the gel (Figure 13-B). Similarly, Guide RNAs named gRNA3 and gRNA5 were generated via in vitro transcription successfully generated for this coding sequence deletion mutation strategy (Figure 13-C). RNA concentration was measured (Figure 13-D), each RNA was aliquoted at a concentration of 500 ng/µl and stored at -80ºC.

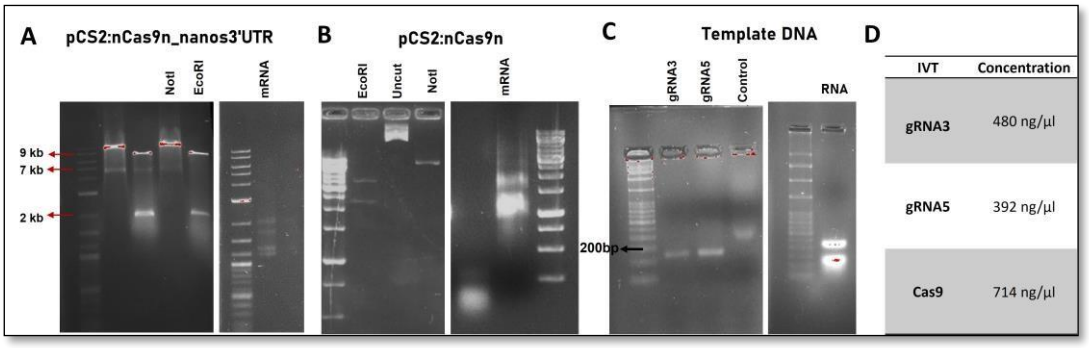

Figure 13 Production of Cas9 and gRNAs. Agarose gel images of A) pCS2:nCas9n_nanos3'UTR and B) pCS2:nCas9n plasmid confirmed with EcoRI, linearized with NotI, and capped mRNA after IVT. C) Template DNA and RNA of gRNA3 and gRNA5 confirmation on agarose gel. D) Concentration of gRNAs and cas9 after IVT is shown.

4.2. GENERATING OF THE CHST6 CRISPR MUTANTS

To generate mutations in the zebrafish genome mixture of gRNA3, gRNA5 and Cas9 mRNA was injected into 1-cell stage embryos. First Cas9 mRNA with nuclear localization signal (nlsCas9nls) was used primarily for gRNA3 and gRNA5 injection, which lead to high rate of death in embryos 24 hours after the injection. To prevent embryonic lethality nanos_nlsCas9nls, germ cell localized Cas9, was used. To this end, a total of 500 ng/µl Cas9 was injected with nanos_nlsCas9nls mRNA alone or mixed with an equal amount of nlsCas9nls. Embryo death was prevented by using nanos_nlsCas9nls. PCR was performed with primer pair OGC452-463 from DNA lysates from mosaic embryos 24 hours after injection. A 150-160 bp mutant DNA band was expected upon successful generation of the targeted deletion. Presence of WT (1.3 kb) and mutant (150 bp) bands were examined (Figure 14-A). After injection, mutation screening was performed among pooled 24 hpf embryos. Groups with mutant DNA bands were taken into the system to be raised. However, since 90% of the fish died in the juvenile period, the injection was repeated. Finally, by reducing the amount of Cas9mRNA to 250 ng, only nanos_nlsCas9nls and only nlsCas9nls were used. As a result of this last experiment, survival was partially increased and a total of 22 adult fish were obtained (Figure 14-E).

Obtaining the coding region deletion mutant with gRNA3+5:

Four injections were made for gRNA3+5, but only 21 fish reached adulthood and were analyzed. Two founder fish with mutations were identified. Only a small deletion was observed in one of these fish (Fish 3) and this fish died before obtaining progeny (Figure 14-B). A large deletion was detected in 1 fish (FF5) (Figure 14-B). In the DNA analysis of the single embryo, a DNA band of approximately 350 bp was seen and F_1 generation was obtained from this fish (Figure 14-C).

After the injection with a total of 500 ng Cas9 mRNA, the PCR product amplified from the embryo DNA, the WT DNA and the short mutant DNA formed because of the deletion are seen in the gel (Figure 14-A). In the 4th experiment, the amount of cas9 mRNA was reduced to 250 ng and two different Cas9 were injected separately, pools of embryos were analyzed for presence of mutant DNA by PCR and gel analysis

(Figure 14-A). In nanos-Cas9 group, less mutant DNA was seen in embryonic DNA lysate because Cas9 is concentrated in germline precursors. In the nls-Cas9 group, the mutant DNA ratio was higher, since Cas9 tends to be equally distributed in all cells. Sibling embryos were raised (30) were raised from both groups. The deletion allele was named chst6^{del5}.

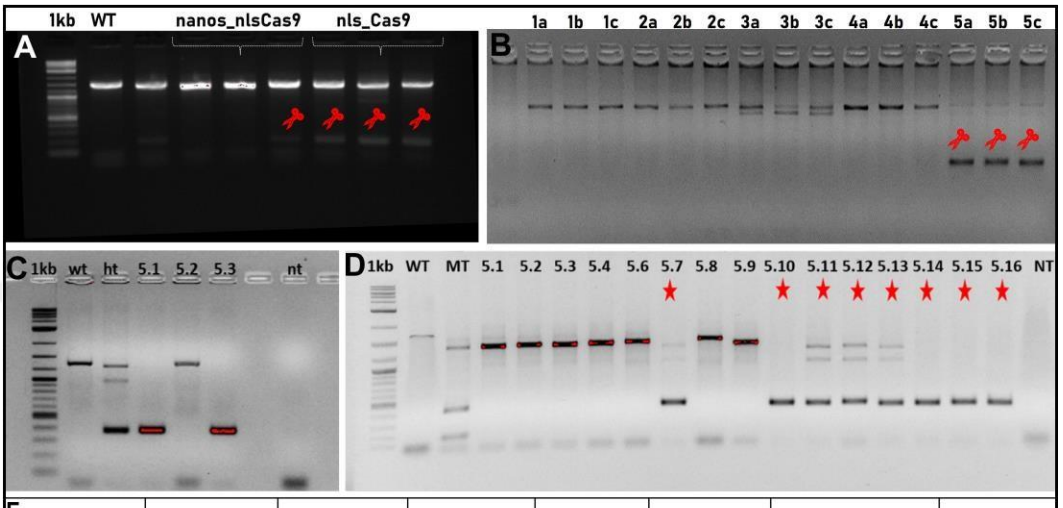

E

gRNA	Number of mosaic fish	Analyzed F_0	Number of FF	% Positive	Analyzed F_1	Number of Heterozygous	% Positive
gRNA3+5	21	20	1	% 5	30	8	%26.6

Figure 14 Mutations screening of chst6^{del5} allele. **A**) Mosaic analysis of deletion mutants. Red scissors indicate mutant DNA band. **B)** Founder fish screening **C)** Single embryo screening of 5th mutant fish. **D)** Heterozygous mutant fish screening of deletion mutations raised from FF5. Red asterisk shows mutant DNA bands. **E)** Table as a summary of transmission rate and number of mutant fish.

21 mosaic adult fish were screened for mutagenesis by obtain in F_1 embryos. Mutation screening was performed by PCR in 3 DNA pools obtained from 5 embryo pools. An image of the gel (Figure 14-B) in which mutant fish were detected is shown. The double band indicates that a small deletion occurred in the a, b, c DNA sets obtained from the embryos of FF3. In the analysis performed on embryos obtained from FF5, the density of a DNA band at the level of 300-400 bp draws attention, while the WT band is seen at low intensity. In Figure 14-C, WT, 5c pool DNA and PCR products of 5.1,5.2, and 5.3 single embryo DNA were analyzed. According to this analysis, only a mutant DNA band of approximately 350 bp in length is seen in fish 5.1 and 5.3.

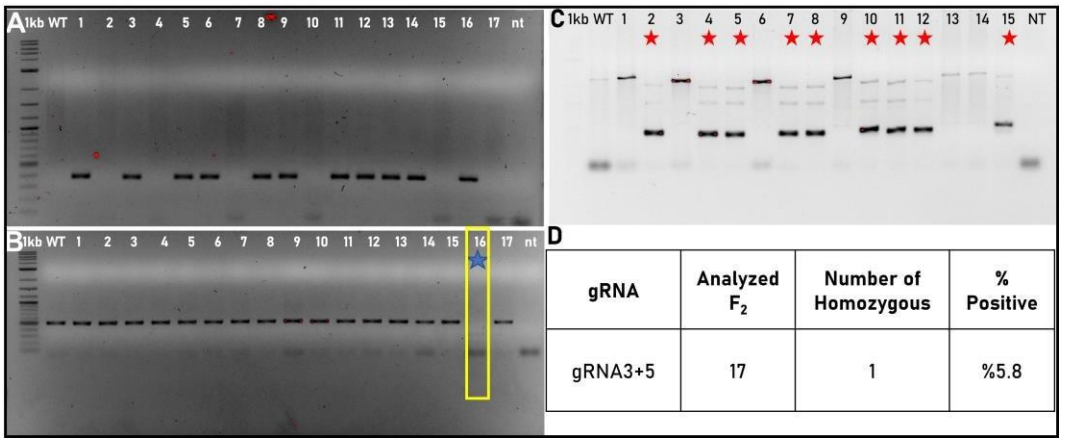

gRNA	Analyzed F_2	Number of Homozygous	% Positive
gRNA3+5	17	1	%5.8

Figure 15 Coding region deletion mutant chst6^{del5} F_2 homozygous screening **A)** Homozygous screening for the chst6^{del5} allele. Although heterozygous DNA bands at the level of 300-400 bp are seen, no definitive interpretation of homozygosity can be made because wildtype DNA bands are not seen. **B)** If the samples carried wildtype DNA or heterozygous DNA, it was expected to see 500 bp of wildtype DNA. Fish 16, marked in yellow, does not appear to carry wildtype DNA. Homozygosity was confirmed by sequencing. **C)** Genotyping PCR in A was repeated with the new primer, heterozygous fish marked with red were detected and included in the system. **D)** Table of transmission rate and number of mutant fish.

As a result of PCR, in which the entire coding region was amplified by using OGC452 and OGC463 primers, no wildtype DNA bands were seen in the gel image of the samples, PCR products less than 400 bp were seen in some of the scanned fish, while no PCR products were formed in the others, as in the WT control. Therefore, differentiation of heterozygosity or homozygosity could not be made according to this gel image (Figure 15-A). To show the presence of wildtype DNA, PCR was established with primers OGC452 and OGC453 including the cut region of gRNA5. It was expected that wildtype and heterozygous fish had wildtype DNA bands in the gel image, and PCR would not work if there was homozygosity.

In fact, it is seen that the 16th sample does not have a wildtype DNA band (Figure 15-B). Considering the 16th fish to be homozygous, it was decided to confirm it by sequence analysis (Figure 16). As a result of the sequencing analysis, cut-off is seen 250 bp from the cut-off site of gRNA5. On the other hand, cleavage on the gRNA3 side occurred where expected. A large deletion appears to have occurred, although not the entire coding region. 16th fish were taken into the system as homozygous. Heterozygous fish of the F_2 generation are also needed for the healthy maintenance of the line. The samples were re-analyzed with the new OGC463 primer (Figure 15-C). Red asterisk shows heterozygous fish: 2,4,5,7,8,10,11,12,15 according to the

PCR result. Fish were genotyped to be heterozygous and used for stock maintenance. 1 homozygous and 9 heterozygous fish were obtained from the chst6^{del5} allele.

Table 13: Coding sequence deletion mutation A) Shows the number of F1 embryos, B) shows the number of F2 embryos.

F_0 Founder Fish (FF)	Sex	Allel Name	Number of raised F_1 Fish	Number of F_1 Heterozygous Fish	Transmission Rate
#5	Female	chst6 $^{del5/+}$	30	8	26.6%

F_1 Genotype	Number of raised F_2	Number of survived F_2 Fish	Number of F_2 Heterozygous Fish	Number of F_2 Homozygous Fish	Homozygous Rate
chst6 $^{del5/+}$	25	17	9	1	5.8 %

Although this strategy, which aimed to delete the entire coding region, was shown to be effective in mosaic embryo analyzes, high lethality was observed in the larval and juvenile stages of these fish. By using nanos-Cas9 localized to the germ cells, this lethality was partially reduced, but despite many attempts, only 22 mosaic, and 1 FF adult fish were obtained.

4.3. SEQUENCING ANALYSIS OF MUTANTS

As a result of using gRNA3 and gRNA5 together, it was aimed to create a deletion of approximately 1150 bp with simultaneous breakage at the beginning and end of the coding region. A 1302 bp long genomic region containing the entire coding region was amplified by PCR and sequence analysis was performed. When DNA sequence analysis was performed from the F_1 heterozygous generation of mutant fish obtained as a result of this strategy, it was seen that a 943 bp region, slightly smaller than the target, was deleted. As a result of the alignment analysis, it was observed that no mutation occurred in the region targeted with gRNA5, but deletion started 200 bp below this region. On the other hand, it is seen that mutation occurred in the region targeted by gRNA3. Nucleotides 236-1179 of the coding sequence were deleted (Figure 16- A)

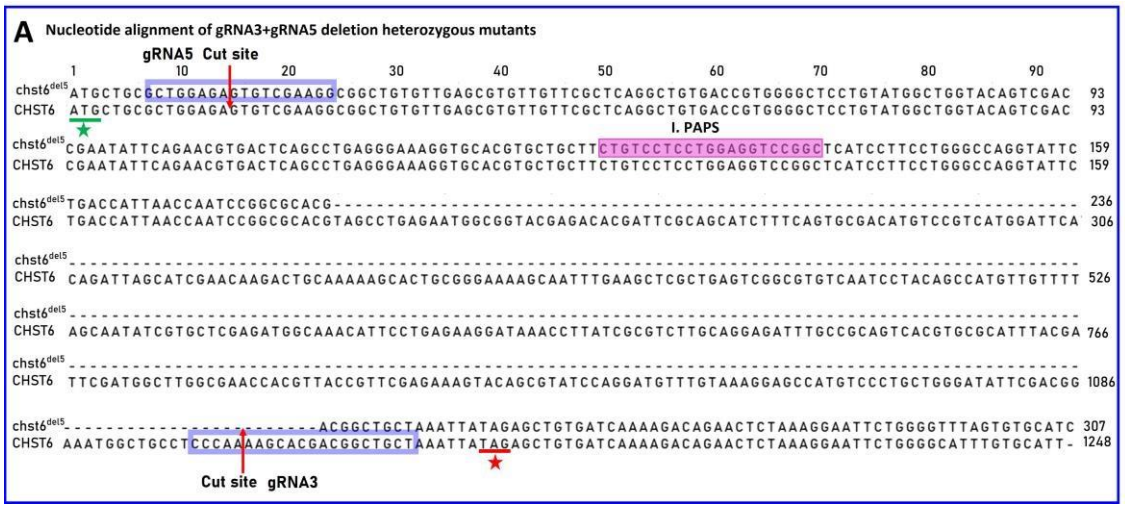

Figure 16 chst6^{del5} allele heterozygous single embryo sequence analysis. The deletion allele obtained because of injection of gRNA5 and gRNA3 was named del5. After the sequence analysis was performed with Clustal Omega, the sequence alignment from the beginning of the coding sequence, ATG (Green), is shown. The deletion started at 236T and continues until 1179A. The stop codon is marked with a red line and an asterisk. The gRNA5 and gRNA3 binding sites are shown in blue outline, PAPS region 1 in magenta box.

After screening homozygous candidate fish, the mutant DNA shown on the agarose gel was sent for sequence analysis (Figure 15-B). Sequence analysis confirmed that the mutant DNA was homozygous. The sequence results were mostly identical to the heterozygous mutant sequence. In the homozygous sequence, the deletion started at 236(T) and continued until 1179(A). When the protein sequence was examined, it is deleted since 89th amino acid. It was observed that deletion started 200 bp below gRNA5 cut region. In other words, although a large part of the gene was deleted in these mutants, the PAPS region remained the same. But this was not enough for the mutant fish to survive.

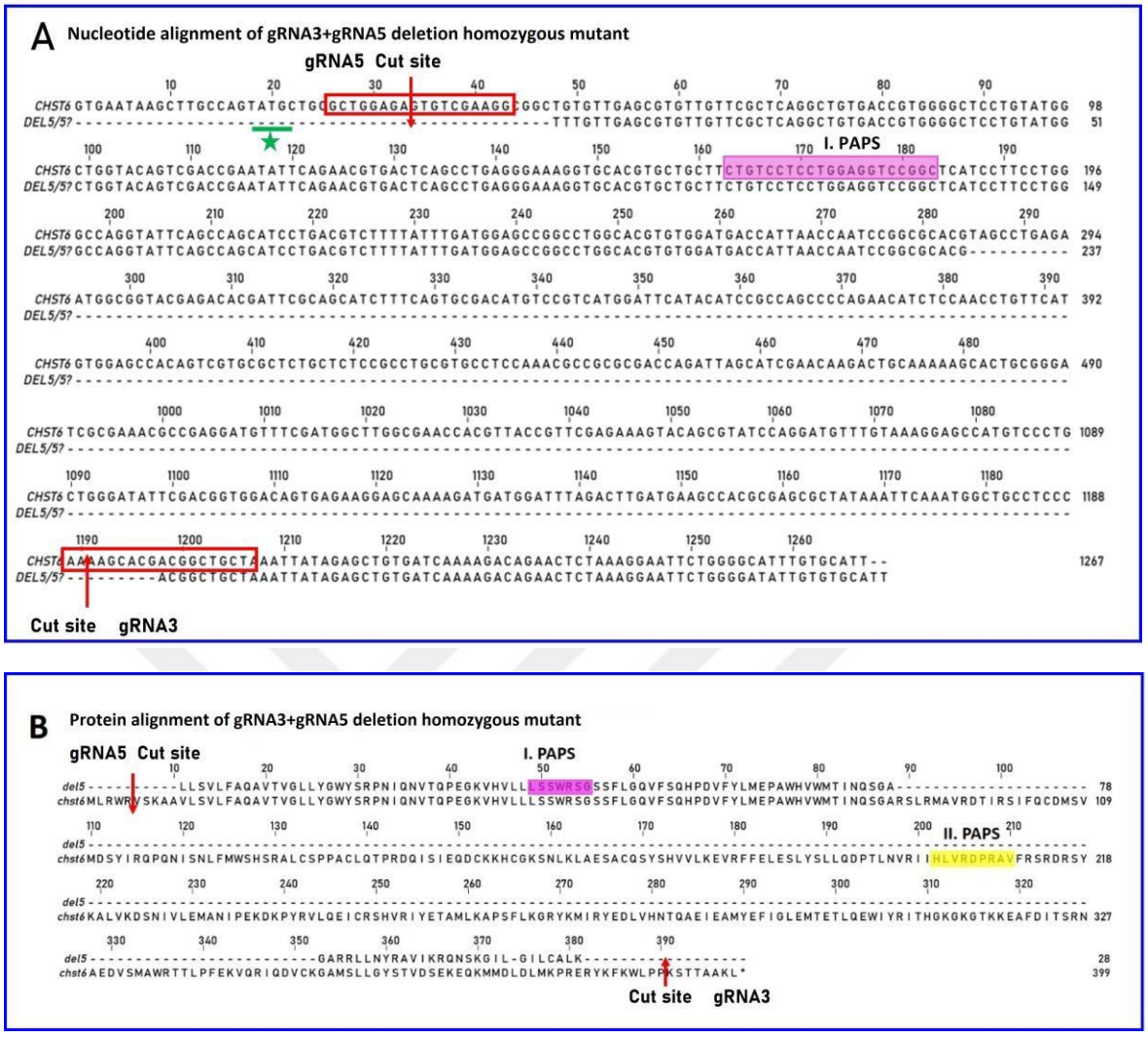

Figure 17 Sequence analysis of coding region deletion mutants with gRNA3+5. A) Nucleotide alignment of chst6$^{del5/5}$ mutant and wildtype fish. B) Protein alignment of chst6$^{del5/5}$ homozygous mutant.

Due to high mortality rate, small number of homozygous fish, and the inability to obtain a new generation, it was not possible to use these mutants in the following experiments.

4.4. SELECTION OF MUTANTS

Although in this thesis it was aimed to generate CDS deletion, alternative strategies to generate CHST6 mutant was also applied in Cakan Lab. These efforts generated mutants that inactivated the 1. PAPS region via smaller deletions.

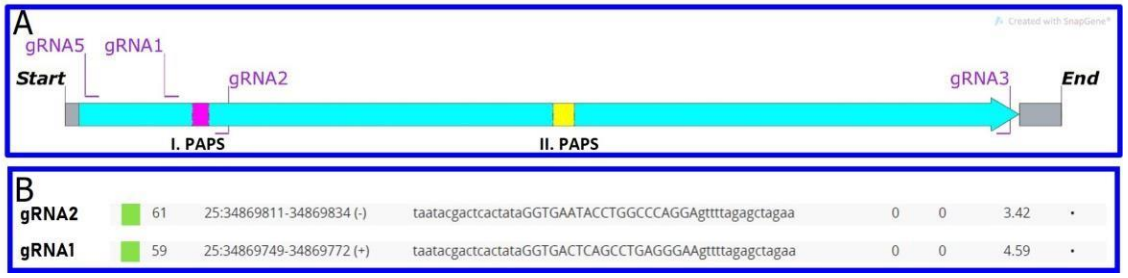

Figure 18 Targeted mutation sites in the zebrafish chst6 gene: A) chst6 mRNA is shown in the graph. Noncoding regions are shown in gray, the protein-coding sequence in turquoise, PAPS region 1 in magenta, and PAPS region 2 in yellow. B) Sequence of select sequence of selected gRNAs based on Crispr scan web-based program.

These mutants are reported in in Merve Başol's thesis " Generation of Chst6 Zebrafish Mutants Via Crispr/Cas9 System, And Phenotypic Analysis of Mutants ", and patent application was submitted (**2022/021668).** The first of these strategies is the deletion of the PAPS region. For this, guide RNAs called gRNA1 and gRNA2 were used together (Figure 18-A). One of the alleles obtained from this strategy, the chst6^{pd4} allele was decided to be used in the experiments due to low mortality, high heterozygous fish numbers and homozygous fish numbers (Table 14). Also, the homozygous sequence of this allele was obtained.

Table 14 Transmission and homozygous rates of chst6pd4 allele.

F_0 Founder Fish (FF)	Sex	Allel Name	Number of raised F_1 Fish	Number of F_1 Heterozygous Fish	Transmission Rate
#4	Female	chst6 $^{pd4/+}$	79	7	8.8%
F_1 Genotype	Number of raised F_2	Number of survived F_2 Fish	Number of F_2 Heterozygous Fish	Number of F_2 Homozygous Fish	Homozygous Rate
chst6 $^{pd4/+}$	40	34	15	7	17 %

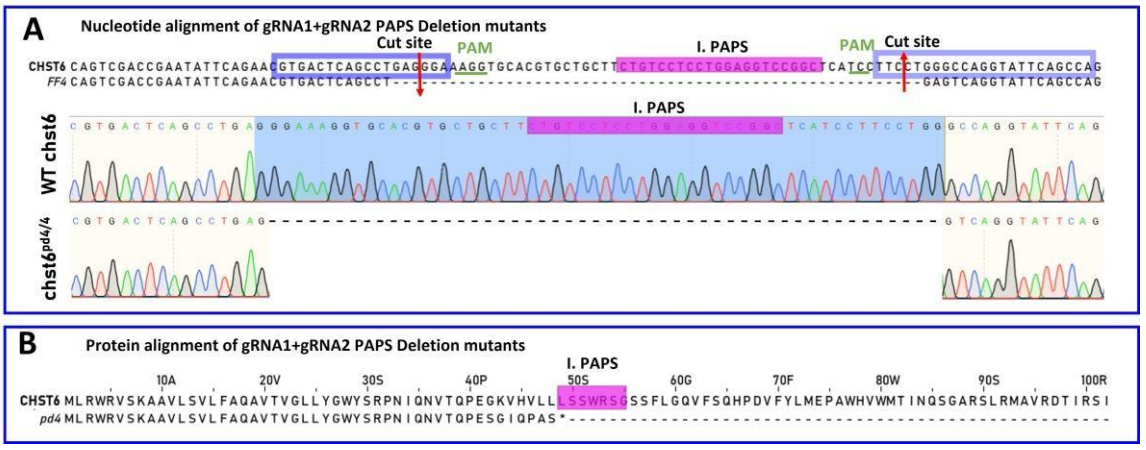

Figure 19 Sequence analysis of the chst6^{pd4} deletion homozygous mutant. Sequence analysis of the obtained sequences with Clustal Omega. The gRNA1 and gRNA2 binding sites, cut sites are indicated, and the PAPS region is shown in magenta. A) DNA sequence analysis B) Protein sequence analysis.

As can be seen because of the alignment of the sequence results shown in Figure 19-A with the gene coding sequence, deletion in the chst6^{pd4} allele starts immediately after the GAG nucleotides encoding the 41st amino acid. Therefore, the region enclosing the GGC codon encoding 42nd and 60th amino acid, the second cut site, was deleted.

A G>T mutation occurred after the first cut site and a frameshift occurred after this single nucleotide insertion. When the protein sequences are compared, it is seen that 7 aa just before the 1. PAPS region in the chst6^{pd4} allele are completely deleted, 7 new residues (SGIQPAS) are added because of the frameshift, and then a stop codon is formed. Thus, a 48 aa-long truncated protein that does not contain PAPS is formed in the chst6^{pd4} allele (Figure 19-B).

Another mutation strategy is to generate frameshift mutation using only gRNA1 just before the PAPS region. Due to the high success and survival rate, high heterozygous and homozygous fish numbers, the chst6^{f42} allele which is one of the alleles obtained in this strategy (Table 15), was selected for use in the further experiments. It was also confirmed by homozygous mutant sequence.

Table 15 Transmission and homozygous rates of chst6f42 allele.

F_0 Founder Fish (FF)	Sex	Allel Name	Number of raised F_1 Fish	Number of F_1 Heterozygous Fish	Transmission Rate
#42	Female	chst6 $^{f42/+}$	16	13	81.25%
F_1 Genotype	**Number of raised F_2**	**Number of survived F_2 Fish**	**Number of F_2 Heterozygous Fish**	**Number of F_2 Homozygous Fish**	**Homozygous Rate**
chst6 $^{f42/+}$	50	36	14	10	20 %

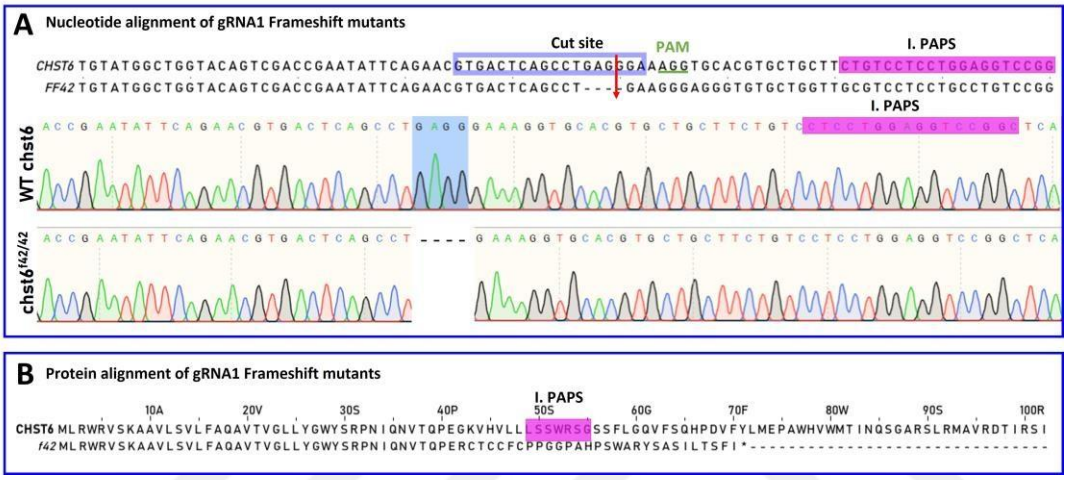

Figure 20 Sequence analysis of the chst6^{f42} frameshift mutation homozygous mutant. Sequence analysis of the obtained sequences with Clustal Omega. The gRNA1 and gRNA2 binding sites, cut sites are indicated, and the PAPS region is shown in magenta. A) DNA B) Protein sequence alignment.

The mutations obtained occurred prior to the 1st PAPS region in accordance with the gRNA1 binding site. In the chst6$^{f42/42}$ allele, there was a frameshift after deletion of 4 nucleotides, 1 amino acid, and all amino acids were mutated, and a stop codon was formed after 29 amino acids.

As a conclusion the chst6$^{f42/42}$ allele carries a 4-nucleotide deletion that causes protein truncation just before the 1st PAPS region while in the PAPS deletion strategy, the 19 amino acid truncated PAPS region in the chst6$^{pd4/4}$ mutant allele was completely lost and an early stop codon was formed.

4.5. PROTEIN EXPRESSION ANALYSIS OF MUTANTS BY WESTERN BLOT

Western blot analysis with anti chst6 and anti-cKS antibody was performed. When western blot was performed with chst6 antibody on lysates, it was seen that the antibody did not cross react with zebrafish chst6 protein (Figure 21- A). However, beta actin and cKS antibodies worked in zebrafish lysates. It was quantitatively shown that the amount of cKS was decreased in eye lysates of chst6$^{pd4/+,}$ and chst6$^{f42/42}$ alleles compared to wildtype fish (Figure 21-B). The amount of keratan sulfate in the lysates was normalized according to beta actin bands and quantified (Figure 21-B'). According to these results, it was shown that the amount of keratan sulfate in chst6$^{pd4/+}$ mutants decreased by 85 % compared to wildtype fish. Similarly, it appears to be reduced by half in chst6$^{f42/42}$ mutants (Figure 21, B'). Figure 21-C shows the membrane of heterozygous larvae lysates blotted with cKS antibody. Signal of bands were reduced in chst6$^{pd4/+}$ larvae lysates compared to WT larvae.

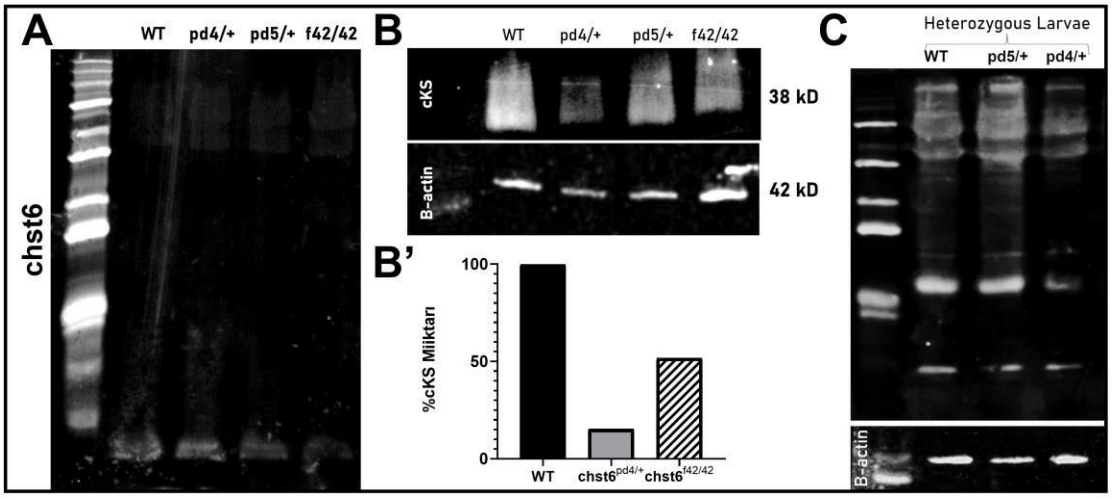

Figure 21 Western blot results: A) Western blot membrane image using anti-chst6 (abcam) antibody. B) Western blot membrane image of eye lysate made with anti-cKS antibody, using actin as control. B') % cKS amount plot because of normalization of cKS amount with beta actin control quantitatively C) Western blot membrane image performed in wildtype and heterozygous larval mutants using cKS antibody.

4.6. FUNCTIONAL ANALYSIS OF MUTANTS BY ELISA

Next the amount of sulfated KSPG in whole larvae lysates were quantified with KS ELISA Kit (My BioSource). For this purpose, 50 larvae (5 dpf) of wildtype, and mutants chst6$^{pd4/+,}$ chst6$^{pd4/4}$or chst6$^{pd5/+}$ were lysed in 600 µl E3 medium. 50 µl of standards, blanks and samples were added to the antibody-coated wells, absorbance was read at 450 nm. Concentrations were calculated by applying the formula in the Microsoft Excel program. It was found that the amount of cKS obtained from 50 larvae decreased by 90% in heterozygous and homozygous chst6^{pd4} allele (Figure 22-C). If the obtained KS amounts are normalized to the total protein, the difference is much higher.

A Table1 : KS-ELISA results of wildtype and mutant fish

Sample	Total Loaded Protein Amount (µg)	cKS Concentration (pg/ml)	Amount of cKS (pg)
WT	220,4	701	35
chst6$^{pd4/+}$	955	99	4,9
chst6$^{pd4/4}$	362	68	3,4

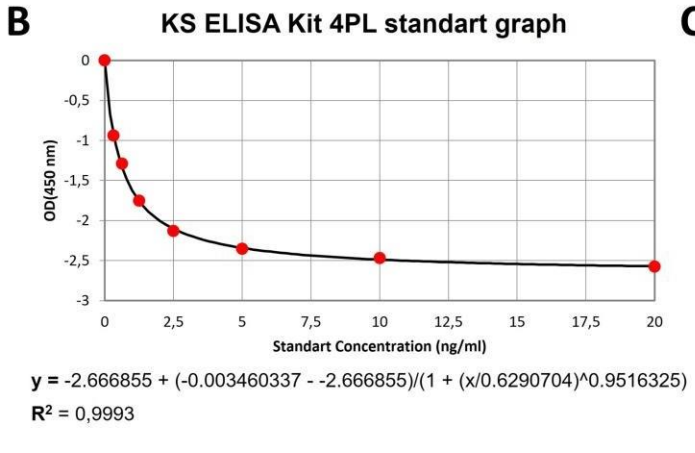

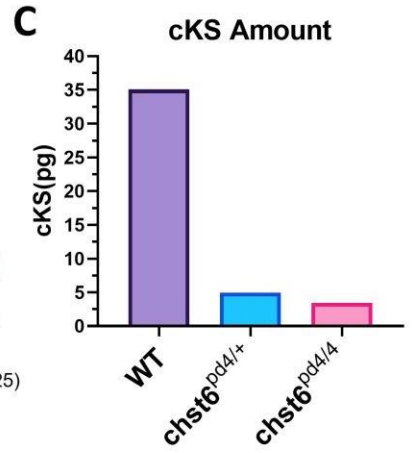

Figure 22 cKS amount decreased in mutants: A) Table of total protein amount, KS sulfate concentration and total cKS amount in 50 larvae of wildtype and mutant fish. B) Concentration calculation formula was obtained by drawing the standard graph. C) KS amount comparison plot of wildtype fish and mutants is shown.

4.7. TISSUE DISTRIBUTION OF SULFATED KSPGs IN MUTANT AND WT LARVAE

Tissue distribution and localization of sulfated KSPGs were detected with anti-cKS antibody that recognizes fully sulfated GlcNac-Gal epitope of keratan sulfate.

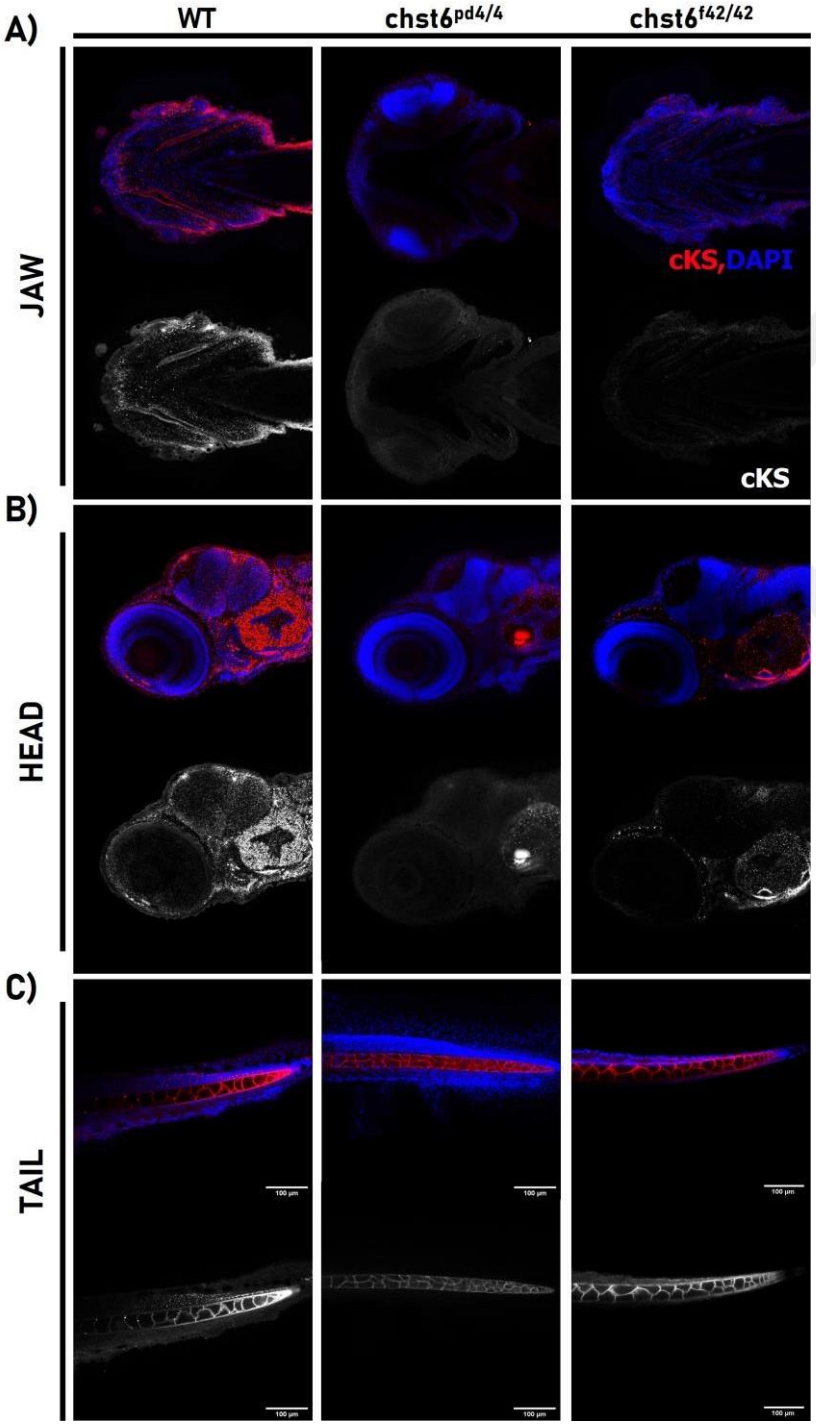

Figure 23 Inhibition of keratan sulfate proteoglycan sulfation in CHST6 mutant zebrafish larvae. sulfated KSPGs were detected with cKS antibody, expression in A) jaw cartilage, B) brain, cornea and otic vesicle C) posterior half of the notochord is detected in WT. cKS signal is undetectable in mutant A) jaw cartilage B) brain, otic vesicle and cornea whereas C) the signal is mildly reduced notochord of pd4 allele and unchanged in f42 allele. Overlay images are shown in first row (Blue: DAPI nucleus stain, red: cKS), and cKS image is shown in second row in gray scale. Images are acquired with Zeiss LSM880, scale bars: 100 µm.

cKS was found in brain, eye, jaw and end of the notochord of WT larvae. In mutant larvae, the cKS signal is either completely lost or dropped significantly in most of these tissues. Larvae of chst6$^{pd4/4}$ allele, cKS in cartilages and brain tissues is not detected and the level of signal was noticeably reduced at posterior end of the notochord, compared to WT (Figure 23). Similarly, the amount of cKS is considerably reduced in chst6$^{f42/42}$ homozygous mutants in all stained tissues, except for the notochord.

Western blot, ELISA, and finally cKS immunofluorescence staining with both PAPS deletion chst6$^{pd4/4}$ allele and PAPS Frameshift mutation chst6$^{f42/42}$ allele support each other, and it has been clearly proven that the mutation causes changes in the amount of keratan sulfate with loss of function of the chst6 enzyme.

In summary, PAPS inactivated and deleted in chst6 mutants. Protein level of KS decreasing were shown with WB and reducing cKS amount in mutants were shown with ELISA. Finally, KS expression decreased in brain, ear and jaw tissues was shown by immunostaining.

4.8. GENERATION OF XENOGRAFT MODEL

A xenograft model was used to evaluate the effect of KSPG composition of host tissues on the metastatic capacity of tumor cells. WT and mutant larvae with reduced KSPG sulfation were used as hosts. Xenografts were performed by injecting fluorescently stained cancer cells into the yolk regions of larvae at 2 dpf. After injection, larvae with low number of injected cells or those in which injected cells were seen in the vasculature were removed from the experiment. After injection, E3 medium was cleaned daily and dead larvae were removed, if any. Four days after the injection, the fish were grouped into metastatic and local groups. When more than 5 cells invaded the body of the host larvae these xenografts were considered metastatic, while the others were considered non-metastatic (local) xenograft tumors.

The tissues to which the cells metastasized were examined. Images of the larvae were recorded with a fluorescent stereo microscope and analyzed with ImageJ. Workflow is shown in Figure 24.

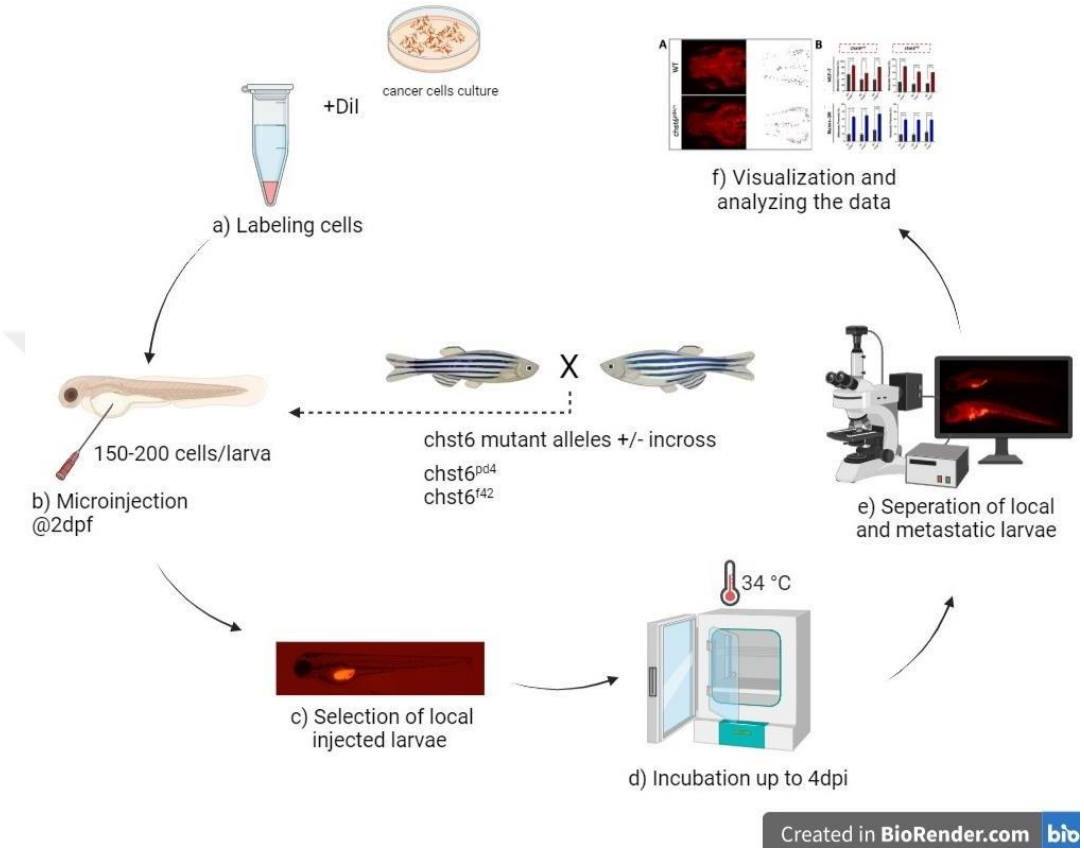

Figure 24 Workflow of a xenograft experiment and analysis

-Metastatic potential of MCF-7 cell line increased in the mutant host:

MCF7 cells are injected to the yolk of 2 dpf WT or chst6^{pd4} heterozygous incross mutant larvae. To obtain the mutants 3 independent experiments each with 3 replicates of 25 larvae was conducted. An average of 45 % of the MCF7 xenografts generated in WT larvae showed metastasis whereas this rate was 76 % when xenografts were generated in the mutant group (Figure 25-E). In addition, it was observed that the metastatic xenograft in both groups has cells in the tail region, and some in the jaw region. The difference between jaw metastasis in control and mutant hosts was further quantified. MCF-7 cells metastasized to the jaw in 26 % of WT host and 80 % of chst6^{pd4} mutant host (Figure 25-F).

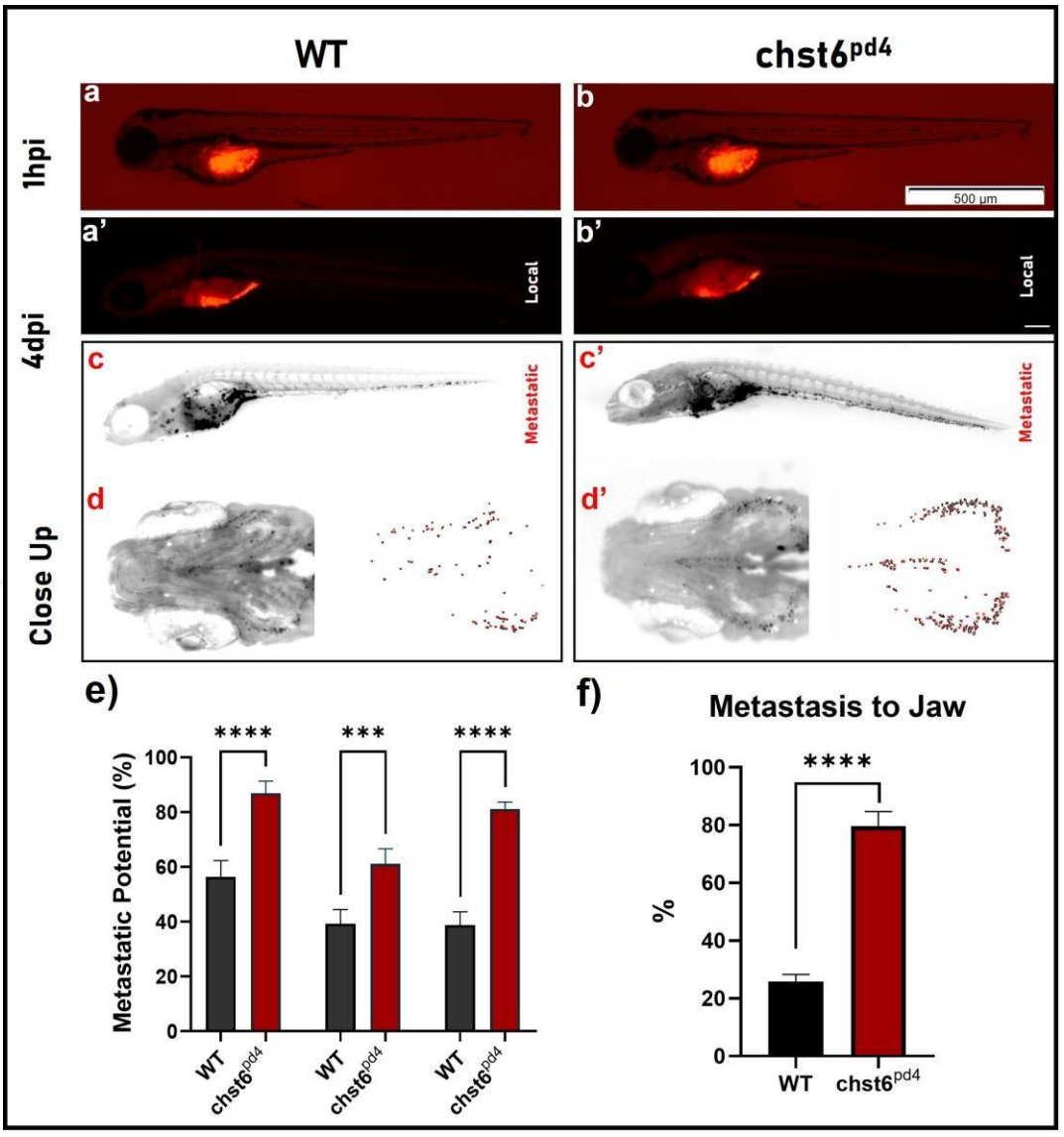

Figure 25 Results of Metastatic Capacity change of MCF7 cells in mutant larvae. Representative images of xenografts generated with DiI (red) stained MCF7 cells of A) WT, B) pd4 mutant larvae at 1 hpi. Representative images of local tumors in A') WT, B') pd4 mutant larvae, and metastatic tumors in C) WT, C') pd4 mutant larvae at 4 dpi. Cells are shown red in A-B', and in black in C-D'. Close-up ventral images of the jaw show metastatic cells in D) WT, E) pd4 mutant host. Cells are outlined by ImageJ and shown on the right. E) The percentage of metastatic xenografts are depicted for 3 independent experiments. F) The percentage of xenografts with jaw metastasis is depicted. In each group n= 25, with 3 replicas. Error bars represent standard deviation.

MCF7 cells are injected to the yolk of 2 dpf WT or chst6^{f42} heterozygous incross mutant larvae. An average of 40 % of the MCF-7 xenografts generated in WT larvae showed metastasis whereas this rate was 67 % when xenografts were generated in the mutant group (Figure 26-E). In addition, it was observed that the metastatic xenograft in both groups has cells in the tail region, and some in the jaw region as

chst6^{pd4} allele. The difference between jaw metastasis in control and mutant hosts was further quantified. MCF-7 cells metastasized to the jaw in 27 % of WT host and 78 % of chst6^{pd4} mutant host (Figure 26-F).

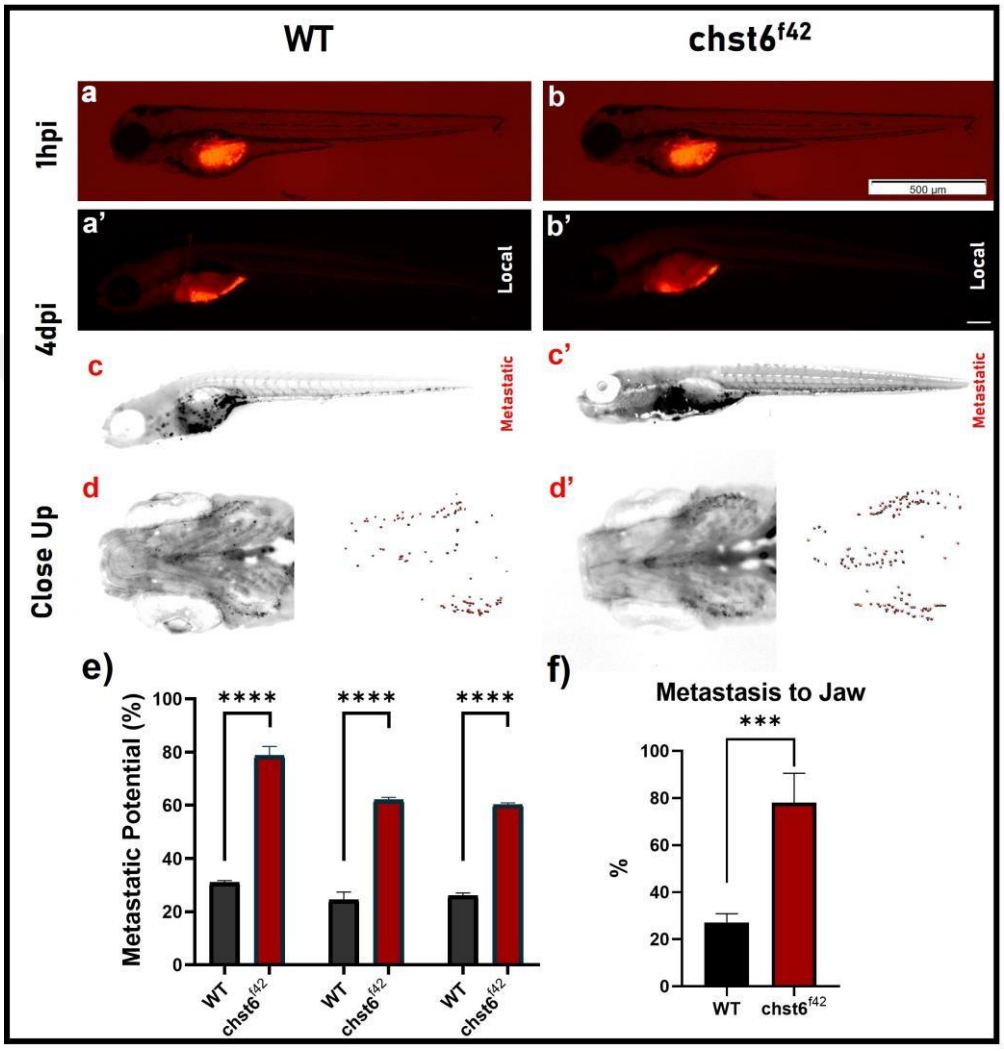

Figure 26 Results of Metastatic Capacity change of MCF7 cells in mutant larvae. Representative images of xenografts generated with DiI (red) stained MCF7 cells of A) WT, B) f42 mutant larvae at 1 hpi. Representative images of local tumors in A') WT, B') f42 mutant larvae, and metastatic tumors in C) WT, C') f42 mutant larvae at 4 dpi. Cells are shown red in A-B', and in black in C-D'. Close-up ventral images of the jaw show metastatic cells in D) WT, E) f42 mutant host. Cells are outlined by ImageJ and shown on the right. E) The percentage of metastatic xenografts are depicted for 3 independent experiments. F) The percentage of xenografts with jaw metastasis is depicted. In each group n= 25, with 3 replicas. Error bars represent standard deviation.

-Metastatic Potential of Malme-3M Cell Line Increased in Mutant Host

Malme-3M cells are injected to the yolk of 2 dpf WT or chst6^{pd4} heterozygous incross mutant larvae. To obtain the mutants 3 independent experiments each with 3 replicates of 25 larvae was conducted. An average of 22 % of the Malme-3M xenografts generated in WT larvae showed metastasis whereas this rate was 70 % when xenografts were generated in the mutant group (Figure 27-E). In addition, it was observed that the metastatic xenograft in both groups has cells in the tail region, and some in the jaw region. The difference between jaw metastasis in control and mutant hosts was further quantified. Malme-3M cells metastasized to the jaw in 17 % of WT host and 70 % of chst6^{pd4} mutant host (Figure 27-F).

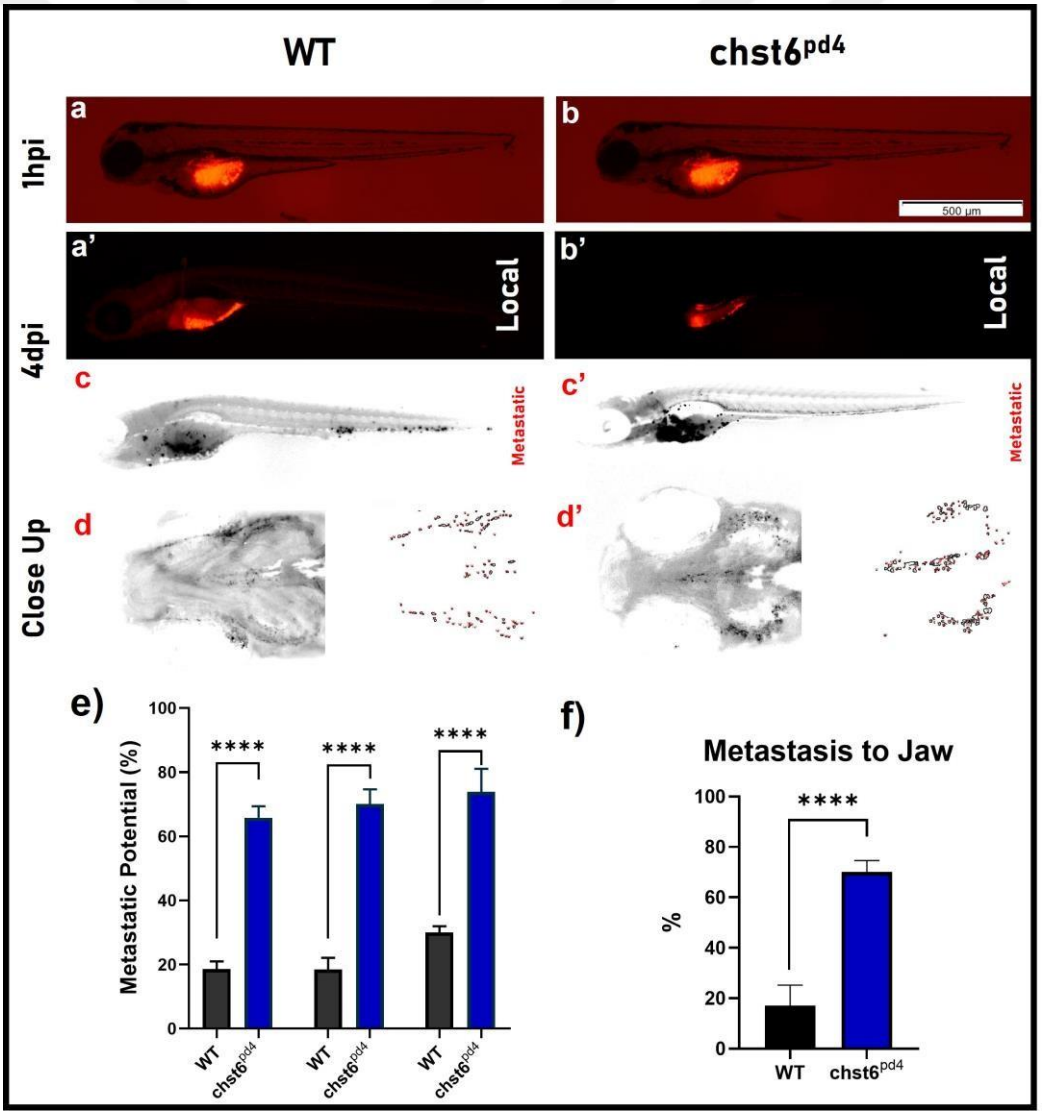

Figure 27 Results of Metastatic Capacity change of Malme-3M cells in mutant larvae. Representative images

of xenografts generated with DiI (red) stained Malme-3M cells of A) WT, B) pd4 mutant larvae at 1 hpi. Representative images of local tumors in A') WT, B') pd4 mutant larvae, and metastatic tumors in C) WT, C') pd4 mutant larvae at 4 dpi. Cells are shown red in A-B', and in black in C-D'. Close-up ventral images of the jaw show metastatic cells in D) WT, E) pd4 mutant host. Cells are outlined by ImageJ and shown on the right. E) The percentage of metastatic xenografts are depicted for 3 independent experiments. F) The percentage of xenografts with jaw metastasis is depicted. In each group n= 25, with 3 replicas. Error bars represent standard deviation.

Malme-3M cells are injected into the yolk of 2 dpf WT or chst6^{f42} heterozygous incross mutant larvae. An average of 22 % of the Malme-3M xenografts generated in WT larvae showed metastasis whereas this rate was 58 % when xenografts were generated in the mutant group (Figure 28-E). In addition, it was observed that the metastatic xenograft in both groups has cells in the tail region, and some in the jaw region as chst6^{pd4} allele. The difference between jaw metastasis in control and mutant hosts was further quantified. Malme-3M cells metastasized to the jaw in 17 % of WT host and 59 % of chst6^{pd4} mutant host (Figure 28-F).

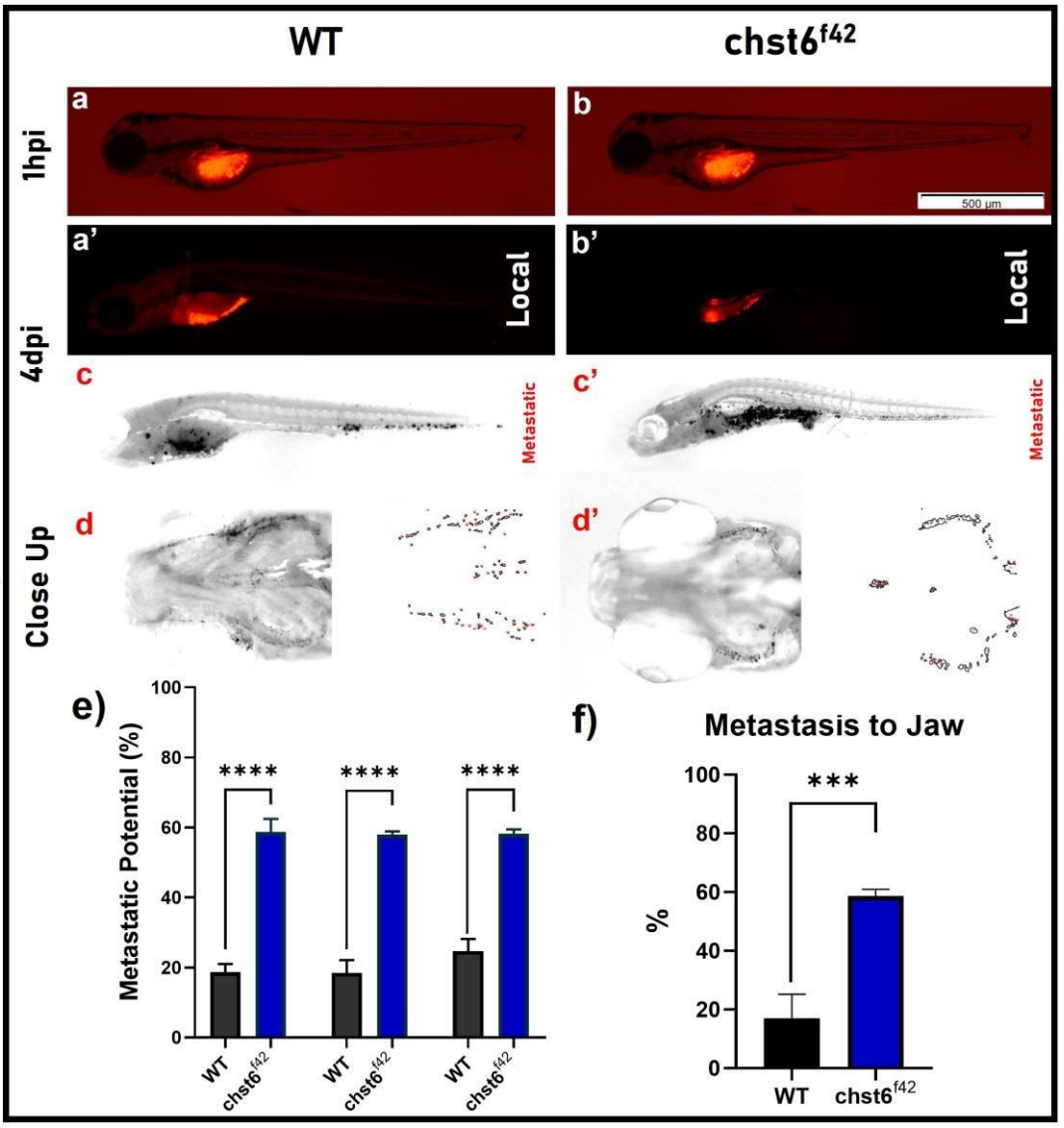

Figure 28 Results of Metastatic Capacity change of Malme-3M cells in mutant larvae. Representative images of xenografts generated with DiI (red) stained MCF7 cells of A) WT, B) f42 mutant larvae at 1 hpi. Representative images of local tumors in A') WT, B') f42 mutant larvae, and metastatic tumors in C) WT, C') f42 mutant larvae at 4 dpi. Cells are shown red in A-B', and in black in C-D'. Close-up ventral images of the jaw show metastatic cells in D) WT, E) f42 mutant host. Cells are outlined by ImageJ and shown on the right. E) The percentage of metastatic xenografts are depicted for 3 independent experiments. F) The percentage of xenografts with jaw metastasis is depicted. In each group n= 25, with 3 replicas. Error bars represent standard deviation.

After examining all the xenograft results, it is seen that both breast cancer and melanoma cancer cell lines show more metastatic capacity in mutant hosts (Figure 29). Moreover, metastasis to the jaw region, where the amount of KS is also considerably reduced, is more often a metastatic target.

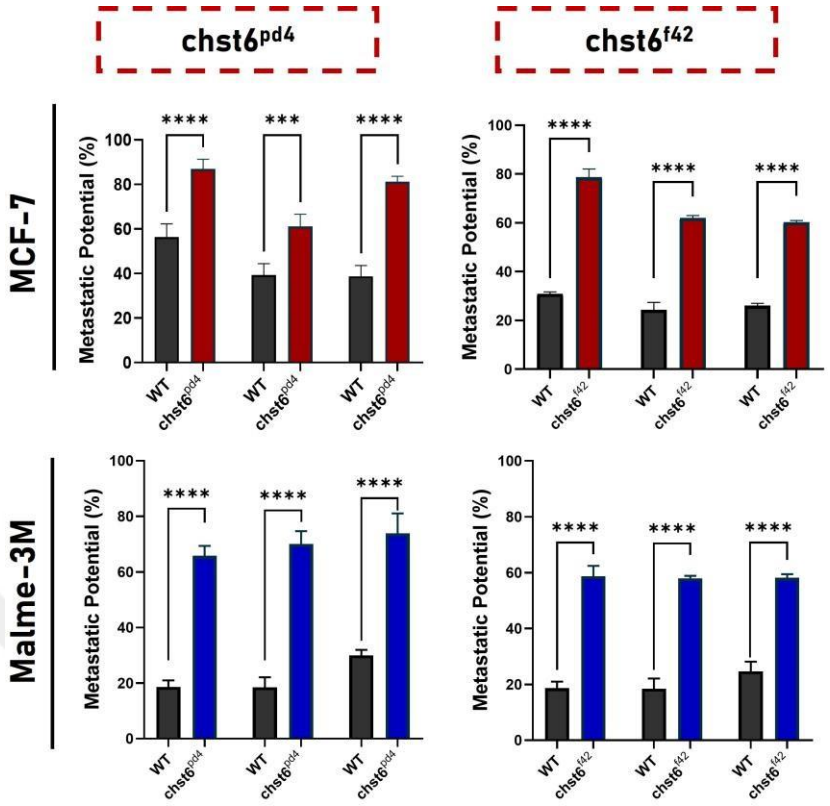

Figure 29 Summary of Metastatic potential comparison of xenografts which are used chst6 mutants as hosts.

- **Non-motile epithelial cells become invasive in chst6 mutant host.**

In order to test whether change in host tissue KSPG content alters motility of non-motile epithelial cells mutant and wildtype fish xenografts were made using non-transformed mouse mammary gland epithelial cell line (NMuMG). It was observed that these epithelial cells, do not show motility and invasive capacity when injected into the yolk of WT larvae, only in 4 % of the xenografts less than 10 cells exit the yolk and invaded the tail of wildtype larvae. On the other hand, in 49 % of the NMuMG xenografts generated in chst6^{pd4} host, high number of transplanted cells invaded the host tissues, displaying a metastatic-like phenotype. In addition, the experiment was stopped 3rd day after the injection because high rate of metastasis was observed in the chst6^{pd4} allele.

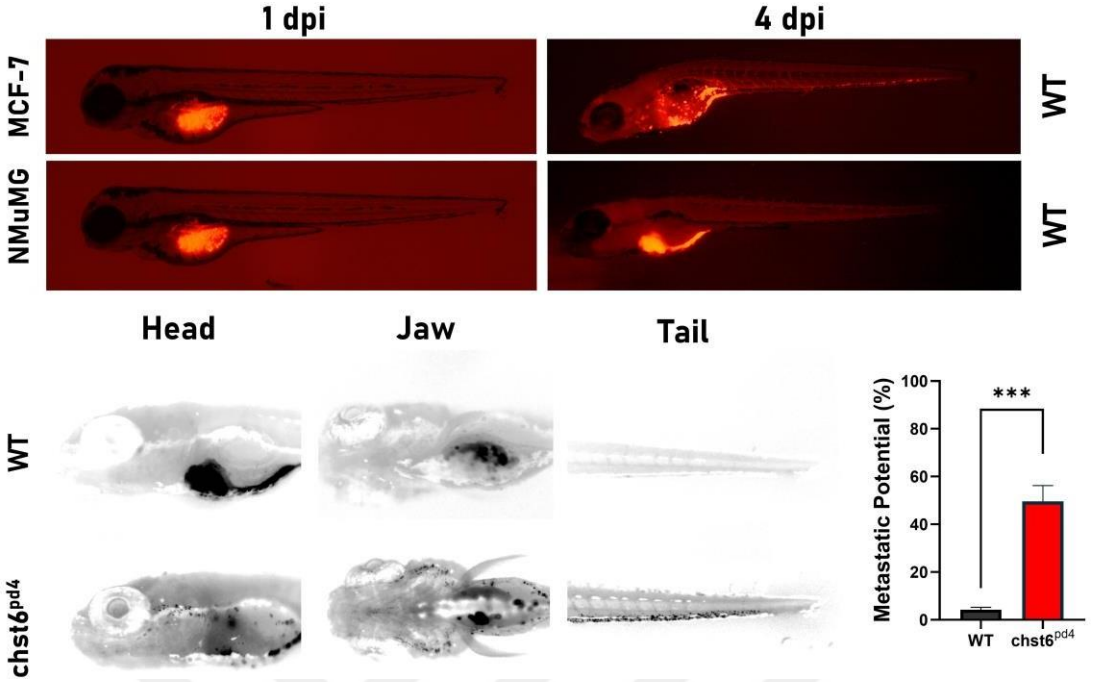

Figure 30 Representative images of DiI stained NMuMG cells injected wildtype and chst6$^{pd4/+}$ incross mutants zebrafish larvae. Black dots represent NMuMG cells.

5. DISCUSSION

The effects of keratan sulfate proteoglycans in the host tissues on the metastatic potential of cancer cells were investigated using the zebrafish model organism. The balanced distribution, amount, and type of glycosaminoglycans in the extracellular matrix is emerging as an important regulator of cancer progression. In this thesis, we focused on keratan sulfates from the glycosaminoglycan family, because among other glycosaminoglycans, keratan sulfates are the most recently discovered and the least understood glycosaminoglycan in cancer studies. nevertheless, some studies indicated to the importance of keratan sulfates, specifically Lumican (See chapter 2.5) in cancer cells (Karamanou et al., 2017, 2021; Leygue et al., 2000; Nikitovic et al., 2014; Sifaki et al., 2006). These studies have shown that lumican can act like both tumor suppressor and inhibitor in melanoma and breast cancer (Karamanou et al., 2017, 2021).The importance of KSPG in the ECM has not been tested in any experimental model to our knowledge.

The main proteins that carry KS GAG decorations are lumican, keratocan and fibromodulin. In addition, Aggrecan is one of the structural proteins of cartilage besides the collagens also carry KS side chains (Figure 6). Due to the large number of proteoglycans that carry keratan sulfate decorations, genetic ablation of any one gene coding for one KSGP is not expected to affect the overall keratan sulfate proteoglycan composition. Therefore, in order to affect functions of all keratan sulfates, we aimed to inhibit the sulfation of keratan sulfates. Therefore, we opted for mutating the carbohydrate sulfotransferase 6 gene that encodes the GlcNac6ST enzyme that is essential for sulfation of keratan sulfates. chst6 gene mutations are linked to macular corneal dystrophy, a disease that causes bilateral blindness due to accumulation of unsulfated KSPG aggregates in corneal extracellular matrix. Although the chst6 gene is cornea specific in humans, the zebrafish chst6 expression is not restricted to the cornea. The thesis work of Merve Basol in Cakan lab has postulated that chst6 gene is expressed in the jaw, brain, and cornea of developing zebrafish larvae. Moreover, skeletal detection of sulfated corneal keratan sulfate (cKS) in the jaw cartilage, and notochord of zebrafish larvae indicates that sulfated

KSs take roles in the ECM of these tissues in zebrafish (Hayes et al., 2013). Therefore, we hypothesized that chst6 loss of function mutants will have non-sulfated keratan sulfates in the tissues in which chst6 is the sole GlcNac6-ST.

5.1. DELETING THE CODING SEQUENCE OF THE CHST6 GENE IS FATAL

Loss of function chst6 mutants were generated by CRISPR/Cas9 mediated mutagenesis. To obtain null mutants without any remaining partial mRNA, it was aimed to delete the entire coding region. 2 guide RNAs that target 5th amino acid (gRNA5) and 391st amino acid (gRNA3) positions on the coding sequence were used simultaneously to induce double strand DNA breaks in the 5'UTR and 3'UTR regions of chst6. However, this strategy did not result in 100 % success. The rate of mutagenesis was low, with only 1 founder fish. Propagation of the mutant lines was challenging due to low survival rate. Finally, the entire coding region could not be deleted. A smaller deletion that begins below the gRNA5 targeted site was generated. This might be due to un synchronicity of ds DNA break generation and better repair in the end that is closer to gRNA5 site. When using a pair of gRNAs to create mutations, the efficiency is much higher than with a single gRNA. ((Zheng et al., 2014). It is aimed to delete the coding region corresponding to approximately 1100 bases using grna3 and grna5. As a result of the micro-injections, the survival rate was quite low. The Cas9 used to increase survival rate and obtain founder fish was replaced with Cas9 nanos localized to germ cells. In this way, survival is slightly increased. Of the 21 fish, only 1 mutated close to the targeted deletion. Single embryo DNA from the obtained founder fish was sent for sequencing, it was clearly seen that a smaller region than the targeted region was deleted shown by the sequencing. As a result of the sequence analysis, it is seen that 943 nucleotide (314 residues) deletion occurred. Homozygous fish were tried to be obtained by crossing 1 female and 1 male from heterozygous fish. 25 fish were obtained and raised, however 8 of them died in the juvenile stage, and only 1 homozygous fish obtained. However, a new generation could not be obtained from this homozygous fish. Since enough embryos could not be obtained from heterozygous fish for the experiments,

they could not be used in the experiments. Deletion of the entire coding region of the chst6 gene is thought to be fatal because of low survival in the early stage, failure to delete the entire coding region, and early deaths in the F_2 generation.

To continue the thesis work, we focused on the alleles that were generated in Cakan lab that generated smaller deletion of the chst6 CDS targeting the first PAPS region.

5.2. MUTATION OF THE PAPS REGION WAS CONFIRMED BY SEQUENCE ANALYSIS

The chst6 mutant were produced within the scope of the thesis Generation of Chst6 Zebrafish Mutants Via Crispr/Cas9 System, And Phenotypic Analysis of Mutants, (BASOL Merve, 2022) and are in the patenting process with patent application number 2022/021668. The $chst^{pd4}$ allele from the PAPS region deletion strategy mutants, and the $chst6^{f42}$ allele from the pre-PAPS region frameshift mutation strategy were selected for use in the thesis studies. Homozygous DNA sequences of both alleles were confirmed.

After validation of the sequences, western blot trials were performed to find out if there was loss of function. Early 3-day and 5-day-old whole body larval samples were used for western blot. Since an antibody developed against zebrafish CHST6 protein is not available in the market, epitopes of antibodies developed against human CHST6 protein were compared with zebrafish CHST6 protein. Novus recognizes the CHST6 antibody protein at residues 289-340th. The lysate preparation and western protocol were optimized, but cross reactivity with zebrafish proteins was not detected in the CHST6 antibody. Similarly, another antibody raised against a peptide that has 57-340. residues of the human chst6 gene (abcam, ab154332) did not cross react with the zebrafish chst6 protein.

5.3. MUTATION OF THE PAPS DOMAIN LEADS TO LOSS OF FUNCTION IN THE CHST6 GENE

The CHST6 gene encodes the enzyme N-acetylglucosamine-6-O-sulfotransferase (GlcNAc6-ST), which sulfates GlcNacs in keratan sulfate chains from the 6th carbon, and the antibody anti-cKS that recognizes keratan sulfates sulfated by this enzyme recognizes the same epitope in zebrafish (Hayes et al., 2013b). Since western blot results could not be obtained in the experiments with the chst6 antibody, western blot was performed with cKS antibody (mab2022, Millipore) in wildtype and mutant fish to show loss of function. Western blot analysis of larval lysates with the cKS antibody confirmed loss of function in mutants. According to these results, it was observed that the amount of keratan sulfate in chst6$^{pd4/+}$ mutants decreased approximately 6 times compared to wildtype fish, decreased by half in chst6$^{f42/42}$ mutants, and there was a noticeable decrease in cKS in whole body lysates of heterozygous chst6$^{pd4/+}$ and chst6$^{pd5/+}$ larvae (Figure 21). The fact that chst6 mutations lead to loss of function of the enzyme has been confirmed by the reduced and almost absent amount of keratan sulfate. Furthermore, total amount of KS in the larval lysates was quantified with ELISA, and supporting results were found. In order to analyze the levels of KSPG sulfated with keratan sulfate antibody in zebrafish mutants, ELISA protocol optimization studies were conducted, the process was optimized, and ELISA measurements were made using the KS ELISA Kit (Mybiosource). It was found that the amount of cKS obtained from 50 larvae decreased by 90 % in heterozygous and homozygous chst6^{pd4}. While 35 pg KS was measured in the WT sample, 3-5 pg KS was measured in the chst6^{pd4} allele. If the obtained KS amounts are normalized to the total protein, the difference is much higher (Figure 22). Finally, whole body immunofluorescence staining was performed in wildtype and mutant zebrafish larvae using the anti-cKS primary antibody used in western blot. This analysis not only showed loss of function but also indicated which tissues the chst6 encoded enzyme is functional. When WT fish was stained with cKS, it was detected in the jaw cartilages, brain, otic vesicle and end of the notochord.

The cKS staining showed that the KS in chst6$^{pd4/4}$ allele is almost negligible, especially in jaw cartilages, and brain tissues. It has been shown that the amount of cKS is considerably reduced in also chst6$^{f42/42}$ homozygous mutants in cartilages, jaw and brain compared to wildtype fish. Also, it was observed that the staining in the otic vesicle was not as strong as in wildtype fish, the intense cKS signal seen in wildtype fish is decreased in all mutants. Additionally at the end of notochord did not change significantly in mutants, indicating that chst6 is not required for KSPG sulfation in the notochord.

Western blot, ELISA, and finally cKS immunofluorescence staining with the mutants support each other, and it has been clearly proven that the mutation causes changes in the amount of keratan sulfate with loss of function of the chst6 enzyme.

5.4. METASTATIC CAPACITY OF BREAST AND MELANOMA CANCER CELLS ARE INCREASED IN CHST6 MUTANT XENOGRAFT MODELS

Wildtype and chst6 heterozygous mutant larvae were used in xenografts using the MCF-7 and Malme3m cell lines. Xenografts were performed in heterozygous incross larvae of the chst6$^{pd4/+}$ and chst6$^{f42/+}$ alleles, which were sequence-confirmed and demonstrated loss of function by results such as ELISA, IF. Unfortunately, heterozygous incross mutants were preferred for experiments because the number of homozygous larvae could not be obtained for each experiment and the larvae number was low. Heterozygous incross larvae were considered sufficient for this study, as there was a significant difference between mutants and wild larvae in all experiments. When xenografts made in larvae with 50% heterozygous, 25% homozygous and 25% wildtype genotype were compared with the xenografts made on 100% wildtype larvae, significant results were seen in metastasis potentials. For each mutant, 3 independent experiments were repeated, including 3 independent groups.

Looking at the chst6^{pd4} allele, it induces higher metastatic potential than wildtype larvae in all 3 experiments (Figure 25, 27). It should also be noted that host organisms have heterozygous incross genotypes and 25% of them are still in WT

genotype. In host organisms with a 100% homozygous genotype, the rate of metastasis will increase even more.

When the target tissues to which cells migrated in the chst6^{pd4} allele were examined, it was noticed that there was an increased orientation to the head and jaw regions. Metastatic cells were also randomly observed in the jaw and head of wildtype fish, but when compared quantitatively (Figure 25-F, 27-F), the number of metastatic cells directed to the jaw is significantly higher in the chst6^{pd4} allele. While an average of %21 larvae metastasized to the jaw in wildtype larvae, this rate increased approximately 3 times to 75 in the chst6^{pd4} allele. Similarly, use of chst6^{f42} mutants' hosts resulted in similar increase in overall metastasis and jaw metastasis in mutants when compared to wt hosts. The increased metastatic orientation overall and to the jaw tissue is in alignment with the decrease of keratan sulfates in the mutant tissues.

The effects of the amount of keratan sulfates and sulfation patterns on the tumor microenvironment have been demonstrated by xenograft models. Metastasis rate of tumor cells increased when KS sulfation in the host tissues was inhibited (Figure 29). This increase can be due to the abnormalities in the extracellular matrix structure making the environment more permissible.

Epithelial cells of breast tissue origin become invasive when injected into chst6 mutant host.

In order to test whether the altered KSPGs in the host ECM can induce motility, or invasiveness of non-motile cells we tested the metastatic behavior of NmuMG cells. Although there are nonmotile epithelial cells, they appear to undergo a characteristic change when placed into the yolk of chst6 mutant larvae. Interestingly these cells left the injection site and invaded the larval body indicating a epithelial mesenchymal transition (Figure 30). Further investigation is needed to determine which factors in the injection site or neighboring tissues would induce this change. The cells were injected into yolk site of larvae. Yolk is composed of lipid layers, but its structure did not explain in detail until today. However, yolk's adjacent tissues are belonging important organs such as liver, gut and pancreas. It was shown that chst6 is

expressed in liver and gut via in situ hybridization in Merve Başol's thesis. As explained in chapter 2.5 proteoglycans interact with extracellular signals and growth factors Therefore, the KSPGs produced by these tissues may induce alteration of NMuMG behavior. Moreover, CAFs can promote metastasis by inducing proliferation by secreting numerous growth factors and cytokines. It is not known whether larval yolk harbors fibroblasts that can interact with injected cells, but if they do these may became CAFS and interact with xenograft cells. Among the factors that can be produced by CAFs, TGF-β is shown to induce EMT of NMuMGs, and also TGF-β is known to promote invasion and metastasis in later stages cancer (Bataller & Brenner, 2005; Yeung et al., 2013) . Eventually that the relationship between proteoglycans and extracellular signals affects the properties of cells such as proliferation and migration.

6. CONCLUSION

In this thesis we showed that short deletions generated in the chst6 CDS that causes mutation of the 1. PAPS domain and truncation of the protein leads to loss of function. Moreover, chst6 was shown to be required for sulfated KSPGs in jaw cartilage, otic vesicle and brain of zebrafish larvae.

Here, we showed that inhibition of KSPG sulfation creates and environment that is more permissive to metastasis of cancer cells. Both melanoma and breast cancer cell lines displayed significantly and stronly increased metastasis in zebrafish model. Moreover, the metastatic targeting of the jaw tissue is specifically increased, supporting the importance of KSPG presence in the target tissue for cancer cell colonisation.

Surprisingly the alteration of KSPGs in host also induced character change of epithelial breast cells and enabled them to become motile and invade the larval tissues. It needs to be further investigated how this change is induced and whether it is a EMT or cancerous transformation.

To our knowledge this study is the first to demonstrate importance of host tissue KSPG sulfation for metastasis of cancer cells.

In this thesis, we showed that structural defects caused by mutations of the CHST6 enzyme that disrupt the sulfation of KSPGs increase the metastatic potential of cancer cells.

In future studies, we plan to investigate epithelial mesenchymal transitions in more detail using these hosts. Furthermore, we plan to examine CAFs and altered KS sulfation relationship in terms of migration signals.

7. REFERENCES

Afratis, N. A., Nikitovic, D., Multhaupt, H. A. B., Theocharis, A. D., Couchman, J. R., & Karamanos, N. K. (2017). Syndecans – key regulators of cell signaling and biological functions. In FEBS Journal (Vol. 284, Issue 1, pp. 27–41). Blackwell Publishing Ltd. https://doi.org/10.1111/febs.13940

aging-11-101807. (n.d.).

Ajit Varki, Richard D. Cummings, Jeffrey D. Esko, Pamela Stanley, & Gerald W. Hart. (2022). Essentials of Glycobiology, 4th edition. https://doi.org/10.1101/9781621824213

Bataller, R., & Brenner, D. A. (2005). Liver fibrosis. In Journal of Clinical Investigation (Vol. 115, Issue 2, pp. 209–218). The American Society for Clinical Investigation. https://doi.org/10.1172/JCI24282

Belli, C., Trapani, D., Viale, G., D'Amico, P., Duso, B. A., della Vigna, P., Orsi, F., & Curigliano, G. (2018). Targeting the microenvironment in solid tumors. In Cancer Treatment Reviews (Vol. 65, pp. 22–32). W.B. Saunders Ltd. https://doi.org/10.1016/j.ctrv.2018.02.004

Burgeson, R. E., & Nimni, M. E. (1992). Collagen types. Molecular structure and tissue distribution. Clinical Orthopaedics and Related Research, 282, 250—272. http://europepmc.org/abstract/MED/1516320

Cabezas-Sáinz, P., Pensado-López, A., Sáinz, B., & Sánchez, L. (2020). Modeling Cancer Using Zebrafish Xenografts: Drawbacks for Mimicking the Human Microenvironment. In Cells (Vol. 9, Issue 9). NLM (Medline). https://doi.org/10.3390/cells9091978

Cakan-Akdogan, G., Ersoz, E., Sozer, S. C., & Gelinci, E. (2022a). An in vivo zebrafish model reveals circulating tumor cell targeting capacity of serum albumin nanoparticles. Journal of Drug Delivery Science and Technology, 75. https://doi.org/10.1016/j.jddst.2022.103658

Cakan-Akdogan, G., Ersoz, E., Sozer, S. C., & Gelinci, E. (2022b). An in vivo zebrafish model reveals circulating tumor cell targeting capacity of serum albumin nanoparticles. Journal of Drug Delivery Science and Technology, 75.

https://doi.org/10.1016/j.jddst.2022.103658

Caterson, B., & Melrose, J. (2018). Keratan sulfate, a complex glycosaminoglycan with unique functional capability. In Glycobiology (Vol. 28, Issue 4, pp. 182–206). Oxford University Press. https://doi.org/10.1093/glycob/cwy003

Chen, X., Li, Y., Yao, T., & Jia, R. (2021). Benefits of Zebrafish Xenograft Models in Cancer Research. In Frontiers in Cell and Developmental Biology (Vol. 9). Frontiers Media S.A. https://doi.org/10.3389/fcell.2021.616551

Cho, S. H., Park, J. Y., & Kim, C. H. (2022). Systemic Lectin-Glycan Interaction of Pathogenic Enteric Bacteria in the Gastrointestinal Tract. In International Journal of Molecular Sciences (Vol. 23, Issue 3). MDPI. https://doi.org/10.3390/ijms23031451

Clause, K. C., & Barker, T. H. (2013). Extracellular matrix signaling in morphogenesis and repair. In Current Opinion in Biotechnology (Vol. 24, Issue 5, pp. 830–833). https://doi.org/10.1016/j.copbio.2013.04.011

Cohen, E., & Merzendorfer, H. (n.d.). Biologically-Inspired Systems Extracellular Sugar-Based Biopolymers Matrices. http://www.springer.com/series/8430

Cross, N. A., Chandrasekharan, S., Jokonya, N., Fowles, A., Hamdy, F. C., Buttle, D. J., & Eaton, C. L. (2005). The expression and regulation of ADAMTS-1, -4, -5, -9, and -15, and TIMP-3 by TGFβ1 in prostate cells: Relevance to the accumulation of versican. Prostate, 63(3), 269–275. https://doi.org/10.1002/pros.20182

Crusio, W. E., Lambris, J. D., & Radeke, H. H. (n.d.). Advances in Experimental Medicine and Biology Volume 1245 Series Editors. http://www.springer.com/series/5584

Derya, M., Yilmaz, I., & Aytekin, M. (2014). The role of extracellular matrix in lung diseases. In European Journal of Physical and Health Education (Vol. 6, Issue 2). Academy of Physical Education and Sport in Gdansk. https://doi.org/10.4172/0974-8369.1000200

Dituri, F., Gigante, G., Scialpi, R., Mancarella, S., Fabregat, I., & Giannelli, G. (2022). Proteoglycans in Cancer: Friends or Enemies? A Special Focus on Hepatocellular Carcinoma. In Cancers (Vol. 14, Issue 8). MDPI. https://doi.org/10.3390/cancers14081902

Faria-Ramos, I., Poças, J., Marques, C., Santos-Antunes, J., Macedo, G., Reis, C. A., & Magalhães, A. (2021). Heparan sulfate glycosaminoglycans: (un)expected allies in cancer clinical management. In Biomolecules (Vol. 11, Issue 2, pp. 1–28). MDPI AG. https://doi.org/10.3390/biom11020136

Filmus, J., & Capurro, M. (2014). The role of glypicans in Hedgehog signaling. In Matrix Biology (Vol. 35, pp. 248–252). Elsevier. https://doi.org/10.1016/j.matbio.2013.12.007

Frantz, C., Stewart, K. M., & Weaver, V. M. (2010). The extracellular matrix at a glance. In Journal of Cell Science (Vol. 123, Issue 24, pp. 4195–4200). https://doi.org/10.1242/jcs.023820

Funderburgh, J. L. (2000). MINI REVIEW Keratan sulfate: structure, biosynthesis, and function. In Glycobiology (Vol. 10, Issue 10).

Funderburgh, J. L. (2002). Keratan Sulfate Biosynthesis. IUBMB Life, 54, 187–194. https://doi.org/10.1080/15216540290114469

Gamble, J. T., Elson, D. J., Greenwood, J. A., Tanguay, R. L., & Kolluri, S. K. (2021). The zebrafish xenograft models for investigating cancer and cancer therapeutics. Biology, 10(4). https://doi.org/10.3390/biology10040252

Giatagana, E. M., Berdiaki, A., Tsatsakis, A., Tzanakakis, G. N., & Nikitovic, D. (2021). Lumican in carcinogenesis—revisited. In Biomolecules (Vol. 11, Issue 9). MDPI. https://doi.org/10.3390/biom11091319

Haldi, M., Ton, C., Seng, W. L., & McGrath, P. (2006). Human melanoma cells transplanted into zebrafish proliferate, migrate, produce melanin, form masses and stimulate angiogenesis in zebrafish. Angiogenesis, 9(3), 139–151. https://doi.org/10.1007/s10456-006-9040-2

Hanahan, D., & Weinberg, R. A. (2011). Hallmarks of cancer: The next generation. In Cell (Vol. 144, Issue 5, pp. 646–674). https://doi.org/10.1016/j.cell.2011.02.013

Hayes, A. J., Mitchell, R. E., Bashford, A., Reynolds, S., Caterson, B., & Hammond, C. L. (2013a). Expression of glycosaminoglycan epitopes during zebrafish skeletogenesis. Developmental Dynamics, 242(6), 778–789. https://doi.org/10.1002/dvdy.23970

Hayes, A. J., Mitchell, R. E., Bashford, A., Reynolds, S., Caterson, B., & Hammond, C. L. (2013b). Expression of glycosaminoglycan epitopes during zebrafish skeletogenesis. Developmental Dynamics, 242(6), 778–789. https://doi.org/10.1002/dvdy.23970

He, Y., Liu, T., Dai, S., Xu, Z., Wang, L., & Luo, F. (2021). Tumor-Associated Extracellular Matrix: How to Be a Potential Aide to Anti-tumor Immunotherapy? In Frontiers in Cell and Developmental Biology (Vol. 9). Frontiers Media S.A. https://doi.org/10.3389/fcell.2021.739161

Heegaard, A. M., Xie, Z., Young, M. F., & Nielsen, K. L. (2004). Transforming growth factor beta stimulation of biglycan gene expression is potentially mediated by Sp1 binding factors. Journal of Cellular Biochemistry, 93(3), 463–475. https://doi.org/10.1002/jcb.20189

Huang, J., Zhang, L., Wan, D., Zhou, L., Zheng, S., Lin, S., & Qiao, Y. (2021). Extracellular matrix and its therapeutic potential for cancer treatment. In Signal Transduction and Targeted Therapy (Vol. 6, Issue 1). Springer Nature. https://doi.org/10.1038/s41392-021-00544-0

Hwang, W. Y., Fu, Y., Reyon, D., Maeder, M. L., Tsai, S. Q., Sander, J. D., Peterson, R. T., Yeh, J. R. J., & Joung, J. K. (2013). Efficient genome editing in zebrafish using a CRISPR-Cas system. Nature Biotechnology, 31(3), 227–229. https://doi.org/10.1038/nbt.2501

Insua-Rodríguez, J., & Oskarsson, T. (2016). The extracellular matrix in breast cancer. In Advanced Drug Delivery Reviews (Vol. 97, pp. 41–55). Elsevier B.V. https://doi.org/10.1016/j.addr.2015.12.017

Iozzo, R. v., & Sanderson, R. D. (2011). Proteoglycans in cancer biology, tumour microenvironment and angiogenesis. In Journal of Cellular and Molecular Medicine (Vol. 15, Issue 5, pp. 1013–1031). https://doi.org/10.1111/j.1582-4934.2010.01236.x

Iozzo, R. v., & Schaefer, L. (2015). Proteoglycan form and function: A comprehensive nomenclature of proteoglycans. In Matrix Biology (Vol. 42, pp. 11–55). Elsevier. https://doi.org/10.1016/j.matbio.2015.02.003

Jao, L. E., Wente, S. R., & Chen, W. (2013). Efficient multiplex biallelic zebrafish

genome editing using a CRISPR nuclease system. Proceedings of the National Academy of Sciences of the United States of America, 110(34), 13904–13909. https://doi.org/10.1073/pnas.1308335110

Jayatilleke, K. M., & Hulett, M. D. (2020). Heparanase and the hallmarks of cancer. In Journal of Translational Medicine (Vol. 18, Issue 1). BioMed Central Ltd. https://doi.org/10.1186/s12967-020-02624-1

Karamanou, K., Franchi, M., Piperigkou, Z., Perreau, C., Maquart, F. X., Vynios, D. H., & Brézillon, S. (2017). Lumican effectively regulates the estrogen receptors-associated functional properties of breast cancer cells, expression of matrix effectors and epithelial-to-mesenchymal transition. Scientific Reports, 7. https://doi.org/10.1038/srep45138

Karamanou, K., Franchi, M., Proult, I., Rivet, R., Vynios, D., & Brézillon, S. (2021). Lumican inhibits in vivo melanoma metastasis by altering matrix-effectors and invadopodia markers. Cells, 10(4). https://doi.org/10.3390/cells10040841

Kolb, M., Margetts, P. J., Sime, P. J., & Gauldie, J. (2001). Proteoglycans decorin and biglycan differentially modulate TGF-mediated fibrotic responses in the lung. http://www.ajplung.org

Kolset, S. O., & Tveit, H. (2008). Serglycin - Structure and biology. In Cellular and Molecular Life Sciences (Vol. 65, Issues 7–8, pp. 1073–1085). https://doi.org/10.1007/s00018-007-7455-6

Lazebnik, Y. (2010). What are the hallmarks of cancer? In Nature Reviews Cancer (Vol. 10, Issue 4, pp. 232–233). https://doi.org/10.1038/nrc2827

Lee, W. Y., Kuo, C. C., Lin, B. X., Cheng, C. H., Chen, K. C., & Lin, C. W. (2017). Podocalyxin-like protein 1 regulates TAZ signaling and stemness properties in colon cancer. International Journal of Molecular Sciences, 18(10). https://doi.org/10.3390/ijms18102047

Leygue, E., Snell, L., Dotzlaw, H., Troup, S., Hiller-Hitchcock, T., Murphy, L. C., Roughley, P. J., & Watson, P. H. (2000). Lumican and decorin are differentially expressed in human breast carcinoma. Journal of Pathology, 192(3), 313–320. https://doi.org/10.1002/1096-9896(200011)192:3<313::AID-PATH694>3.0.CO;2-B

Li, Z., Zheng, W., Wang, Z., Zeng, Z., Zhan, H., Li, C., Zhou, L., Yan, C., Spitsbergen, J. M., & Gong, Z. (2013). A transgenic zebrafish liver tumor model with inducible Myc expression reveals conserved Myc signatures with mammalian liver tumors. DMM Disease Models and Mechanisms, 6(2), 414–423. https://doi.org/10.1242/dmm.010462

Meirson, T., Gil-Henn, H., & Samson, A. O. (2020). Invasion and metastasis: the elusive hallmark of cancer. In Oncogene (Vol. 39, Issue 9, pp. 2024–2026). Springer Nature. https://doi.org/10.1038/s41388-019-1110-1

Merida-De-Barros, D. A., Chaves, S. P., Belmiro, C. L. R., & Wanderley, J. L. M. (2018). Leishmaniasis and glycosaminoglycans: A future therapeutic strategy? 11 Medical and Health Sciences 1108 Medical Microbiology 06 Biological Sciences 0601 Biochemistry and Cell Biology. In Parasites and Vectors (Vol. 11, Issue 1). BioMed Central Ltd. https://doi.org/10.1186/s13071-018-2953-y

Moreno-Mateos, M. A., Vejnar, C. E., Beaudoin, J. D., Fernandez, J. P., Mis, E. K., Khokha, M. K., & Giraldez, A. J. (2015). CRISPRscan: Designing highly efficient sgRNAs for CRISPR-Cas9 targeting in vivo. Nature Methods, 12(10), 982–988. https://doi.org/10.1038/nmeth.3543

Neill, T., Painter, H., Buraschi, S., Owens, R. T., Lisanti, M. P., Schaefer, L., & Iozzo, R. v. (2012). Decorin antagonizes the angiogenic network: Concurrent inhibition of met, hypoxia inducible factor 1α, vascular endothelial growth factor A, and induction of thrombospondin-1 and tiMP3. Journal of Biological Chemistry, 287(8), 5492–5506. https://doi.org/10.1074/jbc.M111.283499

Nikitovic, D., Berdiaki, A., Spyridaki, I., Krasanakis, T., Tsatsakis, A., & Tzanakakis, G. N. (2018). Proteoglycans-Biomarkers and targets in cancer therapy. In Frontiers in Endocrinology (Vol. 9, Issue MAR). Frontiers Media S.A. https://doi.org/10.3389/fendo.2018.00069

Nikitovic, D., Papoutsidakis, A., Karamanos, N. K., & Tzanakakis, G. N. (2014). Lumican affects tumor cell functions, tumor-ECM interactions, angiogenesis and inflammatory response. Matrix Biology, 35, 206–214. https://doi.org/10.1016/j.matbio.2013.09.003

Oxford, J. T., Reeck, J. C., & Hardy, M. J. (2019a). Extracellular matrix in

development and disease. In International Journal of Molecular Sciences (Vol. 20, Issue 1). MDPI AG. https://doi.org/10.3390/ijms20010205

Oxford, J. T., Reeck, J. C., & Hardy, M. J. (2019b). Extracellular matrix in development and disease. In International Journal of Molecular Sciences (Vol. 20, Issue 1). MDPI AG. https://doi.org/10.3390/ijms20010205

Patton, E. E., Widlund, H. R., Kutok, J. L., Kopani, K. R., Amatruda, J. F., Murphey, R. D., Berghmans, S., Mayhall, E. A., Traver, D., Fletcher, C. D. M., Aster, J. C., Granter, S. R., Look, A. T., Lee, C., Fisher, D. E., Development, F.-N., & Zon, L. I. (2005). BRAF Mutations Are Sufficient to Promote Nevi Formation and Cooperate with p53 in the Genesis of Melanoma the p53 and BRAF pathways interact genetically to produce melanoma. Results and Discussion Activated BRAF Is Sufficient to Promote Melanoma arises from the malignant transformation of 2A-2G; www.xiphophorus.org). F-nevi melanocytes ap. Current Biology, 15, 249–254. https://doi.org/10.1016/j

Pez, F., Lopez, A., Kim, M., Wands, J. R., Caron De Fromentel, C., & Merle, P. (2013). Wnt signaling and hepatocarcinogenesis: Molecular targets for the development of innovative anticancer drugs. In Journal of Hepatology (Vol. 59, Issue 5, pp. 1107–1117). https://doi.org/10.1016/j.jhep.2013.07.001

Ren, Q., Wang, J., Liu, C., Meng, L. xin, Qian, R. kun, Gao, H. jie, Qin, W., Zhou, C. ju, Qiao, S., Wang, H. yun, Zhang, L. tao, & Zhang, Y. tao. (2021). Exploring the sulfate patterns of chondroitin sulfate/dermatan sulfate and keratan sulfate in human pancreatic cancer. Journal of Pharmaceutical and Biomedical Analysis, 205. https://doi.org/10.1016/j.jpba.2021.114339

Sander, J. D., Cade, L., Khayter, C., Reyon, D., Peterson, R. T., Joung, J. K., & Yeh, J. R. J. (2011). Targeted gene disruption in somatic zebrafish cells using engineered TALENs. In Nature Biotechnology (Vol. 29, Issue 8, pp. 697–698). https://doi.org/10.1038/nbt.1934

Santoriello, C., Gennaro, E., Anelli, V., Distel, M., Kelly, A., Köster, R. W., Hurlstone, A., & Mione, M. (2010). Kita driven expression of oncogenic HRAS leads to early onset and highly penetrant melanoma in zebrafish. PLoS ONE, 5(12), 1–11. https://doi.org/10.1371/journal.pone.0015170

Sharma, B., Ramus, M. D., Kirkwood, C. T., Sperry, E. E., Chu, P. H., Kao, W. W., & Albig, A. R. (2013). Lumican exhibits anti-angiogenic activity in a context specific manner. Cancer Microenvironment, 6(3), 263–271. https://doi.org/10.1007/s12307-013-0134-2

Sifaki, M., Assouti, M., Nikitovic, D., Krasagakis, K., Karamanos, N. K., & Tzanakakis, G. N. (2006). Lumican, a small leucine-rich proteoglycan substituted with keratan sulfate chains is expressed and secreted by human melanoma cells and not normal melanocytes. IUBMB Life, 58(10), 606–610. https://doi.org/10.1080/15216540600951605

Soares Da Costa, D., Reis, R. L., & Pashkuleva, I. (2017a). Sulfation of Glycosaminoglycans and Its Implications in Human Health and Disorders. https://doi.org/10.1146/annurev-bioeng-071516

Soares Da Costa, D., Reis, R. L., & Pashkuleva, I. (2017b). Sulfation of Glycosaminoglycans and Its Implications in Human Health and Disorders. https://doi.org/10.1146/annurev-bioeng-071516

Souza, A. R. C., Kozlowski, E. O., Cerqueira, V. R., Castelo-Branco, M. T. L., Costa, M. L., & Pavão, M. S. G. (2007). Chondroitin sulfate and keratan sulfate are the major glycosaminoglycans present in the adult zebrafish Danio rerio (Chordata-Cyprinidae). Glycoconjugate Journal, 24(9), 521–530. https://doi.org/10.1007/s10719-007-9046-z

Theocharis, A. D., Skandalis, S. S., Gialeli, C., & Karamanos, N. K. (2016). Extracellular matrix structure. In Advanced Drug Delivery Reviews (Vol. 97, pp. 4–27). Elsevier B.V. https://doi.org/10.1016/j.addr.2015.11.001

Theocharis, A. D., Skandalis, S. S., Tzanakakis, G. N., & Karamanos, N. K. (2010). Proteoglycans in health and disease: Novel roles for proteoglycans in malignancy and their pharmacological targeting. In FEBS Journal (Vol. 277, Issue 19, pp. 3904–3923). Blackwell Publishing Ltd. https://doi.org/10.1111/j.1742-4658.2010.07800.x

Vejnar, C. E., Moreno-Mateos, M. A., Cifuentes, D., Bazzini, A. A., & Giraldez, A. J. (2016). Optimized CRISPR-Cas9 system for genome editing in zebrafish. Cold Spring Harbor Protocols, 2016(10), 856–870.

https://doi.org/10.1101/pdb.prot086850

White, R., Rose, K., & Zon, L. (2013). Zebrafish cancer: The state of the art and the path forward. In Nature Reviews Cancer (Vol. 13, Issue 9, pp. 624–636). https://doi.org/10.1038/nrc3589

Winkler, J., Abisoye-Ogunniyan, A., Metcalf, K. J., & Werb, Z. (2020). Concepts of extracellular matrix remodelling in tumour progression and metastasis. In Nature Communications (Vol. 11, Issue 1). Nature Research. https://doi.org/10.1038/s41467-020-18794-x

Xiong, G.-F., & Xu, R. (2016). Function of cancer cell-derived extracellular matrix in tumor progression. Journal of Cancer Metastasis and Treatment, 2(9), 357. https://doi.org/10.20517/2394-4722.2016.08

Yeh, L. K., Liu, C. Y., Chien, C. L., Converse, R. L., Kao, W. W. Y., Chen, M. S., Hu, F. R., Hsieh, F. J., & Wang, I. J. (2008). Molecular analysis and characterization of zebrafish Keratocan (zKera) gene. Journal of Biological Chemistry, 283(1), 506–517. https://doi.org/10.1074/jbc.M707656200

Yeung, T. L., Leung, C. S., Wong, K. K., Samimi, G., Thompson, M. S., Liu, J., Zaid, T. M., Ghosh, S., Birrer, M. J., & Mok, S. C. (2013). TGF-β Modulates ovarian cancer invasion by upregulating CAF-Derived versican in the tumor microenvironment. Cancer Research, 73(16), 5016–5028. https://doi.org/10.1158/0008-5472.CAN-13-0023

Zheng, Q., Cai, X., Tan, M. H., Schaffert, S., Arnold, C. P., Gong, X., Chen, C. Z., & Huang, S. (2014). Precise gene deletion and replacement using the CRISPR/Cas9 system in human cells. BioTechniques, 57(3), 115–124. https://doi.org/10.2144/000114196

8. APPENDIX

8.1 ETHICS COMITTEE APPROVAL

İZMİR BİYOTIP VE GENOM MERKEZİ
HAYVAN DENEYLERİ YEREL ETİK KURULU (İBG-HADYEK)
KARARI

Toplantı Tarihi	: 10/02/2021	**Toplantı Günü**	: Çarşamba
Toplantı Sayısı	: 3	**Toplantı Saati**	: 15:30

Sayın Dr. Öğretim Üyesi Hani ALOTAİBİ,

2021-003 Protokol No'lu; yürütücüsü olduğunuz "Tümör Mikroçevresi ve Hücre Dışı Matriks Keratan Sülfat Proteoglikan Kompozisyonun Kanser Metastazındaki Rolünün Araştırılması" başlıklı projenin uygulanmasında etik açıdan sakınca olmadığına oy birliği ile karar verilmiştir.

Bilgilerinizi ve gereğini rica ederiz.

Doç. Dr. Güneş ÖZHAN BAYKAN **Başkan**	**Vet. Hek. Kerem ESMEN** **Başkan Yardımcısı**
Prof. Dr. Ersari GÜNELİ **Üye**	**Doç. Dr. Kasım DİRİL** **Üye**
Dr. Öğr. Üyesi Ayşe Banu DEMİR **Üye**	(Projede araştırmacı) **Dr. Gülçin ÇAKAN AKDOĞAN** **Üye**
Vet. Hek. Umur KELEŞ **Üye** (Katılmadı)	**Vet. Hek. Ceren ÜLKER** **Üye**
Vet. Hek. Gizem ARALAN **Üye**	**İrem KARADAŞ** **Üye**

8.2 Curriculum Vitae

Esra ERSOZ GULSEVEN

Year of Birth	1997
e- mail	
mobile	
address	Çiğli/İzmir/Türkiye

EDUCATION

Country Code	University	Institute	Department	Degree	Year
TR	Dokuz Eylul University	İzmir Biomedicine and Genome Institute	Molecular Biology and Genetics	MSc	2023
TR	Ege University	Engineering Faculty	Bioengineering	BSc	2019

EXPERIENCES

	Field	**Experience Type**	**Year**
İzmir Biomedicine and Genome Center	Çakan Zebrafish Modelling Lab.	Projects - Research and Development	2020-
Ege University Bioengineering	Bioprocess Lab.	Thesis Researcher	2019
Pınar Süt Mam. A.Ş.	Production Department	Intern	2018
İzmir Biomedicine and Genome Center	Özhan Lab. on Development and Regeneration	Intern	2018
Ege University Bioengineering	Microbial Biotechnology	Volunteer Intern	2017

PUBLICATIONS

Cakan-Akdogan, G., Ersoz, E., Sozer, S. C., & Gelinci, E. (2022a). An in vivo zebrafish model reveals circulating tumor cell targeting capacity of serum albumin nanoparticles. Journal of Drug Delivery Science and Technology, 75. https://doi.org/10.1016/j.jddst.2022.103658